United States
Department
of Agriculture

**Pacific Southwest
Research Station**

General
Technical
Report
PSW-130

Proceedings of the IUFRO Technical Session on Geomorphic Hazards in Managed Forests

August 5-11, 1990 Montreal, Canada

Rice, Raymond M., technical coordinator. 1991. **Proceedings of the IUFRO technical session on geomorphic hazards in managed forests**; 5-11 August 1990; Montreal, Canada. Gen. Tech. Rep. PSW-GTR-130, Berkeley, CA: Pacific Southwest Research Station, Forest Service, U.S. Department of Agriculture; 82 p.

The proceedings contains 11 of the 17 papers presented at the technical session on geomorphic hazards in managed forests at the XIX World Congress, International Union of Forestry Research Organizations, August 5-11, 1990, Montreal, Canada, plus one paper not presented orally. Two papers report research on torrents, two are about snow, three concern landslides, and five discuss watershed management problems.

Retrieval Terms: natural disasters, torrent control, watershed management, landslides, snow, avalanches, floods, erosion

Technical Coordinator:

RAYMOND M. RICE was, before his retirement, chief hydrologist in the Effects of Forest Management on Hillslope Processes, Fishery Resources, and Stream Environments Research Work Unit, at the Station's Redwood Sciences Laboratory, 1700 Bayview Drive, Arcata, CA 95521-6098.

Authors assumed full responsibility for the submission of camera-ready manuscripts. Views expressed in each paper are those of the authors and not necessarily those of the sponsoring organizations. Trade names and commercial enterprises are mentioned solely for information and do not imply endorsement of the sponsoring organizations.

Publisher:

Pacific Southwest Research Station
P.O. Box 245
Berkeley, California 94701

December 1991

Proceedings of the IUFRO Technical Session on Geomorphic Hazards in Managed Forests

August 5-11, 1990, Montreal, Canada

Raymond M. Rice, Technical Coordinator

Contents

Foreword iii

Invited Papers **1**

Severe Snow Loads on Mountain Afforestation in Japan 1
Ryuzo Nitta, Yoshio Ozeki, and Shoichi Niwano

Priority Setting for Government Investment in Forestry Conservation Schemes— An Example from New Zealand 6
Colin L. O'Loughlin

Voluntary Papers **11**

Effect of Tree Roots on Shallow-Seated Landslides 11
Kazutoki Abe and Robert R. Ziemer

Watershed Concerns and Recent Policy Formulations in Sri Lanka and Australia 21
Rohan Ekanayake

Surrounding the Consequences of Watershed Disasters in the Periphery of the Indian Triangle 28
Rohan Ekanayake

High-Speed High-Stress Ring Shear Tests on Granular Soils and Clayey Soils 33
Hiroshi Fukuoka and Kyoji Sassa

Morphological Study on the Prediction of the Site of Surface Slides 42
Hiromasa Hiura

Experimental Study on Impact Load on a Dam Due to Debris Flow 48
Iwao Miyoshi

Sediment Dynamics of a High Gradient Stream in the Oi River Basin of Japan 56
Hideji Maita

Contents

Snow-Cover Condition in Japan and Damage of the Sugi (*Cryptomeria Japonica* D. Don) 65
Taira Hideaki

Study on Shearing Force and Impact Force of a Volcanic Mud Flow on Mt. Sakurajima 72
Yoshinobu Taniguchi

Research of Wind Erosion Intensity in the Region of Subotica-Horgos Sands 79
Velizar Velasevic and Ljubomir Letic

Foreword

The Technical Session of the Subject Group on Natural Disasters was held on the afternoon of August 7, 1990 as part of the XIX World Congress of the International Union of Forestry Research Organizations in Montreal, Canada. About 35 scientists representing 10 nations were in attendance. Seventeen papers were presented, addressing the topics of all four Working Parties in the Group. Two papers reported research on torrents, three were about snow, five concerned landslides, and seven discussed watershed management problems. Four of the invited papers can be found in Volume 1 of the Proceedings of Division 1, and two are in this volume. The remainder of this volume includes nine of the contributed papers presented at the technical session plus one that was not orally presented. It is hoped that this volume, together with others supported by the Subject Group in recent years, will foster increased understanding of natural disasters in forested environments.

Raymond M. Rice, Leader
IUFRO Subject Group S1.04
Proceedings Technical Coordinator

Severe Snow Loads on Mountain Afforestation in Japan[1]

Ryuzo Nitta, Yoshio Ozeki, and Shoichi Niwano[2]

Abstract: A simple device for estimating snow settling force on tree branches was used to determine the distribution of snow settling force at various heights in a snowy mountainous region in Japan. A trapezoidal distribution of snow settling force was found to exist at all sites tested. It is thought that a zoning scheme based on the damaging potential of snow on young man-made forests would become possible, with the acquisition of sufficient data.

One of the largest problems in Japanese forestry lies in the low survival rate of young man-made forests in the heavy snow areas. It is rare to see a beautiful conifer plantation where snow reaches over 4 m in depth because of mechanical damage caused by large snow pressure. Both on flat locations and gentle slopes, snow settlement causes branch and stem deformation which often brings fatal breakage. To decrease such unsuccessful plantings much basic data for forest zoning are indispensable. Out of such necessity the authors have devised and set new snow poles in mountains to obtain tree-deforming factors such as maximal snow depth and snow settling force without batteries or power supply. The data from the new snow poles explain to us how severely snow loads work on young trees.

DAMAGES TO CRYPTOMERIA IN SNOW REGIONS

The Forestry and Forest Products Research Institute has a long established snow experiment station at Tokamachi City in Niigata Prefecture, Central Honshu. The Tokamachi Station is encircled by the snowy Naeba Mountains in which the authors have surveyed many conifer plantations of Cryptomeria Japonica D. Don. (Japanese cedar) (Fig. 1). The types of snow damage to Cryptomeria [Iwatsubo and Nitta 1987] are shown in Fig. 2. Straight stems have much higher market value than crooked stems. Therefore in field survey, the authors classify every Cryptomeria tree to

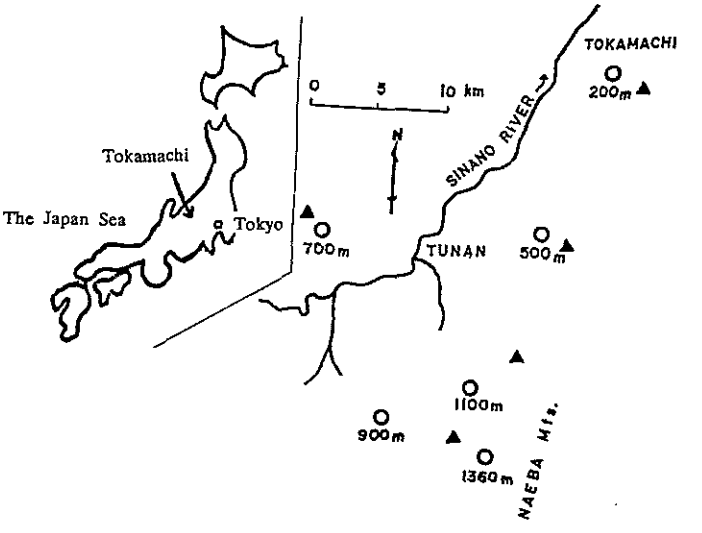

Fig. 1--The sites surveyed.
Circle: Snow settlement recorder
Triangle: Plot of Cryptomeria

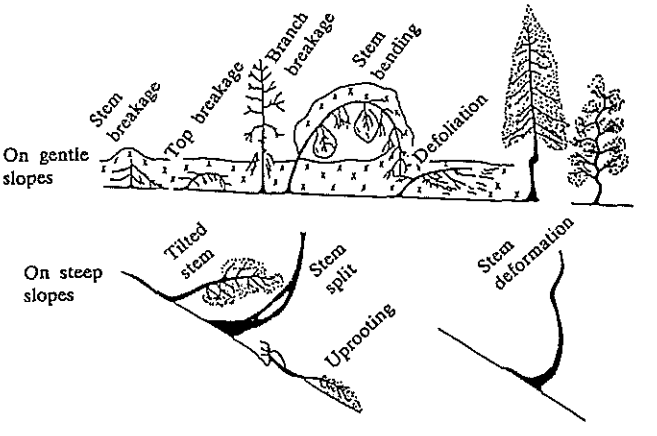

Fig. 2--Damage to Cryptomeria caused by snow loads.

[1]Presented at the Subject Group S1.04 Technical Session on Geomorphic Hazards in Managed Forests, XIX World Forestry Congress, International Union of Forestry Research Organizations, August 5-11, 1990, Montreal, Canada.

[2]Forestry and Forest Products Research Institute, Tsukuba Nohrin, Ibaraki, Japan.

Table 1 Class distribution of Cryptomeria at plots of various altitudes.

Altitude m a.s.l.	Age yr	Share A+B(pct)	Height of B m		Max. snow depth m	Altitude m a.s.l.
300	13	28	7.7	(6)*	3.1	200
620	13	41	4.4	(8)	4.0	500
750	11	39	4.1	(10)	5.2	700
1100	18	5	5.0	(10)	4.7	1100
1250	15	63	4.4	(9)	4.6	1360

*Mean of unsusceptible tree height (meter)

the following four types:

A: Middle and upper stems is straight.
Normal value.

B: Middle and upper stems are crooked, or they have traces of recovery from stem top breakage.
Lower value.

C: Tilted and crooked stem with lower tree height.
No Value.

D: Stem with breakage or large bending, totally suppressed or dead in near future.
No value.

Unless the proportion of trees in classes A and B reaches 50 percent in a surveyed plot (20 m by 20 m) when the tree height reaches twice the mean of maximal snow depth, the planting would end in failure [Shidei 1954].

Table 1 shows the result of plot surveys of Cryptomeria stands on flat sites at several altitudes. The trees at the 1250 m level would receive much more snow damage in the future because their crowns could not project over the snow surface for the next five-year period, though they show a larger share of A + B at the age of 15. In short, all of the man-made forests surveyed would bring no wood market value in the future.

INDICATIONS OF SNOW SETTLEMENT

Lower branches are often bent down due to partial destruction of their bases by heavy snow packing and settling (Fig. 3). The height above ground of the highest bent branches indicates the maximal snow depth. This deformation is being reproduced by an inexpensive recorder for maximal snow depth in Japan. The recorder consists of a pole with horizontal "branches" made of soft metal fixed at every 10 cm height increment [Takahashi K. 1968].

Long term snow settling causes the bending not only of the highest branches,

Fig. 3--Snow damage to a Cryptomeria stand.

but also of the lower branches. If the bent angles of the branches from the horizontal direction show great variety according to above-ground height, the angles would indicate the difference of snow settling power of the layers which catch and deform the branches.

To obtain more information on snow layer settling, 20-cm long galvanized iron wires of regulation quality were fixed horizontally to a 5-m tall pole at every 20-cm height increment. Late each fall, these poles with horizontal wires were set and, after the snow melted, the angles that the wires had been bent down by snow settling were measured (Fig. 4).

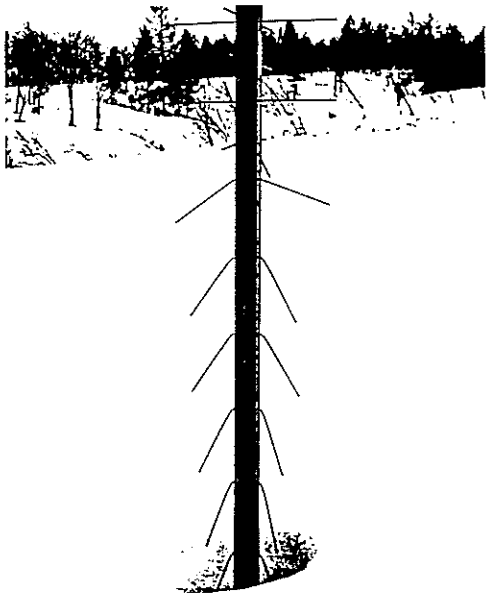

Fig. 4--Snow settling recorder.

Table 2 Average temperature during snow season at Tokamachi Expt. Stn.

Season	Dec	Jan	Feb	Mar	Apr	Mean
1980/81	1.7	-2.2	-1.4	1.8	7.2	1.4
81/82	1.6	-0.3	-1.0	3.0	10.7	2.8
82/83	3.0	-0.2	-0.9	2.3	11.9	3.2
83/84	0.1	-2.4	-2.7	0.3	6.0	0.3
84/85	1.8	-2.1	+0.4	2.7	9.8	2.5
85/86	0.8	-2.1	-2.1	2.7	7.9	1.4

(°C)

The wire was calibrated by loading in the basement of Tokamachi Station where room temperature stays at around 0°C during the whole winter (Tab. 2). Point loads were applied at the free ends of 20-cm long cantilevers for 150 days continuously during winter, and after that the bent down angles were measured (Fig. 5). The calibration curve in relation to wire diameter, angle and point load, shown in Fig.6, provides us a good indication of distribution of snow settling force along the vertical profile of the snowpack.

The data of those angles in winter 1982/83 indicate a feature common to the five profiles, that is, a trapezoidal distribution of the angles (Fig. 7). The wires planted at between +60 cm above ground and -40 cm from the highest snow surface of the season were bent at a large but almost constant angle in each case.

Figure 8 indicates that maximum snow depth at the 1360 m altitude site is about 1 m deeper than that at 500 m altitude and

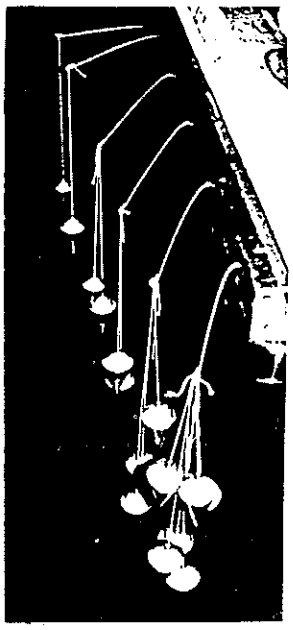

Fig. 5--Calibration of the wires by loading.

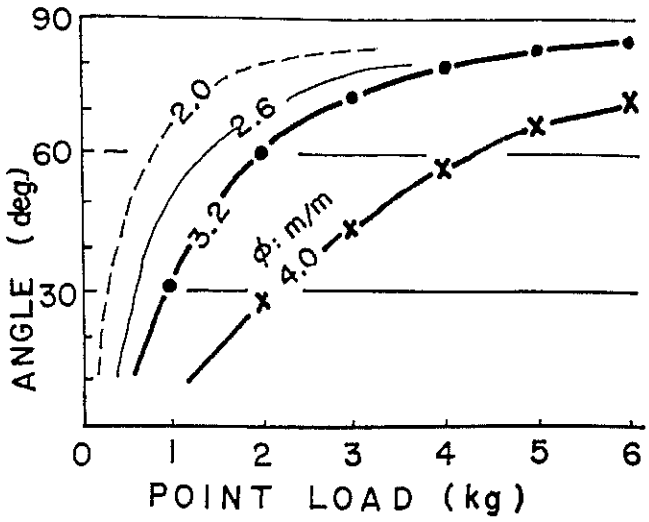

Fig. 6--The calibration curve in relation to wire diameter, bent-down angle and point load (applied at the free end of 20-cm long cantilevers).

that the angle in the middle layers of the former is about 5 degrees greater than that of the latter.

By picking sites where the average bent angle in the middle layers exceeded 60 degrees, and sites where the maximum snow height exceeds 4 m, Table 3 is obtained. It is clear from this table that extremely severe conditions prevail at altitudes over 700 m.

Considering Tables 1 and 3, it is possible to apply a zoning in this region, according to which altitudes of 700 m and over are unsuited to economical forest planning.

Although little data is available at the present, a zoning scheme based on damaging potential should become possible in the future by collecting large amounts of data on damaging potential index with

Table 3 Severity of forestry environment based on max. snow depth and bent angle.

Winter	200	500	700	900	1100	1360
1982/83			A+B	A	ava	A+B
83/84	A	A+B	A+B	A+B	A+B	A+B
84/85			A+B		A	A

A : Angle more than 60 degrees
Diameter of wire: 3.2 mm
B : Max. snow depth more than 4 m
ava: Snow pole lost by avalanches.

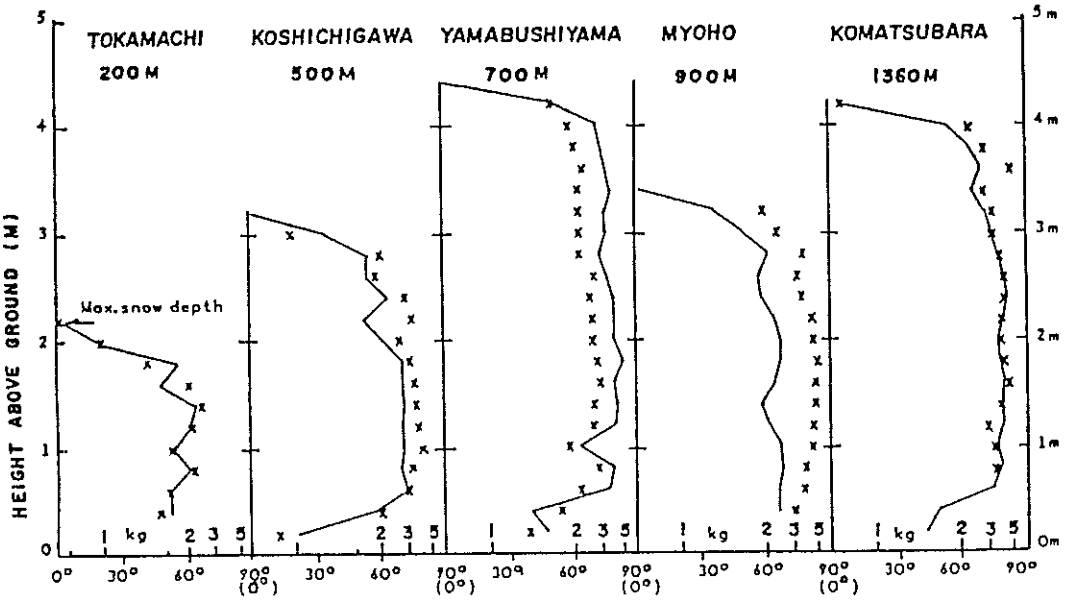

Fig. 7--Distribution of the wire angle along the vertical profile. Data for winter 1982/83 at five altitudes.

Wire diameter: 3.2 mm
x : S-side of snow pole
-- : N-side of snow pole

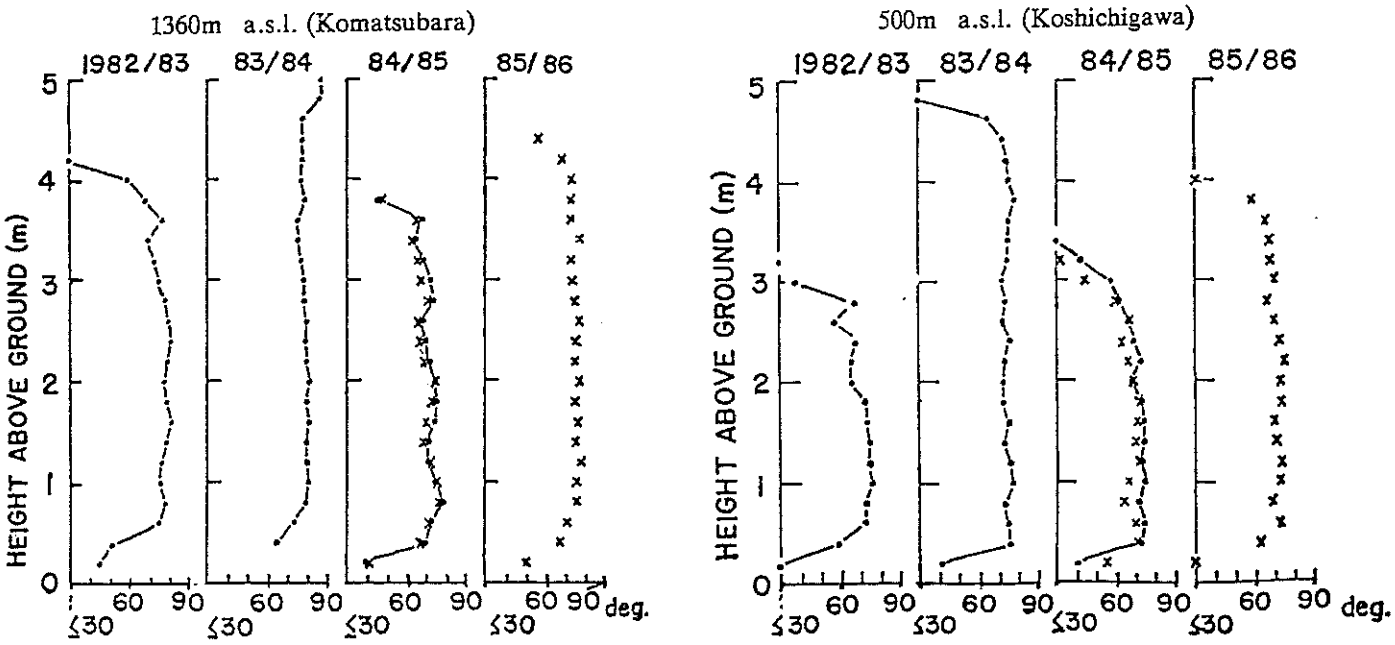

Fig. 8--Distribution of the wire angle along the vertical snow profile. Four season data at the sites on 1360 m and 500 m a.s.l.

Wire diameters:
x x: 4.0 mm
o-o: 3.2 mm

the simplified method stated above. In such belief, data is presently being acquired in several regions in Japan [Takashino and Wakabayashi 1975; Nitta et al. 1982 and 1984].

REFERENCES

Iwatsubo, G. and Nitta, R. 1987. Snow. In [Shidei, T. edited: Forest Protection. 48,Asakura Shoten, Tokyo.]

Nitta, R., Ozeki, Y. and Niwano, S. 1982. Development of simple snow settling recorder. Trans, Jpn. Soc. Snow and Ice. 147.

Nitta, R., Ozeki, Y. and Niwano, S. 1984. Height indicator of branches susceptible to settling snow. Proc. 95th Jpn. For. Soc. 313-314.

Shidei, T. 1954. On the snow damages of forest trees by snow pressure. Res. Bulletin Government Forest Exp. Stn. 73. 1-89.

Takahashi, K. 1968. On the snow scale for measuring maximum snow depth. Seppyo 30. 111-114.

Takashino, K. and Wakabayashi, R. 1975. Wire (branch model) deformation by snow settling. Trans, Jpn. Soc. Snow and Ice. 105.

(All papers written in Japanese)

Priority Setting for Government Investment in Forestry Conservation Schemes—An Example from New Zealand[1]

Colin L. O'Loughlin[2]

Abstract: In New Zealand responsibility for funding flood protection and erosion prevention and control projects rests largely with local regional authorities. However, in 1988 Central Government decided to provide direct funding for a major forestry conservation scheme in the erosion-susceptible East Coast region. Government's investment decision was influenced by a number of factors, the most important being the extent and severity of erosion in the East Coast region and its negative impact on the region's social and economic development.

A large part of New Zealand's wealth depends on pastoral farming. Pastoral land occupies 7.5 million hectares or 28 percent of the country's land surface, much of it steep hill country, and supports about 67 million sheep, 8 million dairy and beef cattle and 1 million deer and goats (New Zealand Department of Statistics 1989). Most of the pastoral land was carved out of indigenous forest between 1840 and 1970. It has been publically acknowledged since the beginning of the present century that high soil erosion rates cause pastoralism to be an unsuitable land use over large tracts of New Zealand's steeplands. Over the last 15 years several studies (Trustrum et al 1983, New Zealand Ministry of Works and Development 1980) have shown that pastoralism on erosion-susceptible hill country is not a sustainable land use. Pastoral farming continues to be a major land use on some of New Zealand's most unstable hill country which, to some, may seem to be an enigma considering New Zealand's international reputation for its technically advanced approaches to conservation and protection of soil and water values. Over the last 5 decades a number of soil conservation schemes have been initiated to stabilise soil on eroding pastoral land.

[1]19th IUFRO World Congress August 5-11 1990, Montreal, Canada.

[2]Assistant Secretary (Research), Ministry of Forestry, Wellington, New Zealand.

It is not the intention of this paper to unravel the reasons why unsuitable pastoral land use practices are widespread in New Zealand but rather the paper will endeavour to examine the way in which conservation schemes on eroding land are initiated and funded and how priorities are set. The role of Central Government will be examined. To this end the paper will concentrate on a forestry conservation scheme known as the East Coast Forestry Project located in the North Eastern part of New Zealand.

In New Zealand, forestry conservation schemes generally involve the blanket planting of eroding land with fast growing exotics, usually Pinus radiata but other species of conifers, Salix or Populus are also often used. Open plantings of poplars are a commonly used soil stabilisation technique in poorly-drained gullies and other localised areas of instability.

POLICIES TO ENCOURAGE EROSION AND FLOOD CONTROL

There exist a number of Government policies that aim to provide protection against or control of erosion and flooding in New Zealand.

(i) *Land use Controls*

There exists legislation known as "the Soil Conservation and Rivers Control Amendment Act 1959" which was again amended in 1988, which provides catchment authorities with the power to control land use to prevent erosion. For instance catchment authorities can require land owners to plant trees on eroding land. However, this legislation is rarely used to enforce tree planting.

(ii) Catchment Grants

The Government contributes to flood protection and erosion control schemes through grants for specific works administered by regional catchment authorities. Nationwide catchment grants have averaged about $90 million per year over the last 20 years. It is planned to replace grants for specific works with a block subsidy system in the near future.

(iii) District Planning Schemes

These schemes can be used under the Town and Country Planning Acts (1954 and 1977) to designate areas of land for particular ultimate land uses (for example forestry). District planning schemes have not been effective in changing land use.

(iv) Disaster Relief

The Government has in the past contributed substantial amounts of money to disaster relief from flooding and siltation. For instance between 1968 and 1981 there were 7 major floods which cost the Government $2.9 billion or $223 million per year. Some of this money has been used for tree planting to stabilise soils and for retiring land from grazing.

(v) Other Subsidies and Grants

In the past the Government provided for encouragement of farm scale forestry and agriculture conservation schemes through a variety of grants and subsidies. However, the present Government has introduced a market-led development strategy for New Zealand which has involved the removal of agricultural and forestry grants and subsidies. This has discouraged private afforestation and other conservation measures by private land holders.

Since 1984 the New Zealand Government has reshaped and reformed local (Regional) Government. The end result has been the amalgamation of more than 600 separate public agencies into 94 new district and regional bodies. New legislation is presently being introduced under the general title "Resource Management Law Reform". Essentially the new legislation will consolidate a large number of existing pieces of legislation covered by a variety of Acts and replace them with a single Resource Management Act. Some of the policies outlined above will probably disappear with the introduction of the new Act which aims to provide Regional Governments (Councils) with greatly increased responsibility for managing natural resources and funding conservation schemes. Central Government is already playing a much reduced role in funding land use projects and conservation/erosion control/flood control schemes compared to the recent past.

EAST COAST FORESTRY PROJECT

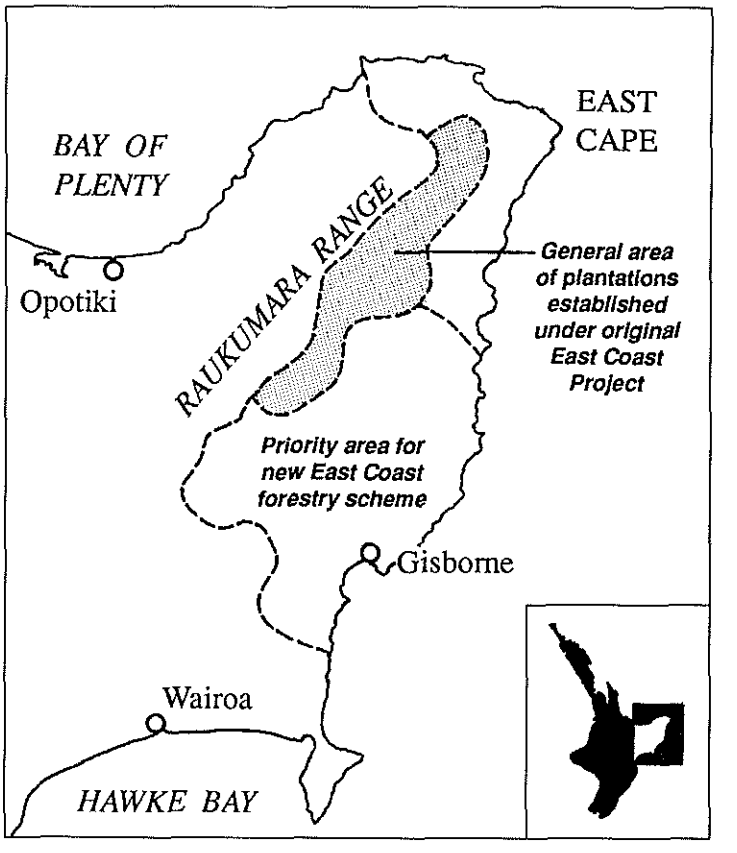

Figure 1: Map showing East Coast region and general area of the East Coast forestry scheme

A major economic appraisal of land use and development options for about 6,500 kilometres^2 of severely eroding pastoral steeplands of the Raukumara Peninsula led to the initiation of a large scale forestry conservation scheme in 1969. The original aim was to plant approximately 1,000 kilometres^2 of fast growing exotics, mainly radiata pine, at a rate of about

2,500 hectares per year. By 1987 when the scheme was halted, 36,100 hectares of dual purpose protection/production forest had been established at a total cost of $229 million. In addition to afforestation a large number of on-farm conservation schemes covering 28,200 hectares of sensitive terrain, had been implemented by 1987. Government contributed 64 percent of the total cost of $14.3 million for these schemes.

The on site benefits of afforestation include substantially reduced earthflow movement rates, cessation of gullying processes and a marked reduction in shallow landsliding (Pearce et al 1987). To date the downstream benefits have not been quantified although in several upper catchment tributaries there are strong indications that a reduction in sediment supply from afforested slopes to stream channels is resulting in stream channel degradation.

Other benefits resulting from the East Coast forestry project are the commercial returns from the production of logs after the forest is 25 years old. Recent projections by the Ministry of Forestry[3] suggest both existing plantings and future plantings are commercially viable in most areas except the areas to the far north and west of the East Coast region. The project also provided social benefits as it helped to prevent rural depopulation and unemployment in this rather isolated and economically depressed region.

EFFECTS OF CYCLONE BOLA AND SUBSEQUENT GOVERNMENT DECISIONS

When a subtropical cyclone, Cyclone Bola, moved across northern New Zealand between 6 and 9 March 1988 the torrential rainfall that fell on the East Coast region caused severe landsliding, erosion, flooding and siltation. Pastoral land was particularly damaged. Some pasture slopes lost 70 percent or more of their grass cover to shallow landslides. However, on hillslopes protected by mature native forest and older pine forests, landslides were less frequent. Damage to farms, forests, horticulture, roads, bridges and houses exceeded $120 million. The Central Government contributed approximately $80 million to the East Coast region as disaster relief to help defray the cost of damages resulting from Cyclone Bola.

[3]Unpublished data, Ministry of Forestry, Wellington, New Zealand.

The impacts of Cyclone Bola extended into the socio-economic area. The East Coast is presently one of the most depressed regions in New Zealand. The region is characterised by a declining total population, falling property prices, a high economic and social dependency on agriculture and forestry which account for 23 percent of the total employment, and a high Maori population which comprises 37 percent of total East Coast population (New Zealand Officials Committee Report 1988). The severe impacts of the cyclone on the agriculture/forestry industries and the inability of the region to cope with the damage from a financial point of view were important factors in subsequent Government decision making. The results of the storm reinforced the fact that the East Coast was New Zealand's most susceptible region to widespread erosion and flooding damage and that erosion and flooding negatively influences the regional economy more than in other parts of New Zealand. The cyclone also highlighted the need for better land use on much of the unstable hill country in the region.

The severe damages caused by the cyclone (the largest of five severe storms to influence the East Coast in 20 years) was a major factor in the setting up of a Government Officials Committee to examine the original East Coast Project and an earlier review of this project. Among other things, the Committee was required to make recommendations to the Government on the future of the project and the Government's involvement in it. In its recommendations the Committee was split between those who recommended no Central Government funding should be provided for restarting the East Coast forestry project and those who strongly recommended that Central Government should intervene and provide additional funding for conservation plantings.

GOVERNMENT DECISIONS

In 1988 Government agreed to provide $8 million to directly subsidise a new East Coast Forestry Conservation Scheme on the East Coast pastoral forelands. The funding was to be spread over a 5 year period; 1989 to 1994; and was aimed at establishing about 3,000 hectares of protection forests per year. The scheme was to be targetted at erosion control on unstable pastoral hill country upstream of Gisborne City, Poverty Bay flats and Tologa Bay where the greatest assets at risk are located. The Government also agreed that the funding would be

provided as a subsidy covering two thirds of the cost of establishment and that the remaining one third of the costs should be met by the region through the East Cape Catchment Board.

The Government also insisted that all protection forests would come under covenants which precluded logging for at least 25 years after planting and then only with the permission of the local catchment authority.

The main factors influencing Central Government to invest in such a scheme included:

- The real extent of severe erosion which is much greater than elsewhere in the country and has substantial negative impacts on the region's social and economic development.

- The need to carry out erosion control quickly and comprehensively to reduce future costs of erosion and flood damage, both to the region and to the Central Government.

- The lack of money and resources within the region for carrying out a comprehensive erosion control scheme.

Under the existing economic environment in New Zealand and the Government's intentions to devolve all responsibility for resource management to regional authorities, it is most unlikely that other regions in New Zealand will qualify for Central Government funding for major forestry conservation schemes in the future.

PROGRESS TO DATE

Despite the generous subsidies available for establishing conservation forests on unstable East Coast hill country, the East Cape Catchment Board who administer the Scheme, have found it difficult to obtain agreement from landowners to provide land for planting. After two planting seasons only about 4,500 hectares have been afforested. Farmers' reluctance to provide erosion prone pastoral land for afforestation stems from several factors:

- Concern that afforestation of sizeable portions of farmland will result in a decline in the stock carrying capacity of farms. The Department of Lands and Survey (1977) concluded that forest planting of poorer grade land within a farm unit generally has little or no impact on stock numbers. However, in the case of a few farm units more than 50 percent of the farm area needed afforestation. Naturally, farmers were reluctant to yield up large parts of their farms for forestry and substantially reduce stock numbers.

- A perception that tree plantations would not yield any return to the land holder in the foreseeable future but rather, would result in additional silvicultural and fencing costs.

- The low profitability of many pastoral farms and low farm incomes which prevents landholders from being attracted by the long term benefits resulting from conservation forestry.

If unstable farmland is not relinquished for conservation forestry at the rate required by the East Coast Forestry Project, then the local regional authorities (the East Cape Catchment Board) may have to enforce afforestation in the priority areas requiring protection. The five year scheme aims at afforesting 15,000 hectares. However, this represents only 20 percent of the total area of severely eroding pastoral hill country in the East Coast region. There is clearly a need for a long term land use rationalisation scheme which will lead to the close integration of exotic and native forests, pastoral farming, horticulture and viticulture. Carefully located forests on the steeper unstable slopes and along riparian areas would provide improved protection to fertile valley bottoms and river plans where horticulture and other types of intensive farming are concentrated. Government Officials and East Cape Catchment Board staff agree that such a scheme would substantially increase farm productivity and reduce the costs of sustaining farming and horticulture on the better classes of land by reducing recurrent storm damage. In addition, recent Ministry of Forestry analyses of the economic viability of exotic forestry on the East Coast indicate that radiata pine forestry on the pastoral forelands has potential internal rates of return exceeding 7 percent[4].

---

[4]Unpublished data, Ministry of Forestry, Wellington, New Zealand.

REFERENCES

Department of Land and Survey (New Zealand) 1977. King Country land use study. Wellington, New Zealand.

Department of Statistics (New Zealand) 1989. New Zealand Official Yearbook 1988-89. 93rd Annual Edition. 884p.

Ministry of Works and Development (New Zealand) 1980. Proceedings of a workshop on the influence of soil slip erosion on hill country pastoral productivity. Aokautere Science Centre Internal Report 21.

Officials Committee Report on East Coast Project Review (1988). A report to the Cabinet Development and Marketing Committee (unpublished), July 1988. 38p.

Pearce, A.J., O'Loughlin, C.L., Jackson, R.J., Zhang, X.B. 1987. Reforestation: on site effects on hydrology and erosion, eastern Raukumara Range, New Zealand. International Association of Hydrological Sciences Publication 167. 489-497.

Effect of Tree Roots on Shallow-Seated Landslides[1]

Kazutoki Abe and Robert R. Ziemer[2]

Abstract: Forest vegetation, especially tree roots, helps stabilize hillslopes by reinforcing soil shear strength. To evaluate the effect of tree roots on slope stability, information about the amount of roots and their strength should be known. A simulation model for the root distribution of Cryptomeria japonica was proposed where the number of roots in each 0.5-cm diameter class can be calculated at arbitrary depths. The pull-out strength of roots was used to analyze the stability of four different types of forested slopes. Root reinforcement is important on slopes where roots can extend into joints and fractures in bedrock or into a weathered transitional layer between the soil and bedrock. Root reinforcement of soil increases quickly after afforestation for about the first 20 years, then remains about constant thereafter.

Sediment disasters by debris flows, mud flows, and landslides occur almost every year during the rainy July to October Typhoon season in Japan. In July 1982, a heavy rainfall of 488 mm in a day, with a maximum intensity of 127.5 mm per hour, caused 4300 debris flows in Nagasaki prefecture, Kyushu Island. This storm destroyed 2200 houses and killed 299 people. During July 1983, intensive rainfall initiated many debris flows and 199 people were killed in Shimane prefecture, along Japan Sea on western Honshu Island.

The cause of so much destruction and death might be unprecedented intensive rainfall. In addition, expansion of cities, resorts, and roads onto hillslopes and mountain areas has been also thought to be a primary cause. In response, national and local governments have adopted a program of aggressively constructing many erosion control works at great expense. But, even so, it is impossible for such construction to protect all mountain hillslopes from debris flows.

An important cause of increased frequency of debris flows is the removal of forests to accommodate urbanization and road construction in mountainous areas. In monsoon areas, like Japan, where steep mountains are covered with forests, mass wasting is the prevailing type of erosion. There is a fragile balance of stability on such steep hillslopes where the forest cover interacts with soil moisture, soil strength, geological condition, historical rainfall, and other factors to stabilize the regolith on a slope. From a viewpoint of soil mechanics, on many hillslopes the factor of safety of a slope (FS) approaches 1.0 during a rainfall event that occurs once every several years. Under conditions of such delicate balance, removal of the trees by logging may result in a reduction in soil strength sufficient to cause landslides.

The influence of forests on slope stability has been one of the most important subjects of study--especially, the role of tree roots on reinforcing soil shear strength. To evaluate the mechanical effect of roots in strengthening soil, however, the quantity and distribution of roots in subsurface soil layers must be quantified.

In this paper, a simulation model for the distribution and stabilizing effect of roots is investigated using an infinite slope stability analysis model.

ROOT DISTRIBUTION

Field Sampling

A stability analysis of forest slopes can be made by adding the soil shear

---

[1]Presented at the Subject Group S1.04 Technical Session on Geomorphic Hazards in Managed Forests, XIX World Congress, International Union of Forestry Research Organizations, August 5-11, 1990, Montreal, Canada.

[2]Research Scientist, Forestry and Forest Products Research Institute, Tsukuba, Ibaraki, 305 Japan; and Principal Research Hydrologist, Pacific Southwest Research Station, Forest Service, United States Department of Agriculture, Arcata, CA. U.S.A. 95521

strength and a reinforcing component provided by the strength of roots (Endo and Tsuruta 1969; Gray and Ohashi 1983). This reinforcing strength is generally shown by equation [1] (Waldron 1977; Wu 1976).

$$Cr = \sum tr_i \ (\sin\theta + \cos\theta * \tan\alpha), \quad [1]$$

where Cr : Reinforcing strength provided by roots
tr_i: Root tensile stress generated in root i at the landslide shear plane
θ : Slope gradient
α : Angle of internal friction of the soil.

The tensile stress for various species has been reported to be a function of root diameter (Ziemer and Swanston 1977; Burroughs and Thomas 1977; O'Loughlin and Ziemer 1982; Abe and Iwamoto 1986). Thus, to model the influence of trees on slope stability, the number and diameter of roots at specific depths must be obtained.

To develop the root model and to understand the influence of different environmental conditions on root distribution, roots of about 16 trees of Cryptomeria japonica, the most popular species planted in Japan, were sampled in five different fields. The sampling was done as follows:

1. The study tree was cut down and its entire root system was carefully excavated.
2. All roots were cut along planes at 10-cm depth intervals below the ground and parallel to the surface (fig. 1).

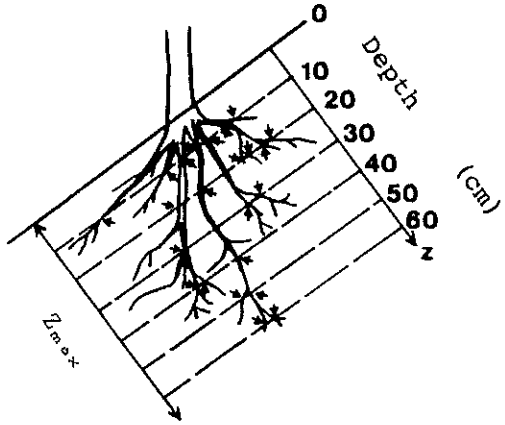

Fig. 1. Method of sampling for root distribution. All roots were cut along planes at 10-cm intervals below the ground surface and diameters of both ends and the lengths of cut roots were measured in each 10-cm thick layer. Z_{max} is a maximum root penetrating depth.
↗ point where diameter is measured.

3. The diameter at both ends and the length of cut roots larger than 0.5 mm in diameter were measured in each 10-cm-thick layer.
4. The number, volume, and total length of roots were then calculated for each layer.

Characteristics of the Root Distribution

Root volume in 10-cm-thick layers (V(z))

About 85 to 90 percent of the total root volume of a tree was found in the upper half of the rooting depth. Root volume decreases exponentially with depth.

To investigate the pattern of root distribution by depth, V(z), the accumulated root volume ratio, F(z), was calculated (eq. [2]).

$$F(z) = \sum_{z=0}^{z} V(z) \ / \ Vr * 100 \quad [2]$$

$$Vr = \sum_{z=0}^{Z_{max}} V(z)$$

where, Vr: entire root volume of one tree
$\sum V(z)$: accumulated root volume from the ground surface to the depth "z"
Z_{max}: maximum depth of root growth.

The relationship between F(z) and depth "z" could be approximated by the probability function of the Weibull-distribution (fig. 2). The solid line in figure 2 is the Weibull probability function, f(z), calculated from equation [3] (Makabe 1966).

$$f(z) = m*(z-1)^{m-1} / \ \alpha*EXP\ [-(z-\gamma)^{m/\alpha}] \quad [3]$$

There are three parameters that must be estimated: α, γ, and m. "γ" is a location parameter that determines a beginning point of the curve. In the root distribution case, "γ" is 0, because the ground surface (z=0) is the initial point. "m" is a shape parameter. It can be read off the Weibull-graph as a gradient of the line, and also calculated by equation [4] with "Z_{max}" and "X0".

$$m = 2.0/(\log Z_{max} - \log X0) \quad [4]$$

X0 is an intersecting point of Fn(z)=0 and the solid line (fig. 2).

From our data, it appeared that if Z_{max} is deeper, the gradient of "m" may be steeper (fig. 2). A regression between Z_{max} and X0 resulted in equation [5].

$$X0 = 0.3522*Z_{max} - 10.799 \quad [5]$$

Substituting equation [5] into equation [4], "m" can be estimated by equation [6].

$$m = 2.0/\{\log Z_{max} - \log(0.3522 * Z_{max} - 10.799)\} \quad [6]$$

"α" is a scale parameter and can be defined as a dependent variable of Z_{max} by equation [7].

$$\alpha = X0^m = (0.3522 * Z_{max} - 10.799)^m \quad [7]$$

Accordingly, the root volume in each 10-cm-thick layer V(z) is obtained by equation [8].

$$V(z) = \{ \int_{z}^{z+10} f(z)\, dz \} * Vr \quad [8]$$

Root Number

In general, the most roots are found 20 to 50 cm deep. The number of roots then gradually decreases with depth. Sixty to 85 percent of the roots are smaller than

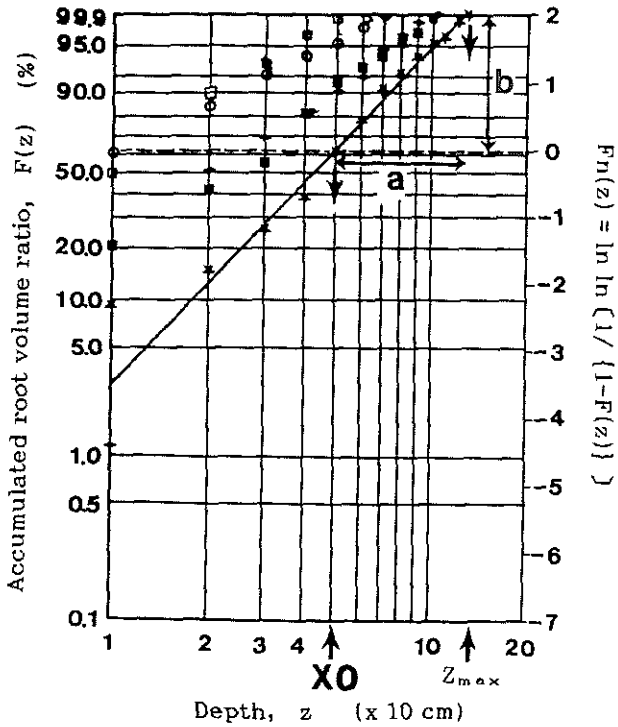

Fig. 2. Relationship between depth (z) and accumulated root volume ratio (F(z)) in the Weibull graph. Weibull coefficient "m" is the gradient of a regression line, obtained by "b/a, "a", and "b".
■ :Tree 1 in Minakami,
○ :Tree 3 in Minakami,
□ :Tree 5 in Komatubara,
◆ :Tree 9 in Misugi,
✶ :Tree 10 in Ksukuba.

Table 1--Root number ratios (Y(i)) in fou field sites

Site	Top zone	Middle zone	Bottom zo
Minakami	$7.91\ i^{-1.47}$	$4.91\ i^{-2.11}$	$5.95\ i^{-1.}$
Komatsubara	$6.01\ i^{-1.76}$	$2.97\ i^{-2.34}$	$0.62\ i^{-3.}$
Misugi	$3.29\ i^{-2.03}$	$1.98\ i^{-2.65}$	$1.13\ i^{-3.}$
Tsukuba	$6.43\ i^{-1.53}$	$4.73\ i^{-1.86}$	$6.04\ i^{-1.}$

0.5 cm in diameter.

To compare root distribution between each field site, the total rooting depth was divided into three zones: top, middle, and bottom. In the top zone, there are many lateral roots that vary widely in diameter. In the bottom zone, most roots grow vertically and there are few roots greater than 1.0 cm in diameter. In the middle zone, many roots develop vertically and diagonally, but there are few lateral roots. Even though the depth zones do not coincide with soil horizons and the thickness of the zones varies between sites, each respective depth zone has similar root distributions. Root distribution was estimated as the root number ratio, obtained by regression between the proportion of the number of roots in each 0.5-cm diameter class, Y(i), and the diameter class, i (table 1).

Mean volume of a root in each diameter class (Vm(i))

There was no difference in the mean volume of a root in each diameter class, Vm(i), among the three depth zones. Consequently, regressions were calculated for each field site (table 2).

Maximum root depth (Z_{max})

It is important to note the depth of root penetration when estimating the effect of roots in stabilizing slopes. The more roots that penetrate a potential shear plane, the greater is the chance that vegetation will increase slope stability. Some of the factors restricting Z_{max} are existence of bedrock, soil porosity, soil moisture, soil structure, soil consistency, and soil fertility. Morimoto (1982) and Ikemoto and Takeshita (1987) reported that Z_{max} could be estimated as the depth where the soil hardness, using a cone penetrometer, is 27 mm, or the N value (number of falls per 10-cm penetration) in the sounding test is 5. However, much more data on this subject is needed.

Table 2--Mean root volume, Vm(i), of the four field sites

Site	Mean root volume Vm(i)	Coefficient of determination	Sample number
Minakami	$7.62\ i^{2.12}$	0.96	51
Komatsubara	$7.84\ i^{2.32}$	0.94	24
Misugi	$6.87\ i^{2.29}$	0.96	59
Tsukuba	$7.81\ i^{2.14}$	0.97	53

MODEL

Figure 3 is a flow chart of the root distribution simulation model. The input factors are field measurements of height (H), diameter (DBH), and Z_{max} of the object tree. The model output is the number of roots in each 10-cm layer and each root diameter class. Yt(i), Ym(i), Yb(i), and Vm(i) are used in the model as variables, so they must be measured for each region having different environmental conditions.

The model was composed as follows:

(1) Input DBH, H, and Z_{max}.

(2) Calculate whole root weight, Wr, in g.
Wr can be calculated by an allometric formula, equation [9] (Karizumi 1977).

$$\log Wr = 0.8216*\log(DBH^2*H)-0.3085 \quad [9]$$

(number of trees = 79; corr. coef. = 0.99).

(3) Calculate whole root volume, Vr, in cm^3.

$$Vr = Wr/Gs \quad [10]$$

(4) Calculate root volume in each 10-cm layer, V(z).
V(z) can be calculated by equation [8], where f(z) is obtained from equation [3] by substituting Z_{max} into equations

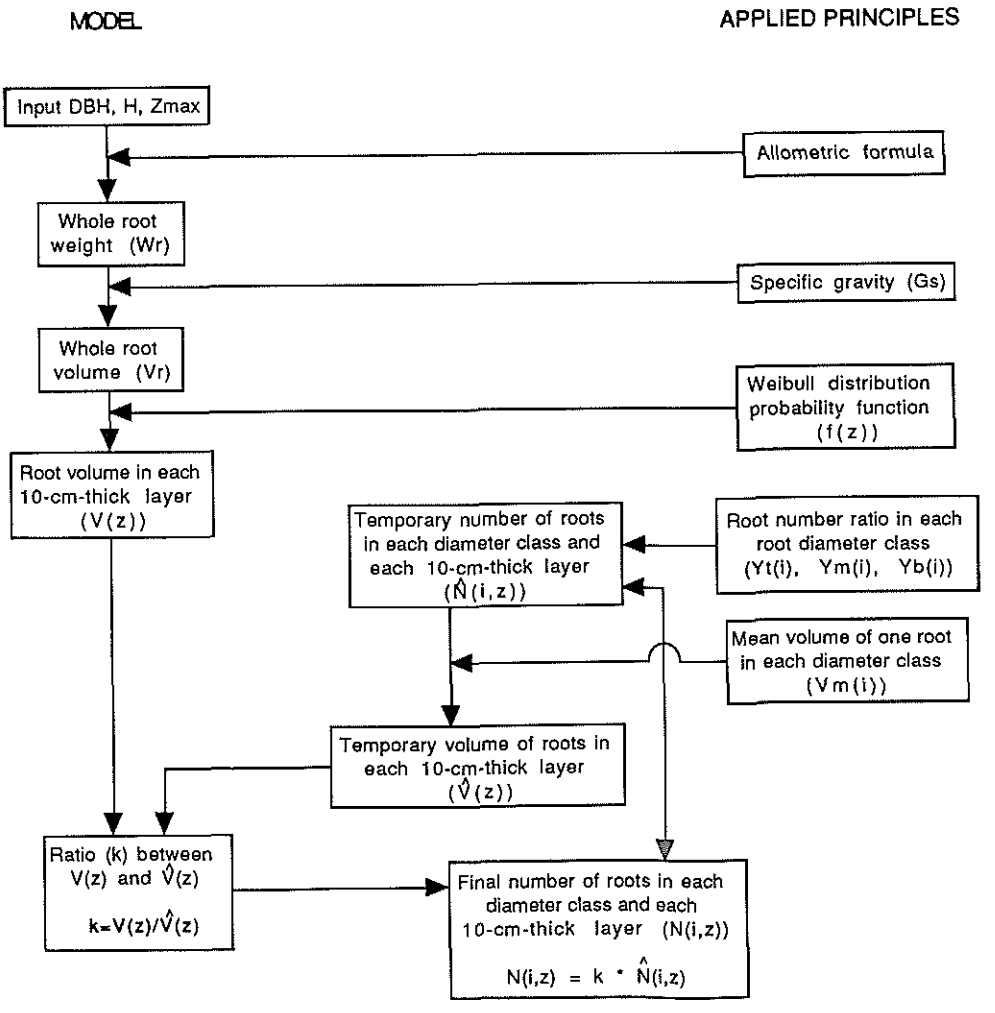

Fig. 3. Flow chart of the root distribution simulation model.

[6] and [7].

(5) Set up the temporary root number in each diameter class and each 10-cm-thick soil layer, $\hat{N}(i,z)$.

The maximum root diameter (i_{max}) should be determined, and $\hat{N}(i,z)$ in each diameter class (0.5-cm intervals in this paper) up to i_{max} in each zone is set up in proportion to the root number ratios Yt(i), Ym(i), and Yb(i). All 10-cm layers that belong to one zone have the same initial value of $\hat{N}(i,z)$.

(6) Calculate temporary root volume in 10-cm layer, $\hat{V}(z)$.

$$\hat{V}(z) = S\ \{\hat{N}(i,z) * Vm(i)\} \qquad [11]$$

(7) Calculate the ratio between V(z) and $\hat{V}(z)$, k.

$$k = V(z)/\hat{V}(z) \qquad [12]$$

(8) Determine the number of roots in each root diameter class and each 10-cm layer, N(i,z).

$$N(i,z) = k * \hat{N}(i,z) \qquad [13]$$

Even fine roots have a strong influence in preventing landslides (Burroughs and Thomas 1977; Abe and Iwamoto 1986). Thus, the model must be able to estimate the number of such fine roots. Also, the landslide shear plane has a tendency to occur near the limit of rooting depth where there are few roots on the shear plane (Abe and others 1985). This model can estimate the number of roots in each diameter class in the deeper layers. Furthermore, it is important that root distribution under different conditions can be expressed by one model.

ROOT STRENGTH

The contribution of roots to increasing soil shear strength has been mainly estimated by four kinds of experiments: tensile test, pull-out test, in-situ shear test, and laboratory shear test.

Many tensile strength tests of roots have been performed. A segment of a root specimen is usually loaded in tension and the maximum value at failure is measured (O'Loughlin 1974; Burroughs and Thomas 1977; Ziemer and Swanston 1977; Nakane and others 1983; Abe and others 1986). From these tests, the tensile strength of live roots and its decline after the roots die have been measured for many of the important tree species.

The pull-out test measures the maximum resistance when a root is pulled out of the soil (fig. 4). Tsukamoto (1987) and Abe and Iwamoto (1986) reported pull-out strength could be predicted by root diameter and was independent of slope conditions and root type, such as lateral, tap, or sinker root. Pull-out strength was composed of tangential friction between soil and roots, and was influenced by root bending, branching, root hairs, and the tensile strength at breakages.

Data from in-situ shear tests (Endo and Tsuruta 1969; Ziemer 1981; O'Loughlin and others 1982; Abe and Iwamoto 1987) are important for evaluating the appropriateness of theoretical concepts. But, it is difficult to perform such tests on steep rocky hillslopes.

Laboratory shear tests have been performed to reveal the mechanism of the root reinforcing effect (Waldron 1977; Wu 1976; Waldron and Dakessian 1981; Gray and Ohashi 1983; Shewbridge 1985). We conducted direct shear tests using sand that contained roots and modified the reinforcement model proposed by Waldron (1977) and Wu (1976):

$$\Delta S=[\{(1+B^2b^2e^{-2bx})^{1/2}-1\} * E*a_r]\ (\cos\theta \tan\phi + \sin\theta) + E*I*b^3*B \qquad [14]$$

where, E: Young modulus
a_r: cross sectional area of the roots
B: one half of a shear displacement
I: modulus of section
θ: root angle at the origin
ϕ: internal friction angle of sand.

From observations of shallow landslide sites, there were only a few fine roots on the bottom shear planes (Abe and others 1985). And, for fallen trees, most of the roots were broken near their tips where the

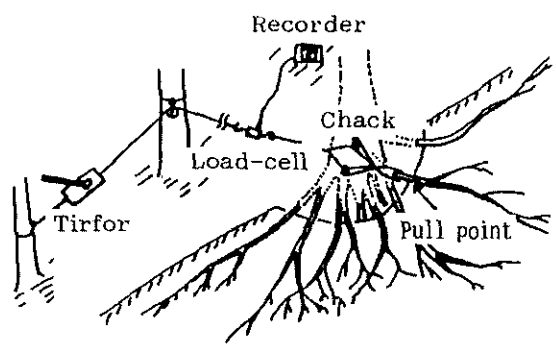

Fig. 4. Diagram of the root pull-out test.

diameter was less than 1 to 2 cm. This suggests that most roots were pulled out. Burroughs and Thomas (1977) reported that the width of the shear zone ranged from 7 to 25 cm and the majority of tree roots had failed in tension. Studies of slope failure in soil over glacial till in Alaska indicated that the expected width of the soil shear zone ranged from 7.5 to 30 cm, and that the expected mode of root failure is in tension (Wu, 1976). We assume that the roots crossing a shear zone generate tensile strength, are elongated in tension, and break at the tips, not in the shear zone. Thus, the mode of root failure is similar to that during a pull-out test. Abe and Iwamoto (1986) conducted tests on Cryptomeria japonica and measured both the pull-out resistance and the tensile strength at the point of breakage (fig. 4). The results were quite different. The pull-out resistance includes the tensile strength at breakage, plus the tangential friction between roots and soil and the mechanical strength caused by pulling bent parts of the root through the soil. Consequently, it is not appropriate to use the maximum tensile strength to represent root reinforcing strength. Although the relationship between pull-out resistance and the theoretical reinforced soil strength is not fully understood, we postulate that both are about equal.

Stability of a forested slope was simulated using the pull-out resistance (PO), obtained by a regression analysis (eq. [15]) of the root diameter (D) at pull points (fig. 4).

$$PO = 126.39D^{1.03}, \quad \text{(kgf)} \quad [15]$$

SLOPE STABILITY ANALYSIS

Slope classification

Geology, soil mechanics, and soil moisture affect slope stability and also affect the distribution of tree roots, especially tap roots. Tsukamoto (1987) classified slopes into four types.

A type--Regolith is thin and underlain by bedrock with few cracks and joints. The roots cannot penetrate the bedrock and are densely distributed in the regolith. Tap roots are not important. Soil water cannot permeate the bedrock, and pore water pressure is easily generated on the bedrock surface. Thus, this type of slope is rather unstable and mostly found on dipping slopes in tertiary parent materials.

B type--Regolith is thin and underlain by bedrock having many joints and cracks. Roots are able to penetrate into bedrock and contribute to stability. Pore water pressure is seldom generated because of high permeability. Accordingly, this type of slope is quite stable and is found in areas with mesozoic and paleozoic parent material.

C type--Regolith is thin and there is a transitional (weathered) layer between the regolith and bedrock. Root growth may be affected by soil density and hardness of this transitional layer. Soil moisture does not easily permeate the transitional layer, because of its high density, and pore water pressure is easily generated. Roots are most effective on this type of slope. As root strength declines after logging, many debris flows would be expected. This type is frequently found in granite mountains.

D type--Regolith is thick and roots can grow without restriction by soil layers. This type of slope is usually found at the base of hillslopes and have a gentle angle. Debris flows never occur on this type of slope.

Stability analysis

The stability of these four types of slope was investigated by assuming reasonable values of important soil and slope characteristics (table 3).

The A-type slope has 80 cm of regolith thickness underlain by bedrock without cracks and the roots can not penetrate more than 80 cm deep. The B-type slope also has 80 cm of regolith, but bedrock is fractured and roots can invade the cracks up to 100 cm deep. The C-type slope also has 80 cm of regolith, plus a 40-cm-thick transitional layer underlain by bedrock. The D-type slope has 150 cm of regolith and a 40-cm-thick transitional layer underlain by bedrock. The stability calculations assumed that the ground water reached the ground surface. Forests of Cryptomeria japonica aged 10, 20, 30, and 40 years were assumed to be growing on each slope. The

Table 3--Characteristics of the four slopes

	Slope type			
	A	B	C	D
Slope angle(°)	32	32	32	15
Thickness of regolith (cm)	80	80	80	150
Transitional zone (cm)	0	0	40	40
Cohesion of soil(ton/m^2)	0.2	0.2	0.2	0.2
Internal angle of soil(°)	30	30	30	30
Cohesion of bedrock(ton/m^2)	20	20	20	20
Internal angle of bedrock(°)	40	40	40	40
Ground water table depth (cm)	0	0	0	0
Density of soil (g/cc)	1.3	1.3	1.3	1.3
Density of bedrock (g/cc)	2.5	2.5	2.5	2.5
Z_{max} (cm)	80	100	100	170

size of trees in each forest was obtained from yield tables. Root distributions (number of roots in each 10-cm-thick soil layer for each 0.5-cm diameter class) were simulated using the model (fig. 3). The reinforcing strength (ΔS) in each 10-cm-thick layer was calculated using equation [16].

$$\Delta S(z) = \sum_{i=1}^{m} N(z,i) * PO(i) \qquad [16]$$

where, ΔS(z): reinforcing strength at depth z cm
N(z,i): number of roots of diameter i cm at depth z cm
PO(i): pull-out strength of a root with diameter i cm.

The simulation results of the four slope types are shown in figure 5. Soil shear strength, Ss, shows an abrupt increase at the boundary between soil and bedrock of the A-type and B-type slopes, but on the C-type slope that has a transitional soil layer, soil shear strength gradually increases. Shear stress, Ps, exceeds the soil shear strength at a depth of 40 to 80 cm on type A, B, and C slopes. This indicates a potential shear zone at these depths leading to the possibility of a landslide. The reinforcing strength by roots (ΔS) was calculated by equation [16] and added to Ss (fig. 5).

On the A-type slope, the growth of tap roots is restricted by the bedrock so there is no reinforcing effect at the boundary (potential shear zone). ΔS is increased by the growing forest only to a depth of 70 cm. In other words, although the number of roots is increased as the forest becomes older, root reinforcement of the soil never develops at the boundary and Ps will exceed Ss at this depth when the ground water surface rises. This condition can lead to a debris flow.

On the B-type slope, however, roots penetrate the cracks in the bedrock, and root reinforcement develops at the soil-bedrock boundary. When the forest is older

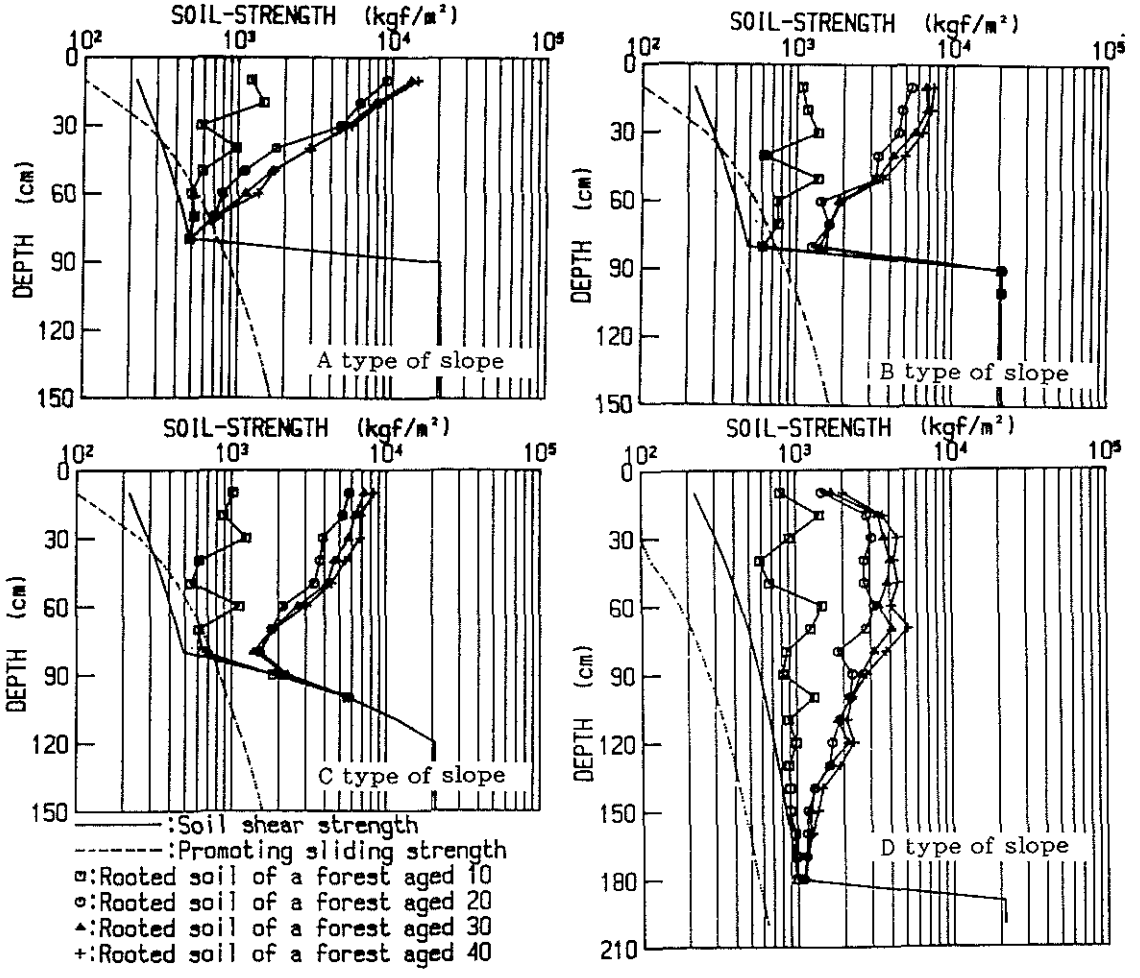

Fig. 5. Simulated rooted soil shear strength of forests having four different ages on A, B, C, and D type of slopes

than 20 years, ΔS becomes stronger than Ss, and Ps never exceeds shear strength of the rooted soil, Sr (fig. 5). But, for the 10-year-old forest, ΔS is not strong enough to prevent a debris flow on the slope.

The C-type slope is similar to the B-type. Roots invade and reinforce the transitional zone, and the probability of landslides decreases as the forest becomes older.

The D-type slope is always stable with or without a forest.

The factor of safety (FS) at the potential shear zone increases for type B and C slopes as the age of a forest increases, up to an age of 20 to 25 years, after which it remains about constant at about 2.0 (fig. 6). For these slope types, the FS of 10-year-old forests is under 1.0, indicating a high probability of landslides. The FS values were calculated for a condition where the ground water reaches the ground surface. For A-type slopes, FS does not change with increasing forest age because roots cannot reinforce the soil and bedrock interface. Type-D slopes remain stable at all ages of forest.

DISCUSSION

As forests grow, root systems develop to provide structural support to the trees and to absorb water and nutrients. Roots are important in stabilizing hillslopes. To quantify the amount of root reinforcement (ΔS), it is necessary to understand the relationship between root growth, slope structure, and depth of sliding surface. In this paper, root reinforcement was modelled for four types of slopes. Previous research has shown that there are high slope failure rates on granite, shattered paleozoic and mesozoic, and tertiary slopes associated with young forests (Tsukamoto 1987). It is expected that there are differences in ΔS related to differences in geologically related slope structure. Thus, it is important to identify those factors that restrict the growth of roots and to quantify the number and size of roots that can penetrate into joints of bedrock or transitional soil layers and reinforce the potential shear zone.

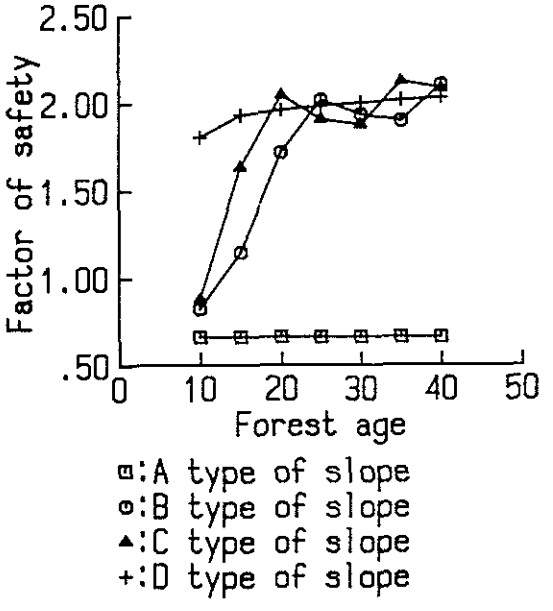

Fig. 6. Change in the factor of safety as the forest ages.

Logging can cause a large decrease in ΔS. As the roots decay, after a 40-year-old forest has been cut, the shear resistance of rooted soil in the potential shear zone will decrease to one third of that in the uncut forest (fig. 5), and the probability of slope failure will increase. Kitamura and Namba (1981) noted that the resistance of tree stumps to uprooting decreases rapidly as the root systems decay following timber harvest. They concluded, when considering the combined effect of root decay of the cut trees and root growth of the planted trees, that the forest soil would reach a minimum strength between 5 and 10 years after cutting and replanting. Ziemer and Swanston (1977) measured the changes in strength of roots remaining in the soil after logging and noted that even the largest roots lost appreciable strength.

In general, the influence of forest logging on debris flows are greatest in granitic and tertiary slopes (C-type). Paleozoic and mesozoic slopes (B-type) generally do not have an increased incidence of debris flow after forest removal. Tsukamoto (1987) explained that the reason for this is that the high permeability of the fractured bedrock prevents the build-up of lateral groundwater flow along the bedrock. Ohta (1986) suggested that roughness of the bedrock also makes this type of slope stable.

ΔS tends to increase as the forest becomes older, up to an age of about 20 years, after which ΔS remains about constant. The contribution of a single tree to ΔS continues to increase as the tree becomes older. However, the number of trees in the forest decreases with forest age (table 4) and the net effect is a constant ΔS after about 20 years. Forty-year-old stands of Cryptomeria japonica

Table 4--Sizes of Cryptomeria japonica

	Tree age (yr)			
	10	20	30	40
DBH (cm)	5.0	13.8	20.0	24.3
Height (m)	5.4	12.1	15.8	18.1
Number (ha^{-1})	3430	2265	1345	1030
Area (m^2)	2.9	4.4	7.4	9.7

have a high density--one tree per 3.1 x 3.1 m. For this stand density, it is acceptable to estimate ΔS on a unit area basis. However, for old-growth and scattered trees, it may not be proper to estimate the reinforced strength by unit area, because tap roots tend to concentrate below the widely-spaced tree trunks.

Most roots in the potential shear zone are less than 1.0 cm in diameter. In this paper, only the effect of roots within the shear zone were considered. However, soil reinforcement by lateral roots should also be considered. Burroughs and Thomas (1977) reported that zones of weakness developed between stumps that could lead to the initiation of slope failure.

CONCLUSIONS

Using a model of tree root distribution and the pull-out strength of roots to estimate the effect of roots upon slope stability, we conclude that:

(1) Root reinforcement could be expected on slopes where roots grow into joints of bedrock or weathered transitional layers. DS in a potential shear zone on such slopes had twice the shear strength of soil without roots.
(2) Most roots directly affecting slope stability are about 1.0 cm or less in diameter.
(3) After afforestation, DS would increase quickly for about 20 years, then remain nearly constant.

REFERENCES

Abe, K.; Iwamoto, M.; Yoshino, S.; Ishigaki, I.; Tarumi, H. 1985. Tree-root distribution on a landslide surface. Tran. 96th. Ann. Mtg. Jpn. For. Soc.: 639-642.

Abe, K.; Iwamoto, M. 1986. An evaluation of tree-root effect on slope stability by tree-root strength. J. Jpn. For. Soc. 68: 505-510.

Abe, K.; Iwamoto, M.; Sammori, T. 1986. Strength of binding soil by tree root. Trans. 38th. Ann. Mtg. Kanto Jpn. For. Soc.: 217-220.

Abe, K.; Iwamoto, M. 1987. Soil mechanical role of tree roots in preventing landslides. Proc. 5th International Conference and Field Workshop on Landslides; 1987; Christchurch, NZ; 1-9.

Burroughs, E. J. Jr.; Thomas, B. R. 1977. Declining root strength in Douglas-fir after felling as a factor in slope stability. Research Paper INT-190. Ogden, UT: U.S. Department of Agriculture, Forest Service. 27 p.

Endo, T.; Tsuruta, T. 1969. The effect of the tree's root upon the shear strength of soil. 68 Ann. Rep. Hokkaido Br., For. Experiment Station: 167-182.

Gray, D. H.; Ohashi, H. 1983. Mechanics of fiber reinforcements in sand. J. Geotech. Div. ASCE 108(GT3): 335-353.

Ikemoto, W.; Takeshita, K. 1987. Effect of tree root on slopes stability. Trans. of Sabo Research Presentation Meeting: 262-265.

Karizumi, N. 1977. Root biomass. JIBPO Synthesis (Shidei, T.; Kira, T., ed.). University of Tokyo Press, Tokyo. 16: 45-52.

Kitamura, Y.; Namba, S. 1981. The function of tree roots upon landslide prevention presumed through the uprooting test. Bull. of For. and For. Prod. Res. Inst. 313: 175-208.

Makabe, H. 1966. Usage of Weibull probability graph. Nippon Kikaku Kyoukai. 81 p.

Morimoto, Y. 1982. Syamen Ryokka Kashima Syuppankai, Tokyo: 94-120.

Nakane, K.; Nakagawa, K.; Takahashi, F. 1983. Change in tensile strength of Japanese red pine roots after death by fire. J. Jpn. For. Soc. 65: 155-165.

Ohta, T. 1986. Forest effect on prevention of sediment disaster. Report of Forest Management Research Meeting. 298: 17-26.

O'Loughlin, C. L. 1974. A study of tree root strength deterioration following clearfelling. Canadian J. of For. Research 4(1): 107-113.

O'Loughlin, C. L.; Rowe, L. K.; Pearce, A. J. 1982. Exceptional storm influences on slope erosion and sediment yields in small forest catchments, north Westland, New Zealand. Proc. of National Symposium of For. Hydrology, Melbourne, Australia.

O'Loughlin, C. L.; Ziemer, R. R. 1982. Importance of root strength and deterioration rates upon edaphic stability of steepland forests. Proceedings of IUFRO Workshop P.1.07-00 Ecology of Subalpine Ecosystems as a Key to Management. 1982 August 2-3, Corvallis, OR. Corvallis, OR: Oregon State University; 70-78.

Shewbridge, S. 1985. The influence of reinforcement properties on the strength and deformation characteristics of a reinforced sand. Berkeley, CA: University of California; Dissertation

Tsukamoto, Y. 1987. Evaluation of the effect of tree roots on slope stability. Bull. of the Experiment Forests. Tokyo Univ. of Agric. and Technol. No. 23: 65-124.

Waldron, L. J. 1977. The shear resistance of root-permeated homogeneous and stratified soil. Soil Science Soc. of America J. 41: 843-849.

Waldron, L. J.; Dakessian, S. 1981. Soil reinforcement by root: calculation of increased soil shear resistance from root properties. Soil Science 136(6): 427-435.

Wu, T. H. 1976. Investigations of landslides on Prince of Wales Island, Alaska. Geotech. Eng. Rep. 5, Columbus, OH: Dept. Civ. Eng., Ohio State Univ. 94 p.

Ziemer, R. R. 1981. Roots and the stability of forested slopes. In: Davies, T. R. H.; Pearce, A. J., eds. Erosion and Sediment Transport in Pacific Rim Steeplands; 1981 January; Christchurch, NZ. IAHS/AISH Publ. No.132 Wallingford, UK: International Association of Hydrological Sciences; 343-361.

Ziemer, R. R.; Swanston, D. N. 1977. Root strength changes after logging in southeast Alaska. Research Note PNW-306. Portland, OR: U.S. Department of Agriculture, Forest Service. 10 p.

Watershed Concerns and Recent Policy Formulations in Sri Lanka and Australia[1]

Rohan Ekanayake[2]

Abstract: Addressing the problems associated with watersheds in both countries is the aim of this paper as well as assessing the respective watershed policies. Attention has been drawn to specific economic, environmental and sociocultural considerations in the recent past. An interesting feature of the most recent policy developments is the tendency to follow a balanced approach to water resource development in either situation. In Australia, it is envisaged to follow a co-ordinated and sustainable use and management of land water, and vegetation resources on a water catchment basis. In Sri Lanka however, after a prolonged lull in policy approaches it is only beginning to prepare the framework towards a bearable watershed resource.

While accommodating a similar population to Australia, Sri Lanka in its tiny 270 miles stretch, has its people clustered on the moist southwestern third of the island known as the 'wet zone'. In Australia, where the main concentration is in the eastern part of the continent, there is heavy reliance on catchments of the Great Dividing Range and the associated run-off for agriculture and hydro electricity. In Sri Lanka, the catchments for nearly all its major rivers rest in the central highlands where most of its hydro electricity is generated and water diverted for downstream purposes. Compared to Australia, Sri Lanka receives a relatively higher rainfall mainly from the monsoonal rains.

WATERSHED MANAGEMENT

Sri Lanka

Irrigation structures in the dry zone of Sri Lanka has a history of 2000 years, and thus, its first water management practices can be related to that time. However, in modern Sri Lanka, soil erosion and watershed problems were first recognised and addressed in the legislature in the early 1940's. But policy formulation did not take place till recent times before a major river basin development programme was initiated surrounding the Mahaweli river. Largely, towards the sustenance of this programme, it was inevitable some policy be introduced to manage the natural resources surrounding its catchments. This materialized only in the late 1989 when an interim report on watershed management was considered by policy makers in Sri Lanka.

Australia

The relevant legislation were first introduced in Australia in 1915, and its maiden water resource assessment programme began in 1963. Australia's main water management programme involves the Murray-Darling river basin that spreads over four of its major states.

More recently, a Bill was tabled in the New South Wales Legislature to implement total catchment management of the State's natural resources, namely, the co-ordinated and sustainable use and management of land, water, and vegetation resources on a catchment basis. Such policy developments followed the recent Federal concerns over a balanced approach to natural resources management in Australia.

---

[1] Presented at the Subject Group S1.04 Technical Session on Geomorphic Hazards on Managed Forests, XIX World Congress International Union of Forestry Research Organisations, August 5-11, 1990, Montreal, Canada.

[2] Research Economist, Water and Land Resources Division, Department of Primary Industries and Energy, and formerly Research School of Social Sciences, Australian National University, Canberra.

CONCERNS

While deforestation in the catchment vegetation is common in both countries and excessive pressure on water resources, is there genuine concern in Sri Lanka and in Australia to ameliorate the situation and achieve a *balance*? The extent of tree clearing in Australia in the main catchment (Great Dividing Range) of the Murray-Darling Basin along the eastern coast is shown in the map. Sri Lanka, having carried out its last partial forest inventory in 1956, faces similar excessive deforestation in the main catchment of the Mahaweli and it is estimated that its forest cover has dwindled from 56 percent in 1956 to a mere 15 percent in the present times.

Extent of Tree Clearing in Australia Since European Settlement

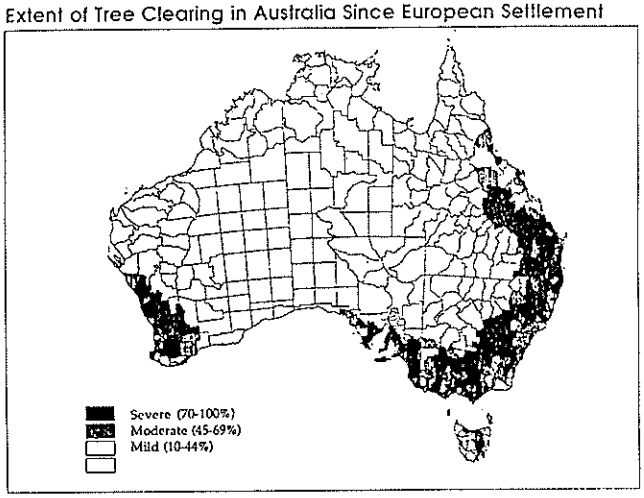

In both situations, environmental flow management and flood mitigation remain unresolved policy issues mainly because of lack of information and the associated social and economic factors. It is in the same interest that it has become apparent those issues be addressed in a coherent policy frame for broad inter-temporal reasons. The *sustainable* frame still remains the same- the Trinity of Soil, Trees and Water (diagram 1).

Trees and Soil Conservation

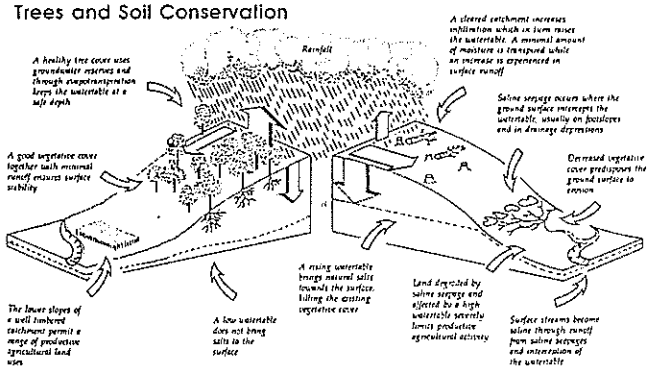

FOCUS

In this paper, an assessment of the watershed policies of both countries has been carried out drawing attention to specific economic, environmental and sociocultural considerations in the recent past.

INSTITUTIONS and policy

Government policy intervention is two-pronged in watershed concerns. Direct and indirect. Direct policies are often regulating measures that affect a watershed.

Indirect policies converge on the integrated land-uses in an overall watershed region. Usually these measures do not fall within the scope of a particular policy consideration. It would be fair to say that in effect, indirect policy once applied has indirect effects on the watershed. These indirect effects are then moulded into explicit policy in the next application.

Indirect Policy

(a typical theoretical explanation of an effect on a watershed)

introduction……price subsidy for agricultural production

intensive and extensive land use……effects from the vegetation cover reduction

increased soil erosion……increased sedimentation

reservoir water levels diminishing…… power cuts, oil imports to fuel extra turbines

overall…economic, resource and environmental effects on society

The political economy within which policies are formed, reshaped and applied is articulated uniquely according to the specific spatial condition in Sri Lanka and Australia.

In Sri Lanka, it is more centrally controlled and regionally applied. In Australia however, it is more regionally controlled and regionally applied. For instance, the role of the Central Government in institutional matters in Sri Lanka is authoritative in nature, whereas in Australia the role of the Federal Government in water affairs is more oriented towards a pro-active participation.

In managed and unmanaged water and watershed affairs, Sri Lanka's centrally dominated and directed policy is essentially a line functional system (not necessarily though they are efficient). In Australia, several regional (States) governments have different policy approaches, institutional structures in place, and legal frameworks in watershed settings (not necessarily though they are inefficient).

Consider the two-nation's main watershed regions. The focus is on the more naturally important as well as socially desired productive regions (i.e. Basins).

These Basins serve as their respective economic and ecological nerves where most social transformations occur, valuable currency exchange earned, more importantly food produced, the people productively employed and scarce and bearable water managed.

The recent phenomenon is not so much an optimistic and problem solving water front to both countries, but consist of overwhelming problem solving horizons. It is infact inheritance in both situations. The greatest tasks that both countries have aspired are the challenges faced with the accentuated environmental consequences from the continued resource degradation.

At cross roads are the favourite concepts for policy manipulation in flood mitigation, energy sustenance, water quality maintenance, total approach to balanced resource use and of course sustainability.

Despite the optimism, this brings us to a third set of policy application. Natural Resources Management Strategy (NRMS) for overall resource planning and management for a Basin wide system. The initiatives are (following the maps);

Sri Lanka- Mahaweli Accelerated Program

Australia- Murray-Darling Basin
Natural Resources Management
Strategy and Program.

Developments

Sri Lanka:

Optimum conservation of catchments is in pursuance.

Land Development Ordinance 1935.

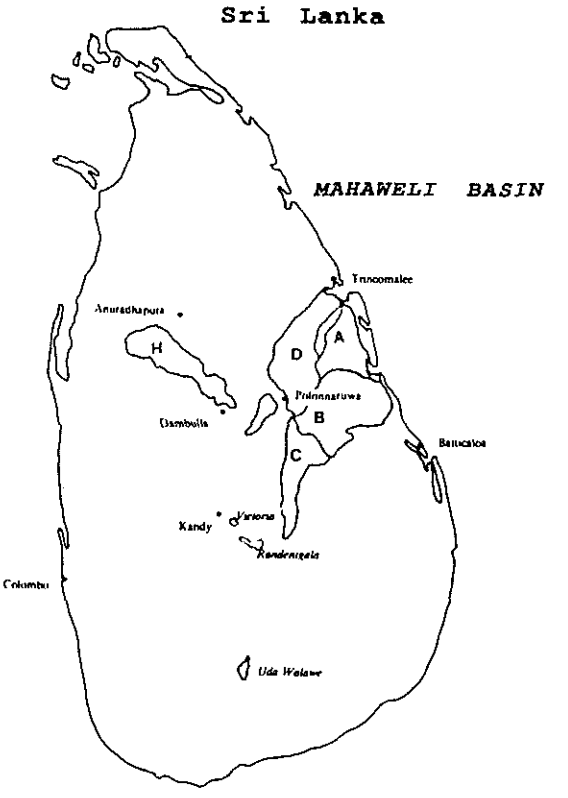

Soil conservation Act follows after a private member Bill in the Legislature in 1940.

A considerable lull in the 1950's through to 1960's.

Absence of integrated Basin wide watershed analysis.

Lack of indepth study on detailed catchment hydrology.

Defficiency in resources and high level of resource degradation with plantation agriculture and private felling in the main catchment.

All Basins:

Rivers 103, total catchment area 59,217 sq km and number of stream gauging stations (River Gauging Stations); 68.

The Mahaweli Basin catchment 10,443 sq km and 18 RGS, number of run-off stations: on a daily basis- nil, monthly-7.

Recent on watershed developments:

First Interim Report on Land 1985.

Second Interim Report on Land 1989.

Basin developments:

In the Mahaweli Accelerated Program total run-off in the project at lowest points of diversion is 10,000 cu m or 25 percent of the total run-off.

A Forestry Master Plan (1986) to circumvent the acute deforestation has been introduced

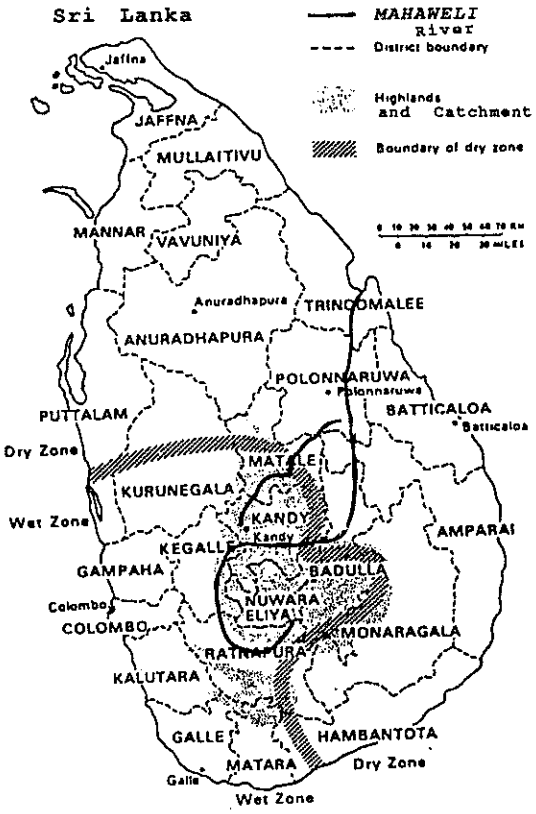

Australia:

First Legislation in 1915 on Murray-Darling Basin Agreement between New South Wales, Victoria and South Australia.and River Murray Waters Amendment Act 1987.

Catchment management and water management follows.

Federal level New directions of Water Management 1987 and Instream Uses of Water.

Recently, NSW State Legislation on Total Catchment Management, 1989 (see community participation as per media publicity).

Basin wide:

135 RGS and 10 within the Murray-Darling Basin.

River Murray Waters Act 1987.

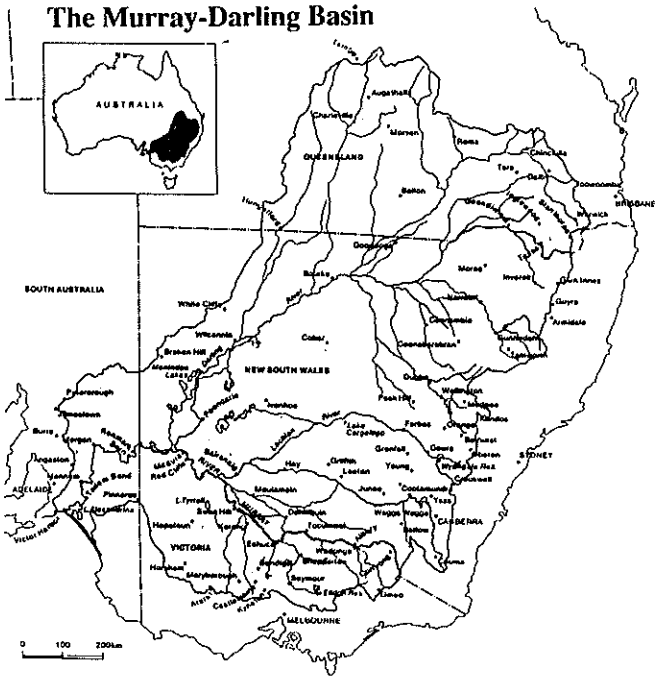

1/7th of Australia's surface catchment falls within the purview of Murray-Darling Basin.

20 major rivers off the Great Dividing Range.

40,000 years history of the Basin associated Aboriginal Culture.

The length of the River is 3780 km .

30 to 40 percent of Australia's total natural resource based production occurs in the Basin.

7000 wetlands within the Murray waters.

Murray yields 12,000 gigalitres and the Darling carries 12 percent of the run-off over 50 percent of the Basin area.

CONSTRAINTS

Conflicts in the institutional arrangements create external diseconomies and in turn have created duplication and overlapping of institutions in both situations.

These impediments have caused disincentives to achieve efficiency and there is a large resource value depletion in both watersheds. This is largely reflected in undercharging for water and lack of appreciation of the resource has been aggravated by the absence of a rent which is the key to secure the resource for intergenerational purposes.

The way the politics interpret priorities, ignorance, postponement of actions and undisclosed defined regimes particularly in the sustainability issues have caused the greatest inequity in watershed concerns in these situations.

In Australia, inter-governmental quangos such as the River Murray Agreement present bona fide commitment by the States to co-ordinated, comprehensive regional approach to interstate water and resource issues.

There is legal opinion that a rational scheme for balancing conflicting interests within the Murray-Darling Basin and for administering the system is unlikely to spring up, alone and unaided, as a voluntary product of State consent.

In Sri Lanka, the infant stage of its handling of natural resources and initiatives, and the slow progress and cautious approach vindicate the whole objective of watershed protection for good economic and environmental reasons. The expectation that foreign help would always be forthcoming to salvage things that have gone wrong for decades due to political mishandling of important issues is in itself a summation of the ideology behind the scene.

In Australia, a major problem that the Murray-Darling Basin watershed planning confronts is the voluntary non-participation of the Queensland state in the Strategy to manage total water, vegetation and environmental flows. In terms of key tributaries, the State's part of the catchment is critical to achieve a bearable level of water flows in the downstream. They are also the underlying causes for most of the flooding in the adjoining State of NSW (during the preparation of this manuscript their has been a positive development to conglomerate Queensland to the River Murray Waters Agreement).

CONCLUSION

Natural resource management is taken up by a broadly modelled total catchment concept which has important parameters and implications. However, it is a brand new phenomena. Only time can determine the significance of the strategy as well as the accelerated initiatives.

Total catchment management has scope for flood mitigation, soil conservation and sedimentation problems in either situation. The concept is in harmony with an overall supply of vegetation resources and sustained productive resource for the respective regions.

Intergenerational issue is another important policy debate that looms giving pertinent attention to inter temporal equity value of total resources in a watershed. At this point in time the best could be achieved is to learn from the past mistakes and accommodate comprehensive sets of objectives not only to circumvent previous impediments but to guard against reoccurrence of degradations and denudations. Because single issue oriented solutions in a watershed region does not carry that much of weight in policy justification anymore.

However, the determining force is not the way that policy is forwarded in a package, but the trade-offs desired politically and implemented concerning whether equity or efficiency is the criterion of the day. It is paramount because neither will be achieved if both criteria are pursued.

A conceptual model of watershed policy

|

Level of policy substitution = level of program/NRMS policy

|

Take NRMS for instance as a function of Total Catchment

|

Management [NRMS *f* (TCM)]

|

TCM *f* (soil, vegetation, watershed)

|

Therefore, the significance for water policy

|

as the institution for watershed concerns

note:

NRMS= Natural Resources Management Strategy

TCM= Total Catchment Management

COMMUNITY REPRESENTATIVES CATCHMENT MANAGEMENT COMMITTEE for the Lower Murray-Darling Region

CATCHMENT MANAGEMENT ACT, 1989

The NSW Government is establishing Catchment Management Committees, under the Catchment Management Act 1989, to implement Total Catchment Management (TCM) objectives.

TCM is a community-based approach to natural resource management. It is the co-ordinated and sustainable use and management of land, water, vegetation, fauna and other natural resources. Its aim is to balance resource use and conservation.

To allow various and differing Western NSW land use management issues to be adequately and effectively addressed it is proposed to divide the Western Region into two regions:

- Lower Murray-Darling Region
- Western Region

The boundary between these regions follows the Sydney-Broken Hill Railway line until Menindee Lakes. The Menindee Lake System, Broken Hill and the entire Lake Victoria catchment lies within the Lower Murray-Darling Region.

The eastern boundary of the Lower Murray-Darling region follows the catchment boundary with the Lachlan and Murrumbidgee, being the boundary to the Lachlan and Murrumbidgee TCM regions. The southern and western boundaries follow the Murray River/Victorian border and South Australian border respectively.

Persons who are landholders, landusers or who have an interest in environmental matters in the Lower Murray-Darling are invited to apply to be representatives of the region on the TCM Committee.

Members of the existing Western Catchment Management Committee will become members of the Committee within which they reside and do not need to reapply.

Applicants should possess the following qualities:

- commitment to sustainable development,
- knowledge, interest or experience in natural resource management,
- ability to represent community views,
- knowledge of natural resource issues in the catchment and how these issues affect the people, and
- such capacities as progressive thinking and the ability to work well with people.

Further information is available from Mr. Brendan Diacono, TCM Co-ordinator; (060) 88 0255.

Written applications providing details in terms of the above qualities should be with Mr. Diacono (c/- NSW Soil Conservation Service, 32 Sulphide Street, Broken Hill 2880) by 31 August, 1990.

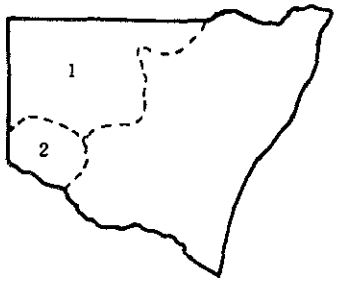

1. Western
2. Lower Murray-Darling

THE NEW SOUTH WALES GOVERNMENT
Putting people first by managing better

ACKNOWLEDGEMENTS

I thank my friend S. Gunatunga, Sri Lanka; for sending research material. This paper was supported by the Scientist Assistance Program of Canada.

REFERENCES

Australia Murray-Darling Basin by Murray-Darling Basin Ministerial Council. 1990. Natural Resources Management Strategy Towards a Sustainable Future; ii.

Clark, S.D.; 1983. Intergovernmental Quangos: The River Murray Commission. Australian Journal of Public Administration XLII (1): 155-171.

Commonwealth of Australia; 19897. River Murray Waters Amendment Act. No. 154 of 1987. Australia; Commonwealth Government Printer.

Day, Diana G.; 1988. River Mismanagement: Policy, Practice or Nature?; Centre for Resource and Environmental Studies Working Paper 1988/1; Australian National University; 1-42.

Democratic Socialist Republic of Sri Lanka; 1985. First Interim Report of the Land Commission; Sessional Paper No.1- 1986. Department of Government Printing Sri Lanka.

Democratic Socialist Republic of Sri Lanka; 1989. Second Interim Report of the Land Commission- 1985. Department of Government Printing Sri Lanka.

Department of Primary Industries and Energy; 1988. Instream Use of Australia's Water Resources; Australian Water Resources Council Water Management Series No.11. Australian Government Printing Press; 1-13.

de Silva, Chandrananda R.K. 1982. Sri Lanka Country Paper. In: Water and Soil Miscellaneous Publication No. 45; Catchment management for optimum use of land and water resources: Documents from an ESCAP seminar; 1982 Wellington; 197-202.

Extent of Tree Clearing in Australia Since European Settlement by Ive and Cock. 1989. Rural Land Degradation in Australia: The Australian Conservation Farmer; 1(3).

Murray-Darling Basin Ministerial Council; 1990. Natural Resources Management Strategy Murray-Darling Basin: Towards a Sustainable Future; August, 1990.

Murray-Darling Basin Ministerial Council; 1987. Murray-Darling Basin Environmental Resources Study; July 1987; State Pollution Control Commission, Sydney. 27-113; 251-281.

NEDECO; 1979. Mahaweli Ganga Development Program Implementation Strategy; Netherlands Engineering Consultants; The Hague September 1979; Volume 1 Main Report; 17-21.

New South Wales Government. Community Representatives Catchment Management Committee. The LAND. 1990 July 26. 2(col.1). New South Wales.

New South Wales (NSW) State Parliament; 1989. Catchment Management Bill. First Print.

Soil Conservation Service of New South Wales; 1990. Total Catchment Management: A State Policy Including State Soils Policy, State Trees Policy.

Sri Lanka Mahaweli Basin and Accelerated Program by IIMI.1986.; 19.

Sri Lanka Mahaweli Basin and Mahaweli River Catchment appeared in a paper presented by Rohan Ekanayake; Economics of Multiple Use of Production Forests in Sri Lanka. 1986. 30th Annual Conference of the Australian Agricultural Economics Society; February 3-5, 1986; 20.

The Global Water Runoff Data Project. 1989. World Climatic Programme Research, Workshop on the Global Runoff Data Set and Grid Estimation, WCRP - 22 and WMO/TD - No. 302, 1988 November 10-15; Klobenz, FRG; 6-12.

Trinity of Soil, Trees and Water based on a diagram in a publication of the NSW Soil Conservation Service.

Surrounding the Consequences of Watershed Disasters in the Periphery of the Indian Triangle[1]

Rohan Ekanayake[2]

Abstract: The watershed of the 'Indian Triangle' is formed by the flow of two mighty rivers which emanate from the Himalaya. The Ganges and Brahmaputra embrace the lands and the peoples of Nepal*, India* and Bangladesh* before emptying into the Bay of Bengal. A recent monsoon submerged two thirds of the low-lying Bangladesh rendering 25 million people homeless. Can the future of these people be secured by lowering the water levels downstream? Are there alternative structural propositions and are they economically and politically feasible ? What effect will the excessive removal of natural barriers to rain in the upper catchments have on policy?

A major issue addressed in this paper is the sustainable development and ecological stability in these watershed regions. A majority of the environmental problems in the region's watersheds in the past have occurred mainly due to undesirable human interference in regional environmental flows and vegetation resources. Plausible solutions to on-going and future environmental crisis will largely depend on how broad the regional consensus is surrounding the conflicting water resource issues. Depending on how the dominant rural social base adjust to important dynamics of the problem, the paper concludes that sustainability will be an issue vulnerable to political interpretation.

Like most watershed regions in the world, the watershed region of the 'Indian triangle' is on its history's rapid growth track. A sudden progress of events on several interrelated fronts-the economic, the ecological and the political has combined to spur significant changes both in the relationships between peoples, policy-makers and governments and in the way these forces interact in the management-use and conservation-of the water and vegetation resources as a whole.

THE PEOPLE

The significance (percent) of rural population to the relevant South Asian nations is shown from the United Nations Population Studies (1989).

	Year			
Nation	1955	1965	1975	1985
India	82.4	81.2	78.5	74.5
B'desh	95.3	93.8	90.9	88.1
Nepal	97.3	96.5	95.2	92.3

The composition of the population in the triangle is not different from the respective national aggregates and thus it is based significantly in the rural areas. Agriculture is predominant and a large dependence on natural resources is common in the region. The importance of water resource to the people in the watershed is immense for their livelihood and so does the forestry resource (Ekanayake 1990).

THE PROBLEM

It is a regular feature in Bangladesh life to experience floods every year and it is not surprising to expect flooding with almost every monsoon followed up by a drought. A recent monsoon submerged two thirds of the low-lying areas of Bangladesh rendering 25 million people homeless. Destructions to crops and economic losses are insurmountable. The September 1988 floods inundated 2 million ha of farmland (FEER 1989).

---

[1] Presented at the Subject Group S1.04 Technical Session on Geomorphic Hazards on Managed Forests, XIX World Congress International Union of Forestry Research Organisations, August 5-11, 1990, Montreal, Canada.

[2] Research Economist working in the Water Branch of the Land Resources Division in the Department of Primary Industries and Energy and formerly Research School of Social Sciences, Australian National University, Canberra.

Like the river dispute involving the Euphrates-Tigris and Shatt al Arab in the Mediterranean, the long-running dispute between India, Bangladesh and Nepal on the control of waterways of Ganges and Brahmaputra has led to a sequence of uncontrolled floods and droughts in the region of the triangle.

Occurrence of heavy floods[3] in the triangle in the past have been;

Decade	1950	1960	1970	1980
Assam (India)	-	2	2	4
Bangladesh	3	3	3	4.

It is claimed that increasing population have added impetus on the watershed disasters by way of extra dimensions of human and economic costs.

Population[4] (to the closest million)

	1955	1967	1977	1987	Increase '77-'87(pct)
India	386	504	626	781	25
B'desh			83	103	24
Nepal	9	11	13	18	38

Consumer Prices Index (CPI) 1980=100

	Average 1964	1972	1980	1987
India	31.5	51.8	100.0	184.4
Bangladesh	12.6	24.9	100.0	212.7
Nepal	33.0	51.3	100.0	204.3

The extra burden of CPI increase on the economy as a result of population increase for the nations is evident from the above data as well as the rural dimension of the problem.

The Triangle

Agriculture accounts for nearly half of the national income of India and it supports about 70 percent of the country's population. But large parts of cultivated land usually experience the problem of insufficient rainfall for crop growth either in terms of precipitation or its distribution to match with crop water requirements. National Commission on Agriculture estimates India's utilisation of annual precipitation would improve in the early part of the next century from its current level of 25 percent.

Bangladesh has an area of 14.4 million ha lying in the delta of the region's three great rivers; the Ganges, the Brahmaputra and the Meghna of which 9.1 million ha (64 percent) are cultivated. About 80 percent of the population are engaged in agriculture (Map indicating Bangladesh and surrounding countries with principal rivers).

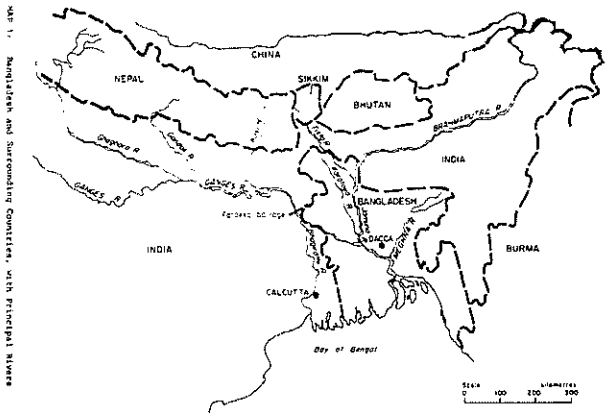

The mean annual rainfall in Bangladesh varies from about 1,300 mm in the western part to almost 5,000 mm in the northeast of the country and is characterised by wide seasonal fluctuations with about 90 percent of the rainfall occurring in the five month period of the monsoon (May to September). In spite of an overall abundance of rainfall, serious droughts do occur.

Nepal has an area of 141,000 sq km lies parallel to the main Himalaya range of mountains. About two thirds of land area is taken up by high mountains and the lower slopes, the remaining one third, a narrow strip to the south called the Terai, is the border-line of the Indo-Gangetic plains. About 10 percent of the population lives in the Himalaya region, 50 percent in the hills of the lower slopes and the remainder in the Terai.

[3] Information on flood occurrence in the region is from Centre for Science and Environment of India.

[4] Population and economic indicators are from International Financial Statistics (1988).

THEORY AND EMPIRICS

The triangle region like many regions in developing economies rely heavily on water resource development to foster economic growth. The nations in the region also have the potential to develop hydro power to ease burden of high import bills on fuel. In addition, flood mitigation is crucial for enhancing the productivity of low-lying lands.

Even with modern mechanisms of water resource management, it has not been able to control floods in the low lying areas of the triangle. None of the countries in the region have realised even half of their hydro power potential.

To sustain production, water and land use policies must be integrated. This is theory. In practice, the countries in the region lack overall water resource and vegetation management strategies. Deforestation in the catchments and excessive removal of natural barriers to rain in the region's highlands have further disturbed the ecological balance.

In summary, it is shown by environmental science that deforestation in highlands reduces the absorptive capacity of its watersheds. When this is related to the current topic, monsoonal rains run inhibited off the denuded slopes, causing erosion in the fertile soil. The sedimentation in downstreams causes floods. The tarnished groundwater retention levels calibrate droughts furthering the imbalance in agricultural production (see Ives and Messerli 1989. 'The Himalayan dilemma: reconciling development and conservation' for a contrasting but subtle *Himalayan Environmental Degradation Theory*).

POLICY

Water has become a diplomatic issue in the region. Bangladesh being a low-lying state is at a disadvantage in negotiations receiving nearly 90 percent of water from across the border. Nepal has an enormous capacity to develop its hydro energy having harnessed only 0.5 percent of its potential so far. Being a upstream state is to its advantage in water negotiations. India, according to Far Eastern Economic Review, by withholding hydrological and climatological information can effectively influence structural undertakings in the triangle region. Some of the most elementary data on hydrology and power generating capacity of North India remain classified as military secrets (ibid).

So far, the efforts to secure wider economic benefits for the region by providing for droughts in Ganges delta have failed. Similarly, finding a solution to annual flooding has been an equally intractable impasse.

While reservoirs in Nepal would relieve flooding in the Ganges, most of inundation is caused by the Brahmaputra-Meghna waterway, which carries twice the Ganges's volume of water (Asiaweek Map). Indian strong view is that the proposed Ganges-Brahmaputra link canal would greatly contain flooding in the delta. This is contrasted by Bangladesh on the lack of appreciable effect of lowering water levels downstream.

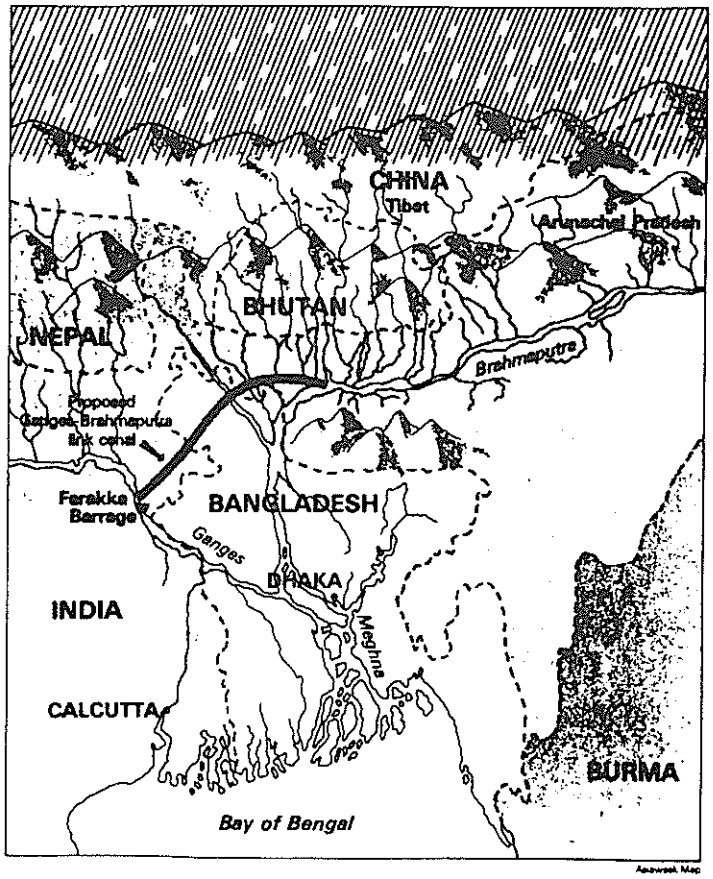

Constructing storage dams in the Indian territory with exclusive benefits to Bangladesh's downstream is not favoured by the cost bearing side. However, considering the northern Indian situation, where the world's highest mountains meet some of the world's flattest plains and the rainfall is concentrated in 90 short-days, it appears that the unrivalled trust for water resource management is contained in upland storage.

Some argue such policy as purely issue centred and brand them as 'makeshifts'. The conflict between energy and irrigation priorities becomes most acute during the dry season when there is more demand for water at farm-level while turbines need to maintain spill levels for energy generation.. The question is, who can suggest equity by displacing highland people in catering to energy needs of the city-dwellers?

Lack of political will in implementing far-reaching forestry oriented flood control measures in the triangle region have been the casualty of opting to more locally beneficial activity. Ignoring the best possible path-the less painful natural ways, and without any glimpse at seismic breaching and excessive melting of snow, the more localised suggestions are carved in small to medium scale intervention to prevent saturation of water-flows.

Bearable Waters

According to Myres (1989), in the cause of sustainable development environmental resource base makes a critical contribution as the ultimate support of much economic activity. Expanding on that, others have added that sustainability concept has major implications for intergenerational responsibility. This means, institutional arrangements should take into account of socially unjustified environmental degradation associated with intragenerational activity.

Economic justification of sustained water provision to any situation must take into account of climatic variability. This has important implications for both dry land water preservation as well as monsoonal-flush situations. The evidence from temperate regional water management initiatives as well as sub-temperate and monsoon regions are important in this respect.

As mentioned in Frederick and Gleick 1988, it is crucial to identify shortcomings in the capacity of the water resource region to adapt to large changes in water-flows in the absence of new infrastructure or institutional changes or technological developments.

This investigative approach with little economic or social strain will be proven useful to the region given future changes in water-flow patterns.

THE OUTCOME

Given the equity questions and sensitive decision making horizons in the region's polity, there is no guarantee to suggest that *sustainable* guide-lines will be easily constituted here. In the vast majority of these societies, subsistence is the main force that drives living beings further. Likewise, the policy makers are overwhelmed by domestic priorities and are unable to suggest any better sustenance. For example, even under a reasonable education system, a majority of the population would be uninterested in environmental problems as economics bite hard. Sri Lanka, with its very high educational attainment levels, is unable to respond to any environmental crisis and this is widely evident in its handling of high occurrence in pesticide contaminated deaths.

Therefore, even at the peril of a region's long-term economic viability, policy may not intervene for remedial action not merely because of their educational background and specific experience. Most environmental crisis are regionally based and need to be handled at regional levels.

The approach is to find tradeoffs to offset gains and losses until no one is worse off (or better off). Until such time that the policy makers are non-ignorant, then a possibility exists for cooperation. However, even at regional levels, sub regional bias engulfs the issue tables. At those levels, decisions based on household sensitivities have priority over the intergenerational issues. The pain of those decisions though is passed on to the *society* or possibly to the next generation for absorption. This is a resemblance of the current issue surrounding its ecology and future economic well-being.

CONCLUSION

The future of a harmonious relationship that the peoples of this region aspire, will largely hinge on the decision-makers' ability to grapple with real issues affecting the waters and forests of the region and their productivity. However, there is no guarantee that they will be sensitive to generational issues or wider benefits outside their horizons. Neither, they can be entrusted with the fullest confidence to handle dynamic issues that we are discussing in a way compatible with natural limitations. At the end of the day, the most respected notions we debate for policy may show vulnerability to the expediency and interpretation of the politician.

ACKNOWLEDGEMENT

This paper was supported by the Scientist Assistance Program of Canada.

REFERENCES

Asiaweek map on Regional-flows Terrains and Locations

Asiaweek; Number 4 1988 Defence plans after the deluge; 34-35.

Bangladesh and Surrounding Countries, with Principal Rivers; Australian National University

Easter, William.K.; Dixon, John A.; and Hufschmidt, Maynard M. 1989 ed. Watershed Resource Management: An Integrated Framework with Studies from Asia and the Pacific. Studies in Water Policy and Management, No. 10. Boulder: Westview Press; 3-15

Ekanayake, Rohan. 1990. Women and access to sources of household energy: value of labour and resource scarcities in peasant economies of South Asia. Contributed Paper to the 34th Annual Conference of Australian Agricultural Economics Society, 1990 February 12-16; Brisbane Australia

Far Eastern Economic Review 2 February 1989. The Wasted Waters, Himalayan Blunder and Resource and Rights; 16-22.

Frederick, Kenneth D.; Gleick, Peter H. 1988. Water Resource and Climate Change. In: Rosenberg, Norman J.; Easterling, William E.; Crosson, Pierre R.; Darmstadter, Joel.ed Proceedings of a Workshop on Greenhouse Warming: Abatement and Adaptation held in Washington, D.C. 1988 June 14-15; 133-143

MacNeill, Jim. 1989. The Greening of International Relations. International Journal 1(1) Winter: 1-35

Myers, Norman ; 1989. The Environmental Basis of Sustainable Development. In: Schramm, Gunter and Jeremy W.Warford ed. Published for the World Bank, The John Hopkins University Press, Baltimore; 57-68.

High-Speed High-Stress Ring Shear Tests on Granular Soils and Clayey Soils[1]

Hiroshi Fukuoka and Kyoji Sassa[2]

Abstract: The purposes of this study is to obtain exact knowledge of the influences on friction angle during shear by shearing speeds. Ring shear tests on sandy and clayey materials have been carried out with a newly developed High-Speed High-Stress Ring Shear Apparatus to examine if there are some changes in the frictional behaviors of these materials at high shearing speeds of 0.01cm/sec~100cm/sec and high normal stress of 0~3.8kgf/cm^2. Samples used for tests were glass beads, tennis court sands in the university campus, the Toyoura standard sands (uniform beach sands) and bentonite clays. All tested samples were dry.

Although result on the glass beads showed that the friction angle during shear was independent of shear speed under the normal stress up to 3.8kgf/cm^2, 2 ~ 5 degrees of change in friction angle were observed on the tennis court sands, the Toyoura standard sands and the bentonite clays. In the tests on the Toyoura standard sands and the bentonite clays, friction angle increased as the shear speed increased. On the contrary, friction angle during shear of the tennis court sands decreased at a shearing speed of 100cm/sec.

Change in grain size distribution implies that heavy crushing or grinding of particles occurred during shear. The grain size distribution become wider during shear by grain crushing in samples except glass beads. It could result in the increase of density and accordingly increase of the friction angle. Crushing or grinding of grains during shear can change the shape of grains. The Toyoura standard sands have round shape, because they are beach sands, it may become angular by crushing during shear. On the contrary, the tennis court sands have angular shape because they are taken from mountain slopes, it may become round by grinding during shear. Round grains have a small friction angle. It may be interpreted that the tennis court sands had a smaller friction angle during shear because of the change of angular grains to round grains by grindings. Hence, it can be said that the friction angle is affected by crushing or grinding of grains during shear, which appears in a higher normal stress and a greater shear speed (shear distance).

To know the frictional characteristics of soils during high speed shearing is very important for the research on motion of landslides.

To measure the friction angle during shear, it is most appropriate to use ring shear apparatus because landslide motion usually causes long distance shearing of about several meters to some hundred meters. Bishop, 1961, developed a ring shear apparatus and carried out ring shear tests on samples of several kinds of clays in order to examine residual strength of clays which is a steady strength appearing after the peak strength. In reactivation of old landslides, the mobilized shear strength is not the peak strength in the virginal shear of the soil, but the residual strength which is a small steady state strength appearing after the peak strength. Bishop's ring shear apparatus had a sample box of which diameter was about 15cm (outside) and 10cm (inside). The maximum normal stress is 2.5kgf/cm^2. The shear speed in his experiment was 1.3×10^{-5}cm/sec and the maximum shear displacement was 132cm. But it is not enough for research of the motion of landslide, it needs a faster shear speed up to some meters per a second, and longer shear displacement up to some meters.

Sassa, 1984, developed a Low-Stress High-Speed Ring Shear Apparatus in 1984 for the research of motion of debris flow. The diameter of the sample box is 30cm (inside)—48cm (outside). The maximum normal stress is 0.4kgf/cm^2. The shear speed is 0.001 to 150cm/sec.

In order to know whether the shear friction during shear depends on shear speed or not, Sassa carried out ring shear tests on glass beads, the Toyoura standard sands. The results of ring shear test on glass beads of 2.0mm diameter are shown in Figure 1. Measured data on normal stress versus shear resistance which has a stress dimension are plotted. The tests were carried out under the normal stress up to 0.3kgf/cm^2. The normal stress was continuously increased under the constant shear speed. Such tests were repeated of same sample on different shear speeds of 0.001, 0.1, 1, 90cm/sec. Almost all data are on a straight line inclined 19° and there are little scatters among the data. So, this

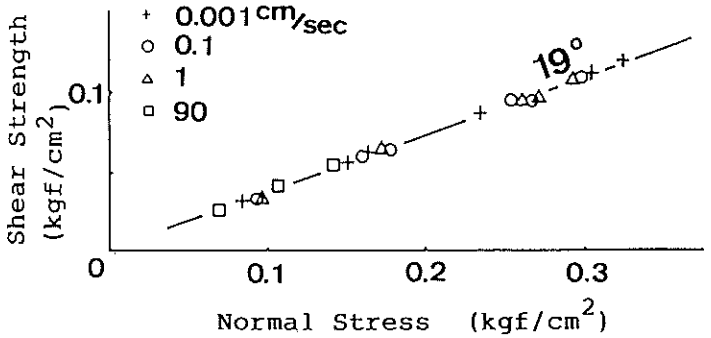

Figure 1—Result of low-stress high-speed ring shear tests on dry glass beads of 2.0mm diameter. Void ratio e=0.65~ 0.67 (Kaibori, 1986).

[1] Paper presented at the XIX World Congress of the International Union of Forestry Research Organizations, 5–11 August, 1990, Montréal, Canada

[2] Post Graduate Student and Associate Professor, respectively, Disaster Prevention Research Institute, Kyoto University, Uji, Kyoto, Japan

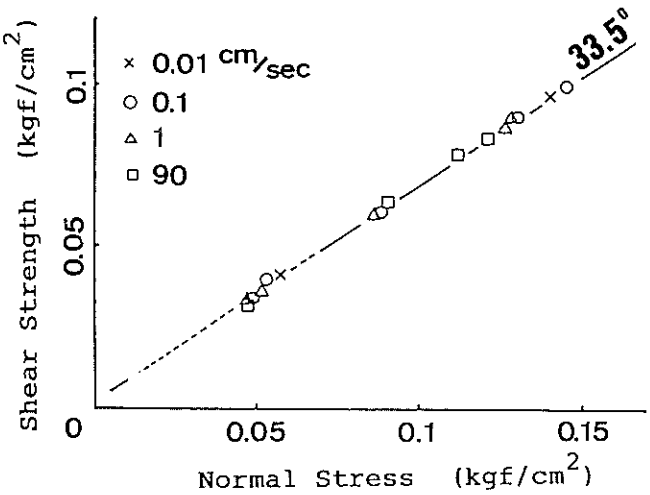

Figure 2—Result of low-stress high-speed ring shear tests on Toyoura standard sands. Void ratio e=0.88~0.91 (Kaibori, 1986).

result means that the shear friction of the glass beads is independent of shear speed in the range of shear speed and the normal stress as mentioned above.

Results of ring shear tests on Toyoura standard sands are shown in Figure 2. Procedure of the tests are almost same with the tests on the glass beads. Shear tests are carried out under the normal stress up to 0.15kgf/cm^2. Shear speeds of these tests are 0.01, 0.1, 1 and 90 cm/sec. The friction angle of all shear speed is 33.5°.

Hungr and Morgenstern, 1984, developed a high velocity ring shear apparatus in 1984. The diameter of the sample box was 15cm (outside) and 11cm (inside). The maximum normal stress is about 2kgf/cm^2 and the maximum shear speed is 2m/sec. In use of the apparatus, they carried out ring shear tests on polystyrene beads and the Ottawa quartz sands of various grain sizes under two shear speeds of 0.025cm/sec and 98cm/sec. Results of the tests showed that the friction angle was almost independent of shear speed.

Sassa, 1988, developed a High-Stress High-Speed Ring Shear Apparatus in 1988 for the research of landslide. It attained high normal stress up to 3.8kgf/cm^2 and it corresponds to the depth of about 19~23m of landslide mass, hence research on the motion of real landslides has become possible. The diameter of the sample box is 33cm (outside) and 21cm (inside). The maximum shear speed is 150cm/sec.

With the apparatus, Vibert, Sassa and Fukuoka, 1989, carried out the ring shear tests on torrent deposit of the Denjo river and soils of the Jizukiyama landslide in order to examine whether the shear friction depends on shear speed or not. Result of the tests on dry torrent deposits of the Denjo river showed that the friction angle during shear under the shear speed up to 10cm/sec is 35.0° but the friction angle at 100cm/sec under the normal stress up to 1.2kgf/cm^2 is 36.5° (Figure 3).

Result of the tests on unsaturated (degree of saturation was 20%) Jizukiyama landslide soil showed that the friction angle during shear was 32.8° at 0.01cm/sec, 35.0° at 0.1cm/sec, and 38.5° at 1cm/sec and 10cm/sec (Figure 4). The magnitude of the variation is about 6°, larger than the result on the sample of the Denjo river. The friction angle during shear of both sample tended to increase as the shear

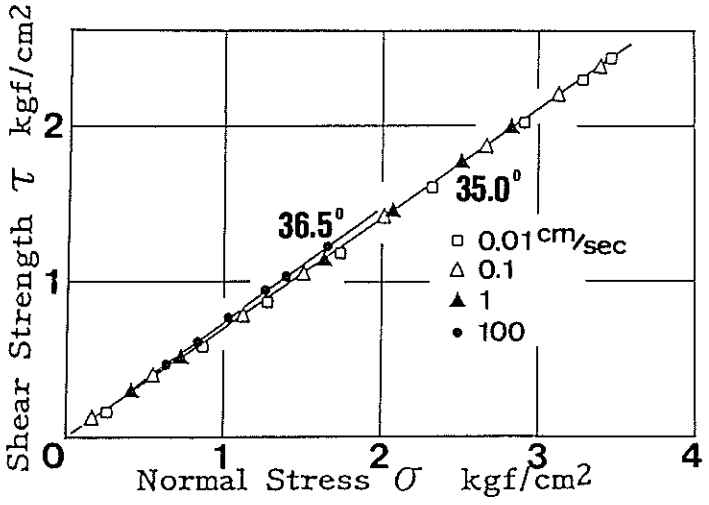

Figure 3—Result of high-stress high-speed ring shear tests on dry torrent deposit of the Denjo river. Void ratio e=0.50~0.57 (Vibert et al., 1989).

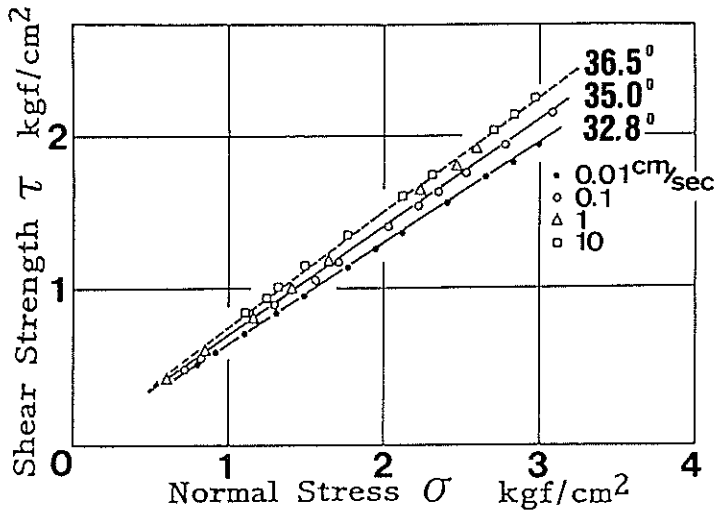

Figure 4—Result of high-stress high-speed ring shear tests on unsaturated Jizukiyama soil. Degree of saturation S_r = 20%. Void ratio e=0.50~0.57 (Vibert et al., 1989).

speed increased.

Examination of both sheared samples after the tests showed that so much fine ground grains were found on the shear plane. It seemed that this grinding of soil particles relates to the variation of friction angle during shear, and the magnitude of the variation relates to the grain size.

So using the High-speed High-stress Ring Shear Apparatus, we have done ring shear tests of various samples at various shear speed to examine what causes the variation of friction angle.

SAMPLES AND APPARATUS

Samples for tests

Samples of different material and different grain size were chosen. Tested samples are glass beads of 0.2mm diameter, tennis court sands, Toyoura standard sands (uni-

beach sands) and the bentonite clay. Because pore pressure of the sample is not measured during shear test, effective stress can not be measured. So when dry or not-saturated sample were used, no excess pore water pressure would be generated and total stress would be equal to effective stress. So all of the samples tested by the apparatus were dry.

Glass Beads

Glass beads are of 0.2mm uniform diameter. The specific gravity of the glass beads is 2.50.

Tennis Court Sands

Tennis court sands are taken from the tennis court in the university campus. They are taken from mountain slope and consist of angular grains. The specific gravity is 2.60. They are dried before the tests.

Toyoura Standard Sands

Toyoura standard sands is Japanese uniform beach sands sold by a Japanese company and used as a standard sands for calibration of test apparatus for soils by Japanese soil mechanics researchers. It is a uniform, clean fine quartz sands with round grains. The grain size is 0.05 ~ 0.5mm. The specific gravity is 2.49.

Bentonite Clays

Bentonite clays used in the tests is a dry clay powder sold in Japan and usually used for civil engineering works. It is well ground and with grain size smaller than 0.3mm. The specific gravity is 2.58. Permeability of the clays is always very small and it takes so much time for dissipation of excess pore water pressure, so the sample used for shear test was completely dry to prevent generation of pore water pressure.

Structure of the Apparatus

Figure 5 is the schematic diagram of High-Speed High-Stress Ring Shear Apparatus. The sample box is shaped circular channel. The diameter of the sample box is 33cm (outside) and 21cm (inside). It is made of transparent acrylic resin, retained by metal frame and the outside of the sample can be observed during test. Section of the sample box is 6cm wide and about 6~8cm high. The width of the section is constant. The loading plate can move vertically, so only the height of the sample can change. The sample box is separated horizontally at about midheight (Figure 6). The lower one is rotated by servo-control motor for shear. Several non-skid needle assemblies are fixed on the base and the ceiling (loading plate) of the sample box and they prevent the sample from slipping on either side. So, rotation of the lower sample box causes shear of sample. After the shear test, horizontal shear plane is usually formed between the upper and the lower part of the sample box. There is a rubber edges at the inside and outside gaps between the upper and the lower part of the sample box and they are bound on the upper part of the sample box to seal the gap, and preventing leak of sample from the sample box.

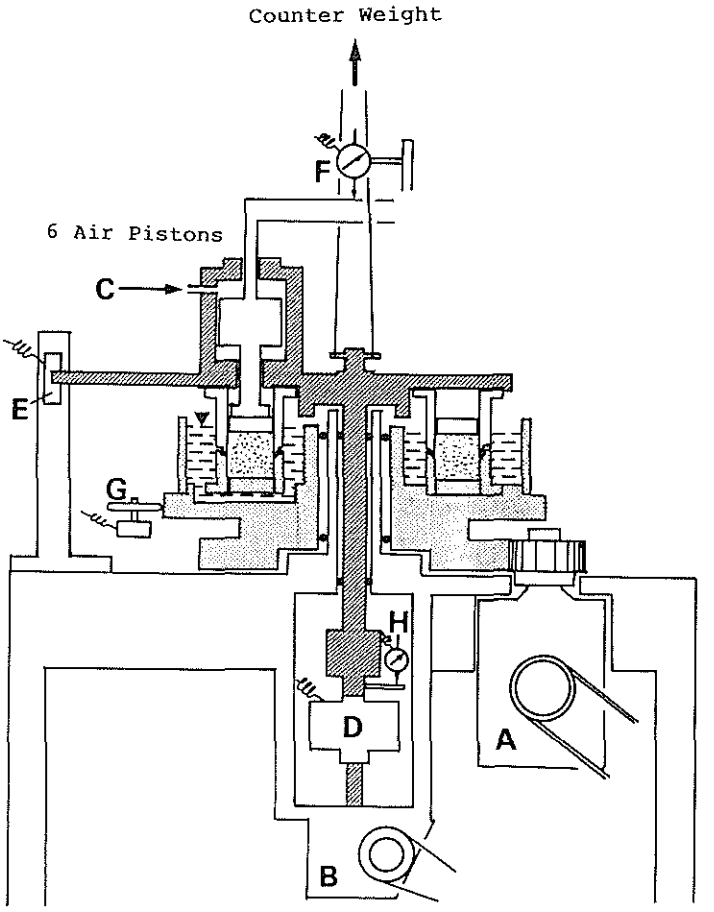

Figure 5—Schematic diagram of the High-Speed High-Stress Ring Shear Apparatus. A: servo-control motor for shear, B: servo-control motor for gap control, C: servo-control air regulator, D: load cell for normal stress, E: load cell for shear stress, F: dial gauge for volume change, G: shear displacement detector, H: dial gauge for gap.

The electric servo-control motor (marked as A in the Figure 5) can rotate the lower part of the sample box at constant speed, so it enables constant shear speed shear test. Available shear speed is from 0.001cm/sec to 150 cm/sec with use of four different gears in the gear box (also in A in the Figure 5).

The normal stress to the sample is given by an air compressor. The compressed air is put into six air pistons through an servo-control air regulator. The air pistons push down the loading plate (ceiling of the sample box) and the normal stress is loaded on the sample uniformly. The maximum normal stress is 3.8kgf/cm^2.

The gap distance between the upper and the lower part of the sample box should be constant throughout the test procedures, because too much narrowing of gap distance or contact of the upper and the lower part of the sample box may increase the measured value of the normal stress. While, too much widening of gap distance may lead to leak of sample from the sample box during shear test.

So, the apparatus has a servo-control motor for gap control (marked as B in Figure 5) and a electric distance meter for gap distance measurement on the order of 1/1000 mm. With them, gap distance is kept constant during a test as the same value at which shearing of the sample starts.

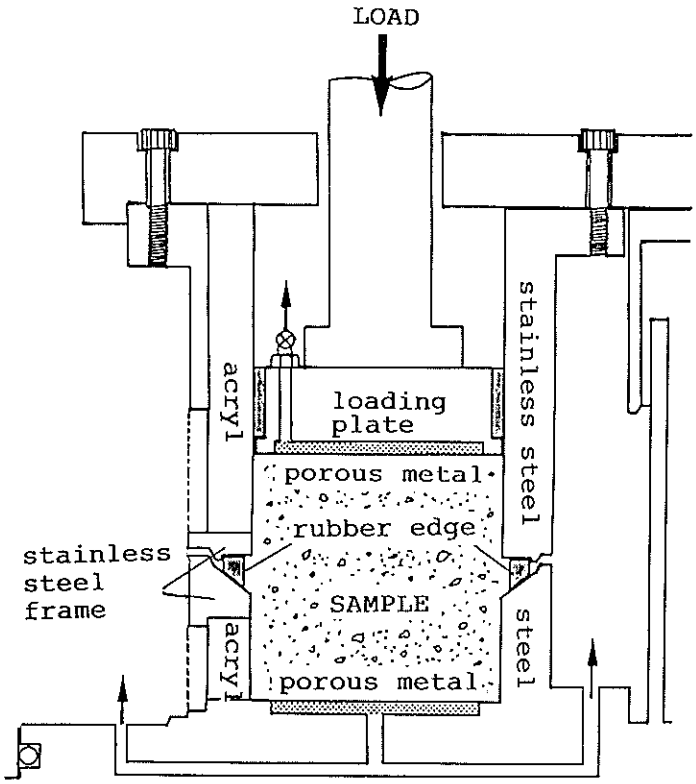

Figure 6—Section of sample box of the High-Speed High-Stress Ring Shear Apparatus.

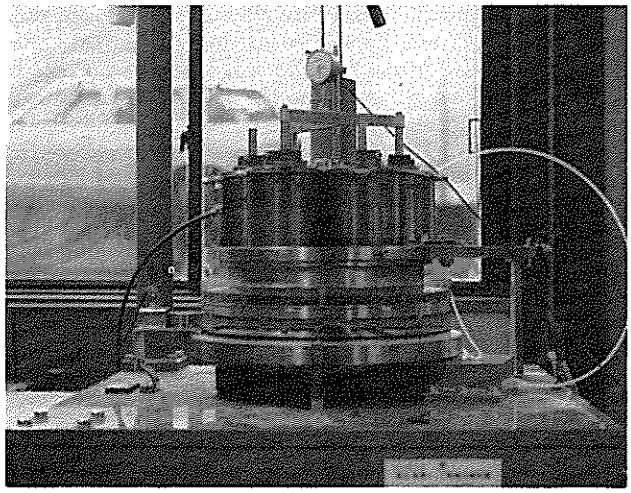

Figure 7—The High-Speed High-Stress Ring Shear Apparatus.

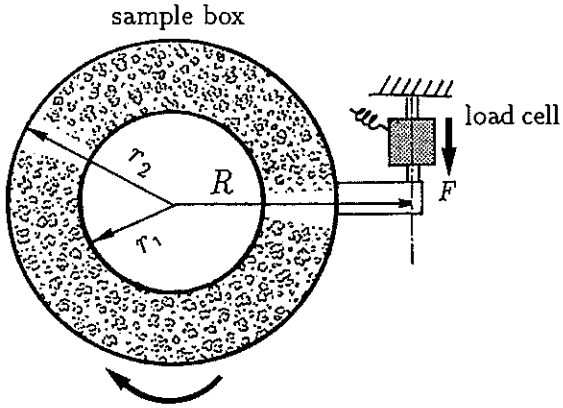

Figure 8—Calculation of shear resistance and shear torque of the High-Stress High-Speed Ring Shear Apparatus.

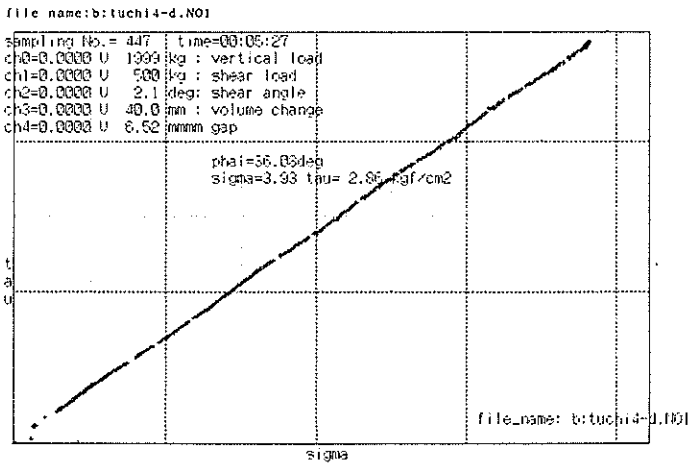

Figure 9—Screen copy of real-time monitoring system of the apparatus, assisted by personal computer. Displaying normal stress and shear resistance relation.

Monitoring System

Normal load on the sample is measured with a load cell set beneath the axis (marked as D in Figure 5). The compressed air which produces the normal load on the sample push up the air pistons and axis, then normal load is measured as tension force.

Shear resistance of the sample is measured with a load cell (marked as E on Figure 5). The upper part of the sample box and the upper unit (including air pistons) are fixed and restricted not to rotate with the lower part of the sample box, (marked E in Figure 5) with load cell for shear resistance. So, shear resistance is measured as tension force. As the shear resistance is supposed to originate uniformly on the shear plane, the shear resistance is easily calculated from the equation of shear torque. Above mentioned two load cells are electrically connected to dynamic strain meters with cables, and tension forces are measured with them.

Vertical displacement of the sample is measured with the dial gauge (marked as F on Figure 5). As the sample box cannot deform sideways, the measured vertical displacement multiplied by the area of loading plate is variation of volume of the sample.

Shear displacement is measured with rotary encoder which contact with the lower part of the sample box which rotates during test. The shear speed is calculated from the rate of rotation and it is displayed at each result of the tests shown below as the shear speed at the center of the sample.

All these measured parameters (normal load, shear resistance, sample height and shear displacement) are output as electric voltage through the amplifier unit. All values are recorded on the sheet of a pen-recorder and also put

into personal computer through A/D converter board in it, then the data are saved on magnetic floppy disk and the normal stress (σ)—shear resistance (τ_f) relation are plotted on the computer display at real time. Figure 9 is the screen copy of the computer display of the real-time monitoring system plotting stress conditions (normal stress and shear resistance).

Pore pressure is not measured because it is difficult to measure pore pressure at the shear plane. Only total stress on the sample can be measured. Therefore, tests were carried out under dry conditions.

Calculation

Normal stress σ (kgf/cm^2) is calculated from:

$$\sigma = \frac{W}{\pi(r_2^2 - r_1^2)} + \gamma_t \cdot h_{up}$$

Here, W: Normal load acting on the sample through loading plate measured by the load cell, r_1: diameter of the sample box (inside), r_2: diameter of the sample box (outside), γ_t: total unit weight of the sample, h_{up}: sample height above shear plane (about 3~4cm). $\gamma_t \cdot h_{up}$ is at most 0.008kgf/cm^2. The normal stress loaded on the sample during the ring shear tests are between 0.5~3.8kgf/cm^2, so this term is almost negligible. So, this term was not calculated during the ring shear tests.

Shear resistance τ (kgf/cm^2) is calculated from the equation of rotational torque (Figure 8):

$$\int_0^{2\pi} r\,d\theta \int_{r_1}^{r_2} r\tau\,dr = RF$$

$$\tau = \frac{3}{2}\pi \frac{RF}{r_2^3 - r_1^3}$$

Here, R: distance from the axis to the load cell for shear resistance, F: shear load measured at load cell which retains the upper part of the sample box from rotation.

PROCEDURE OF TESTS

Sample Preparation

The soils for the sample was compacted inside the sample box up to about 6cm high with steel bar. Compaction is carefully executed to make homogeneous sample.

Then set the upper unit including loading plate and air pistons, connect electric cables of measuring device to amplifiers and strain meters and connect air tubes of air pistons to the air regulator. The air compressor starts to run and supply pressure to air regulator.

Consolidation

Before shear test begins, sample is consolidated with normal stress of 3.8kgf/cm^2. Progress of consolidation is monitored by the dial gauge for measurement of sample height on pen-recorder. All soils for sample except bentonite were sandy soil and dry, consolidation completed quickly within about several seconds. Bentonite clay sample, which was dry powder, also completed consolidation quickly.

Ring shear test

After the sample is consolidated, normal stress is decreased to 0.5kgf/cm^2. Then slowest gear is connected to the servo-control motor, corresponding signal voltage for 0.01cm/sec is set on servo-control unit, and then servo-control motor starts. Confirming that the sample reaches residual condition, increase normal stress gradually up to 3.8kgf/cm^2 at constant rate and decrease to 0.5kgf/cm^2 again, then stop the servo-control motor. During shear test, stress path (relation between normal stress and shear resistance) is drawn continuously on computer display at real time.

Ring shear tests at shear speed of 0.1, 1, 10, 100 cm/sec follow after the test at 0.01cm/sec step by step. At each test, appropriate gear is selected and test is executed in same way except test at 100cm/sec. As it takes about some minutes to complete one cycle of a test, during which servo-control air regulator increases and decrease the normal stress, at the test of 100cm/sec sample sometimes leaks outside through the gap between the upper and the lower part of the sample box. It is difficult to keep running for long time at 100cm/sec. Then the test at 100cm/sec is done in different way, that for about only three or ten seconds the sample box is rotated for the discrete normal stresses of 0.5, 1.5, 2.5 and 3.5kgf/cm^2.

After shear test on each sample is completed, the upper unit, the upper part of the sample box and also the sample above the shear plane is removed and shearing plane of the sample is closely examined.

RESULT OF TESTS

Glass beads

Dry glass beads were tested under the normal stress up to 3.8kgf/cm^2. Figure 10 is the result of uniform dry glass beads of 0.2mm diameter. Ring shear test was executed at constant shear speed of 0.01cm/sec as the normal stress was increased gradually. Then, another test at faster shear speed (0.1, 1, 10, 100cm/sec, step by step) followed it in

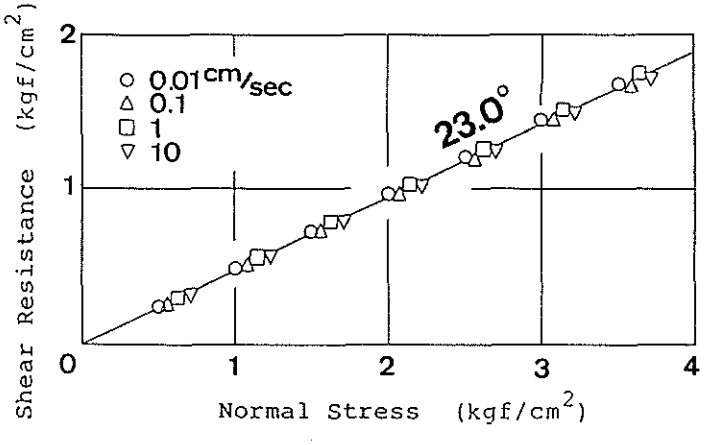

Figure 10—Result of high-stress high-speed ring shear tests on the 0.2mm glass beads. Void ratio during shear test: e=0.87~0.88.

the same procedure. So continuous normal stress–shear resistance relation was gained at each test. Plotted points in the figures of normal stress v.s. shear resistance in this paper are picked up from the recorded data at the normal stresses of every 0.5kgf/cm^2 between 0.5 and 3.5kgf/cm^2.

The friction angle scattered little, mean friction angle is 23.0°, being independent of shear speed of 0.01cm/sec to 10cm/sec. Test at 100cm/sec was carried out, but some sample leaked out of the sample box and the test was terminated. From the examination of sample after shear test, no grinding or crushing of the glass beads occurred.

Tennis court sands

Results of high stress ring shear test on dry tennis court sands are shown on Figure 11. It displays the relation between normal stress and shear resistance. The friction angle at the shear speed slower than 10cm/sec is 35.1°, but it decreases to 31.9° at 100cm/sec. After the test, removing the upper unit and the upper part of the sample box and cross section of the sample was closely examined. So much fine ground grains were observed on and near the shearing plane (Figure 13 (a) and (b)). Variation of grain size distribution between before and after the shear test are shown in Figure 12. Curve of after the test is that of

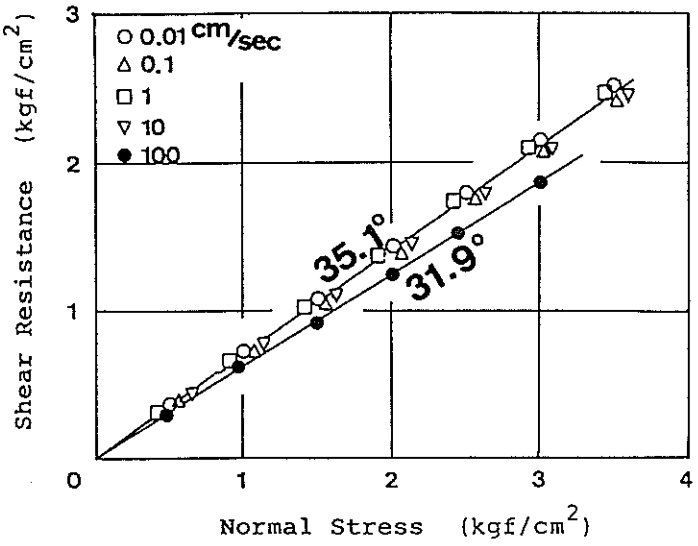

Figure 11—Result of high-stress high-speed ring shear tests on the dry tennis court sands in the university campus. Void ratio during shear test: e=0.51~0.68.

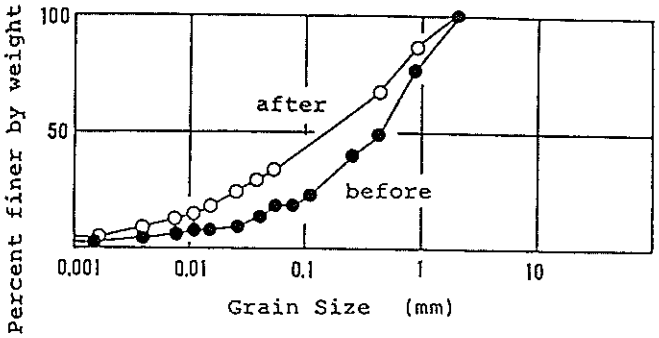

Figure 12—Grain size distribution of the tennis court sands. ●−● : before the test, ○−○ : after the test

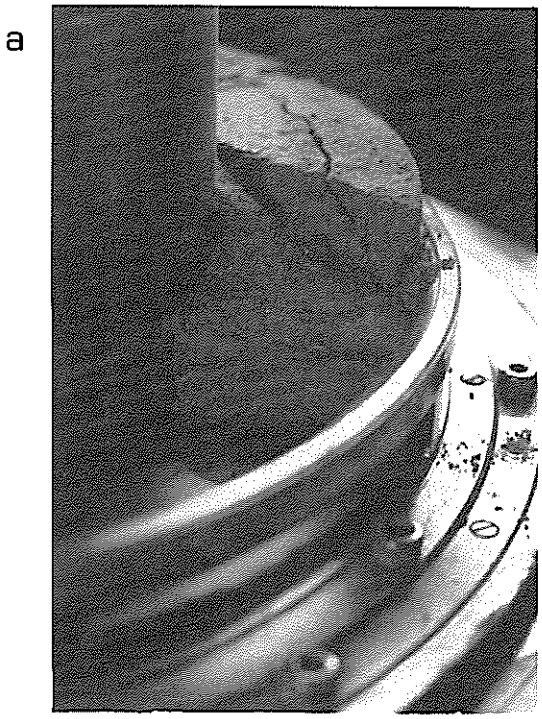

Figure 13 (a) The campus soils after test. (b) Well ground soil particles of the shear zone on the fingers.

the sample taken from fine ground grains around the shear plane. It shows clearly that shearing causes grinding of grains.

Toyoura Standard Sands

Figure 14 is the test results of the dry Toyoura standard sands at shear speed of 0.01~100 cm/sec. The test was done from the slowest speed of 0.01cm/sec to the highest speed of 100cm/sec step by step. The friction angle during shear increased from 31.7° to 33.8° under the respective shear speed. Thereafter, tests were continued at slower speeds; 1cm/sec, 0.1cm/sec, 0.01cm/sec step by step. These tests at reducing shear speeds were carried in

order to examine whether shear friction depends only on the shear speed or not. Results of the tests were shown on Figure 15. Change of the sample height which means change of the sample volume and friction coefficient which is tan ϕ_m (tangent of friction angle) versus shear speed is plotted. Plots with number of 1~5 are the same data of Figure 14. Plots with number of 6~8 are the results of successive tests following Figure 14. Sample height increased untill the test of No. 3 and then continued to decrease during tests of No. 4~7. Increasing process was maybe dilatancy of the sample. The decreasing process seemed to be owing to crushing of the sample. It is proved by the comparison of grain size distribution between before and after the test, shown in Figure 16. Smaller grains finer than 0.05mm which was not included in the sample before

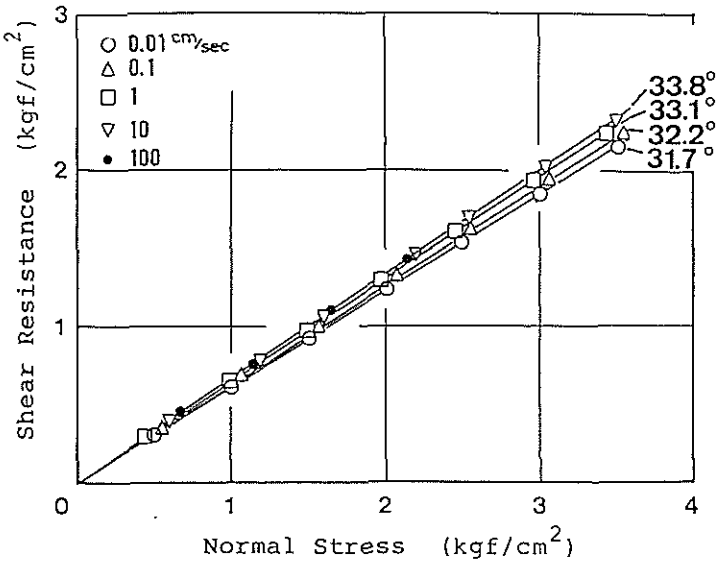

Figure 14—Result of high-stress high-speed ring shear tests on the dry Toyoura standard sands. Void ratio during shear test: e=0.65~0.83.

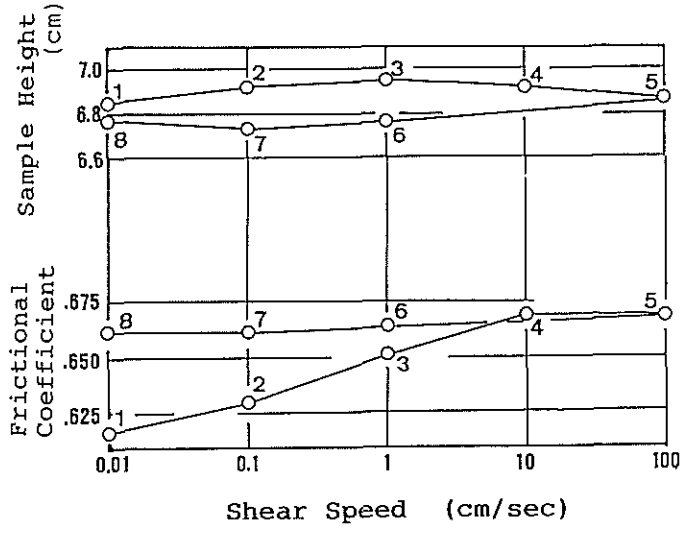

Figure 15—Shear speed v.s. sample height and frictional coefficient relationship for the dry Toyoura standard sands.

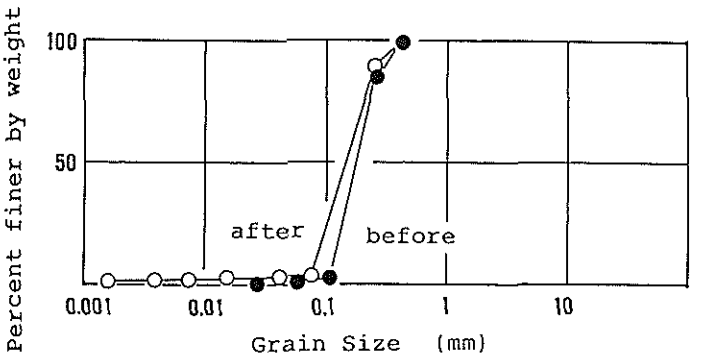

Figure 16. Grain size distribution of the Toyoura standard sands. ● – ● : before the test, ○ – ○ : after the test

the ring shear test appear in the distribution curve of the sample after the test. Although Figure 16 is not comparison of the sample of shear plane, but of total sample, it is obvious that grain crushing occurred in the sample. Friction coefficient tends to increase during the tests of No. 1~5 and almost keep constant (or slightly decreased) during the tests of No. 6~8.

Bentonite Clay

Test result of ring shear tests on the bentonite clays is shown in Figure 17. It showed the greatest difference of friction angle with the change of shear speed. The friction angle was 28.6° at the first test with shear speed of 0.01cm/sec. And then it varied as 34.1° at 0.1cm/sec, and 34.8° at 1 and 10cm/sec. In this test, test at the speed of 0.01cm/sec was executed again after the test at 10cm/sec. But the friction angle remained almost same with that at 10cm/sec speed.

Figure 18 shows the entire process of shear test at shear speed of 0.1cm/sec. The normal stress increased up to 3.5kgf/cm² and decreased again. Shear resistance also changed in proportion with the normal stress. The most important is the behavior of the friction coefficient, namely tangent of friction angle (tan ϕ_m). It increased with increase of normal stress (during the shear displacement of 0~20cm)

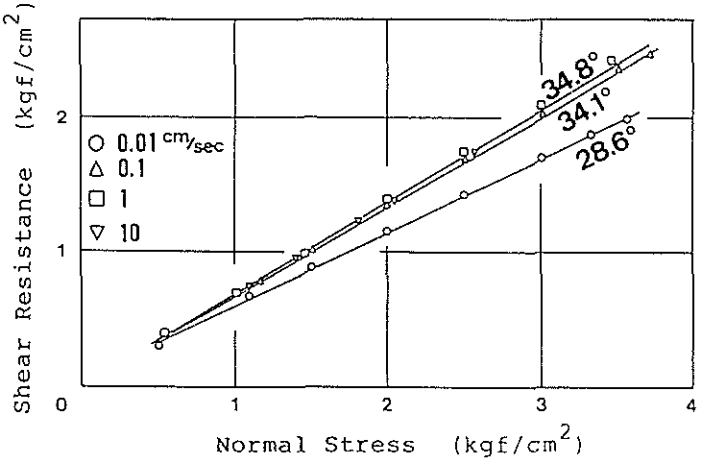

Figure 17—Result of high-stress high-speed ring shear tests on the dry bentonite. Void ratio during shear test: e=1.74~2.04.

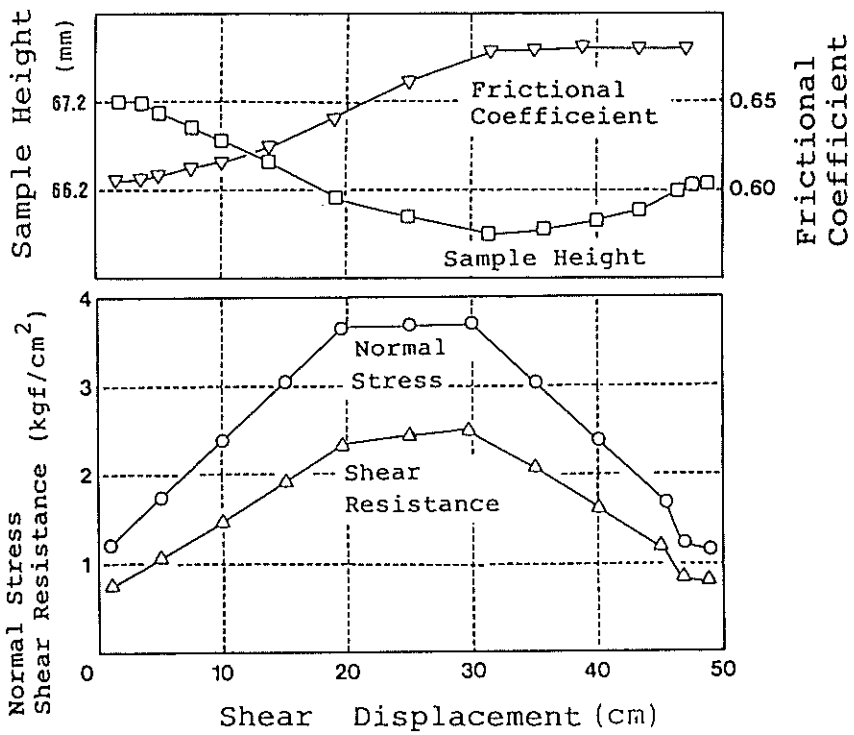

Figure 18—Variation of frictional coefficient, sample height, shear resistance during a cycle of test. (shear velocity:0.1cm/sec)

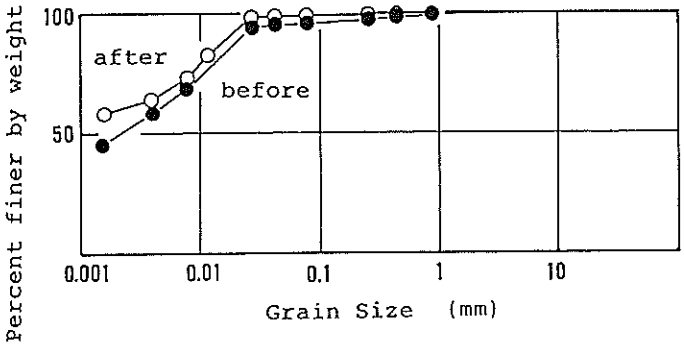

Figure 19—Grain size distribution of the dry bentonite. ● – ● : before the test, ○ – ○ : after the test

and also while the normal stress kept constant peak (shear displacement of 20~30cm). While the normal stress is decreasing, the friction coefficient remained constant (shear displacement of 30~45cm). The sample height decreased during shear and didn't recover the initial height at the end of the test.

Figure 19 is the comparison of grain size distribution of bentonite sample between before and after the test. This is from the sample of shear zone. It still clearly exhibited the effects of grain crushing through shearing.

Influence of Grain-crushing on the Friction Angle during Shear

The results shown above by the High-Speed High-Stress Ring Shear Apparatus suggest that friction coefficient may be affected by crushing (grinding) of grains at increasing

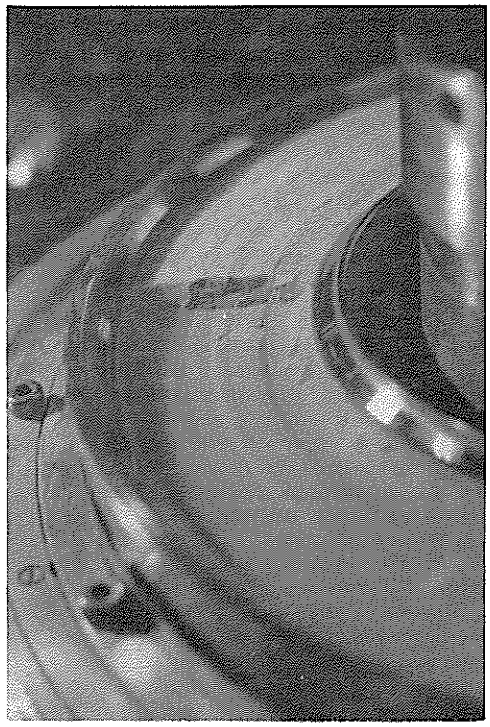

Figure 20—Bentonite sample after ring shear tests, showing polished and striated slip surface (upper portion of the sample is removed).

process of normal stress. And high speed shearing may have worked for a rapid crushing. We observed heavily crushed grains in shear zones after the tests of each sample except the glass beads. Glass beads are enough strong not to be crushed under the normal stress of the apparatus and the friction angle does not change with shear speed.

Here, we suppose two factors influencing the variation of friction angle during shear caused by grain crushing. One is the variation of grain size distribution and another is the variation of grain shape, i.e. round or angular.

As for the variation of grain size distribution, crushing of grains during shear, especially in the material of uniform grains makes a lot of finer grains and the sample becomes wider in grain size distribution. It should increase the density of the sample and the interlocking between grain particles. Increase of density of soils usually causes increase of internal friction angle. This seems to be the reason why the friction angle increased in the test of Toyoura standard sands and bentonite clays.

However, in the test on the tennis court sands, the friction angle at a high speed shearing decreased in spite of occurring of grain crushing. What can be the cause of this is not clear at present, but one possibility is the shape of grains. The initial shape of Toyoura sands which were from beach was round, so crushing can make them angular. So the variation of grain shape in the Toyoura standard sands didn't act for decreasing of the friction angle and so the factor of variation of density had to be dominant. We could not observe the initial and sheared grain shape of bentonite clays by eyes, then the influence of the variation of grain shape on the friction angle of bentonite clays was unknown.

On the contrary, the tennis court sands were mountain sands, the initial shape was rather angular, so crushing

could increase the roundness of grains. Because sample of round grains usually have smaller friction angle than that of angular grains, crushing of grains during shear can reduce the friction angle. It can be one interpretation.

ACKNOWLEDGMENTS

We thank Professor Michiyasu Shima, Disaster Prevention Research Institute, Kyoto University, for his supervision and cooperation to our research. We acknowledge Dr. Christophe Vibert from Ecole des Mines, Paris for his cooperation to the high-speed ring shear tests.

REFERENCES

Bishop, A. W.; Green, G. E.; Garga, V. K.; Andresen, A.; Browns, J. D. 1961. A new ring shear apparatus and its application to the measurement of residual strength. Géotechnique 21(4): 273–328.

Hungr, O.; Morgenstern, N. R. 1984. High velocity ring shear tests on sand. Géotechnique 34(3): 415–421.

Kaibori, M. 1986. Study on the movement of the slope failure materials. Doctor thesis for the Faculty of Agriculture, Kyoto University.; 99 p.

Sassa, K. Computer simulation of landslide motion. 1990. In: Proceedings, XIX World Congress of the International Union of Forestry Research Organizations, volume 1; 351–362.

Sassa, K. and others. 1984. Development of ring shear type debris flow apparatus: Report of Grant-in-Aid for Scientific Research by Japanese Ministry of Education, Science and Culture (No.57860028). 30p.

Sassa, K. 1988. (Special Lecture) Geotechnical Model for the Motion of Landslides. In: Proceedings, 5th international symposium on landslides, volume 1; 1988 July 10–15; 37–55.

also In: Bonnard C., editor. Landslides. Rotterdam: A.A. Balkema Co., Inc.; 37–55.

Vibert C.; Sassa, K.; Fukuoka, H. 1989. Friction characteristics of granular soils subjected to high speed shearing. In: Proceedings of the Japan-China symposium on landslides and debris flows, volume 1; 1989 October 3 and 5; Niigata and Tokyo: The Japan Landslide Soc. and The Japan Soc. of Erosion Control Engineering.; 295–299.

Morphological Study on the Prediction of the Site of Surface Slides[1]

Hiromasa Hiura[2]

Abstract: The annual continual occurrence of surface slides in the basin was estimated by modifying the estimation formula of Yoshimatsu. The Weibull Distribution Function revealed to be usefull for presenting the state and the transition of surface slides in the basin. Three parameters of the Weibull Function are recognized to be the linear function of the area ratio a/A. The mapping of the hazardous zones could be successfully done using the stream line distribution map and the relief map.

Sediment yield produced by frequent surface slides on the mountain slopes of granitic rocks become as dangerous as those produced by gigantic landslides or large scale slope failures, because of the high frequency of occerrence in a basin in spite of the dimension.

It is recognized that surface slides will occur on the mountain slopes of every geology. As for the investigations on surface slides, almost all papers in Japan deal with surface slides which occur on the mountain of granitic rocks which are often severely weathered and distribute widely in the south-western district of Japan and disasters due to this geology occur frequently on the occasion of heavy rain which will be brought about by the typhoon or the frontal storm.

ESTIMATION FORMULA OF SURFACE SLIDES

In order to express the condition of the occurrence of surface slides in a basin, usually the parameter a/A; the ratio of the total area of surface slides to the area of a basin (the terminology "area ratio" is used hereafter)is used. In most of the studies concerning the occurrence of surface slides, efforts were made to express the area ratio as the function of the precipitation and formulas by Uchiogi(1) and Yoshimatsu(2) are the presentative ones. Here, the formula below by Yoshimatsu is taken to be discussed.

$$a/A = K \times Rr \times (R-r)^{1.5} \quad \text{------ (1)}$$

where, "R" is the amount of precipitation of one continual rain which has led to the disaster occurrence of surface slides, "r" is the invalid limited precipitation being of no effect on the occurrence of surface slides, Rr is the relief ratio and K is the coefficient.

In Table 1, values concerning the above formula by Yoshimatsu are indicated;area of the basin, total area of surface slides in the basin, area ratio and relief ratio and Figure 1 shows the relation between the area ratio and the amounts of continual precipitation both for measured and calculated are shown, and both values show good conformity.

Table 1--States of the occurrence of surface slides due to heavy rain(by Yoshimatsu(2))

(i)R.Kamanashi basin

Precipitation(mm)	Area of basin	Total area of slides	Area ratio	Relief ratio
275	4.58	0.0120	0.0026	0.38
300	3.46	0.0510	0.0147	0.51
325	7.67	0.1795	0.0234	0.51
350	13.98	0.5595	0.0400	0.47
375	16.65	0.7693	0.0462	0.57
400	13.27	1.1986	0.0903	0.67
425	6.11	0.9829	0.1609	0.76
450	5.68	0.9632	0.1696	0.80

(ii)R.Tenryuu basin

Precipitation(mm)	Area of basin	Total area of slides	Area ratio	Relief ratio
350	2.00	0.0140	0.0070	0.24
375	5.66	0.0907	0.0160	0.27
400	5.26	0.1230	0.0234	0.24
425	7.72	0.4284	0.0555	0.36
450	12.87	0.7627	0.0593	0.38
475	15.84	1.2451	0.0786	0.36
500	10.05	1.0213	0.1016	0.34
525	7.99	0.8741	0.1094	0.30
550	14.17	1.8614	0.1314	0.30

(iii)R.Kizu basin

Precipitation(mm)	Area of basin	Total area of slides	Area ratio	Relief ratio
425	3.41	0.0446	0.0131	0.18
475	25.28	0.3257	0.0129	0.20
525	22.59	0.5110	0.0226	0.18
575	12.07	0.4371	0.0362	0.18

[1]XIX World Congress of IUFRO, August 5-11, 1990 Montral, Canada

[2]Associate Professor of Forestry, Kohchi Univ. Nangoku City, Kohchi Prefecture (before October 1990; Research Associate of Kyoto Prefectural Univ.)

(iv)R.Arita basin

Precipitation(mm)	Area of basin	Total area of slides	Area ratio	Relief ratio
575	10.49	0.0470	0.0048	0.29
600	32.01	0.1205	0.0038	0.33
625	14.97	0.0605	0.0040	0.38
650	13.24	0.1436	0.0108	0.43
675	9.59	0.1152	0.0120	0.44
700	7.69	0.1801	0.0234	0.35
725	4.02	0.1139	0.0283	0.32
750	1.84	0. 581	0.0316	0.32
775	0.97	0.0374	0.0386	0.33
800	1.50	0.0631	0.0421	0.33

The values of the relief ratio could be considered to have constant value when we think of it for a fixed basin. The value of the coefficient K can be the presentative constant of a basin and when the value of K is bigger, sediment yield due to surface slides or other mass movements seem rather vivid in the basin than others.

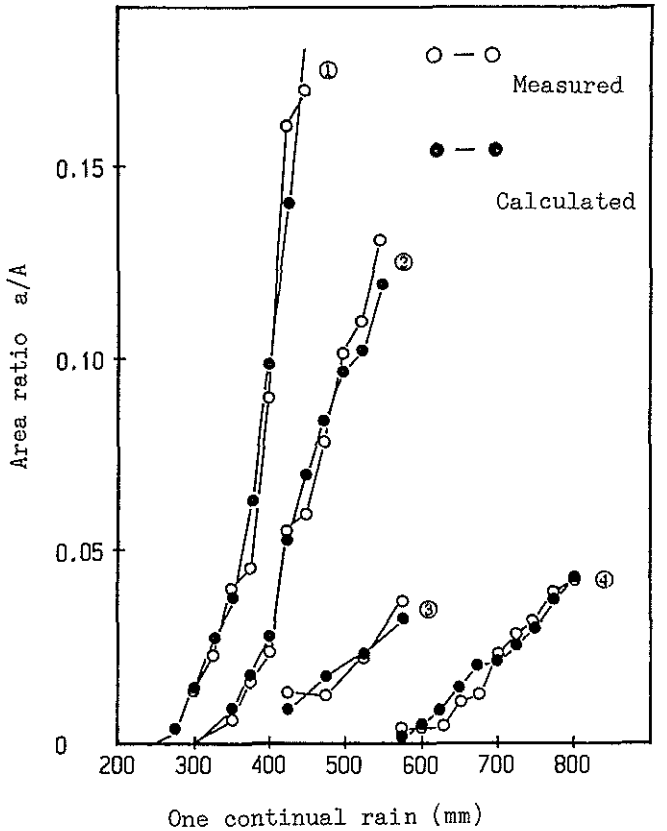

① R.Kmanashi $a/A = 0.8\times10^{-4}(R-250)^{1.5}\times Rr$
② R.Tenryuu $a/A = 1.0\times10^{-4}(R-300)^{1.5}\times Rr$
③ R.Kizu $a/A = 0.45\times10^{-4}(R-325)^{1.5}\times Rr$
④ R.Arita $a/A = 0.325\times10^{-4}(R-500)^{1.5}\times Rr$

Figure 1--Relation between the area ratio and precipitation of one continual rain

As a result, this formula represents only the state of the occurrence of surface slide and only represents that the more the the amount of precipitation augments, the bigger the value of the area ratio becomes. In other words, the temporal increase of the number of surface slides in a fixed basin can not be estimated.

As for the value of the invalid precipitation; r of these formula are determined by the data in order to reduce the formula and subsequently the precipitation of one continual rain which would lead to the occurrence of surface slides is not necessarily bigger than the derived "r" value. So, in the following part, in order to predict the amount of surface slides which will occur repeatedly in the same basin, derived value of "r" are not used, and treating "r" as a variable, determined it to suit the real state of the temporal increase of surface slides.

TRANSITION OF THE AREA RATIO IN A BASIN

Before discussing about the transitionsin of the value of area ratio, it is necessary to know the upper limited value of the area ratio. Figure 2 shows the relation between the total area of surface slides;a and the area of the basin;A. The oblique line in the Figure is the line when a/A = 1.0 and in this case, all part of the mountain of a basin is bare due to surface slides, consequently, the total area of surface slides should be plotted beneath the oblique line.

When the area of two basin are decided arbitrary and if there are no surface slides, the initial states are plotted on the abscissa as shown in Figure 2 by ○ and ●, and these two points move directly upwards as the total area of the surface slides increases. Even when the values of "a" are same for two different basins, the values of a/A differ to each other because of the value of the area of the basin are not the same. In this condition, the larger the area of the basin becomes, the less the value of a/A becomes. Subsequently, in the case of discussing exactly about the area ratio, the value of the area of basins should be made uniform. But, to discuss about it here is not the aim of this paper, the author only point out the importance of this subject.

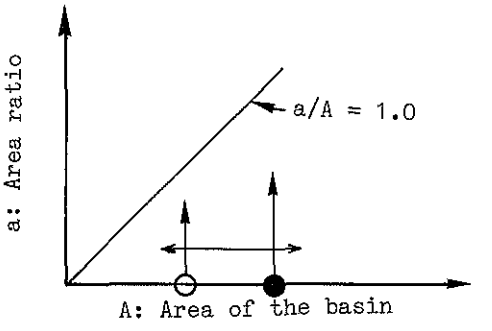

Figure 2--Relation between the total area of surface slides and the area of the basin

Figure 3 and 4 show the relation between the total area of surface slides and the area of the basin by the author and Yoshimatsu respectively. As shown in both figures, common envelope curves are drawn and in this case, the value of the area ratio is 1.5 and this value can be the upper limited value of the area ratio. This value coincides with that of the R.Kamanashi basin which is given by Yoshimatsu, though the conditions of the occurrence of surface slides seems extremely ruined condition.

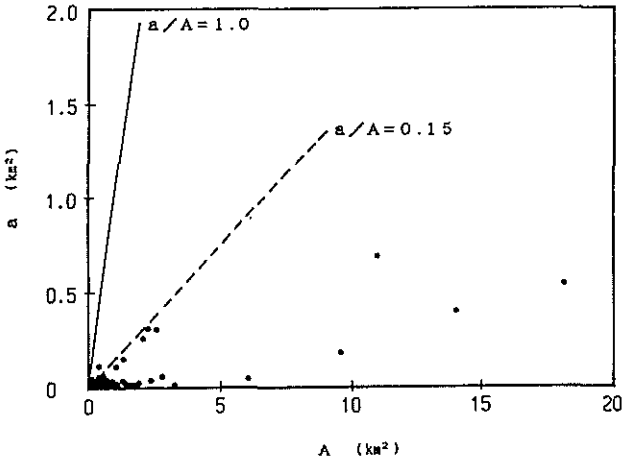

Figure 3--Relation between the total area of surface slides and the area of the basin by Hiura

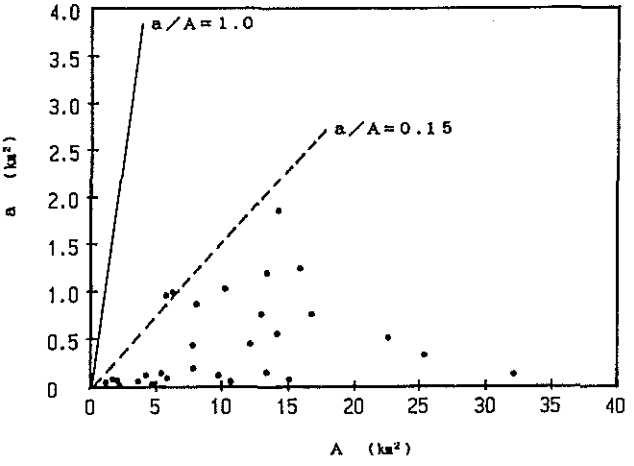

Figure 4--Relation between the total area of surface slides and the area of the basin by Yoshimatsu

Transition of the number of surface slides

Figure 5 shows the yearly fluctuation of surface slides of the Tsuchiyabara district(R.Kizu). As seen in Figure 5, the values of the area ratio tends to increase and converge to a final value. The values of the area ratio in 1971 and 1976 are indicated below;

Year	Area ratio
1971	0.0450
1976	0.0492

and the maximum precipitation of a year during 1971 and 1976 are as follows;

Year	1971	1972	1973	1974	1975	1976
Precp.(mm)	166.3	203.0	133.1	144.0	157.5	240.0

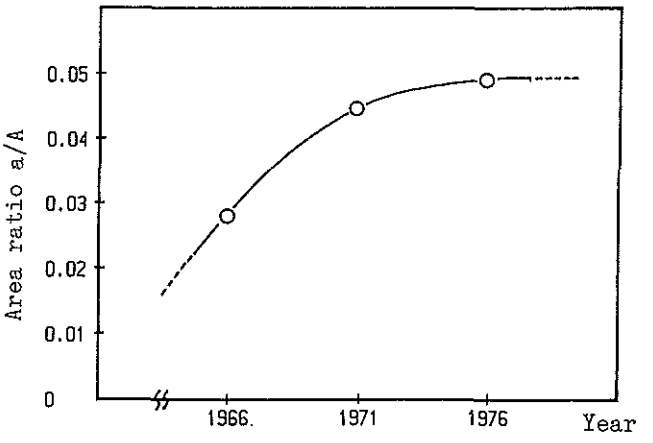

Figure 5--The yearly fluctuation of the area ratio of R.Kizu basin

These values do not exceed the invalid precipitation 325mm which is presented by Yoshimatsu. Thus, it is clear that the formula can not be used for the estimation of the yearly increment of the area ratio. So, as mentioned above, taking the invalid precipitation as a variable, and dividing precipitation into two groups;R>200mm and R<200mm and assuming the value of the area ratio to be a/A =0.0012 and 0.0006 correspondingly to the precipitation respectively. The results of the estimation of the invalid precipitation are indicated in Table 2 as well as the maximum precipitation, the difference of both precipitations;the valid precpitation;(R-r) and the area ratio. As the mean value of the area of the basin is approximately ten km from Table 1, then annually fifty slides when R>200mm and twenty-five slides when R<200mm will occur accoding to the estimation of this paragraph and these values seem reasonable.

Table 2--Maximum continual precipitation;R, area ratio;a/A, invalid precipitation;r and valid precipitation;(R-r) for Tuchiyabara district(R.Kizu basin)

Year	Maximum continual precip.	Invalid precip.	Valid precip	Area ratio
1972	203.0(mm)	175.5(mm)	27.5(mm)	0.0012
1973	133.1	115.8	17.3	0.0006
1974	144.0	126.7	17.3	0.0006
1975	157.5	140.2	17.3	0.0006
1976	240.0	212.5	27.5	0.0012

PRESENTATION OF THE STATE OF SURFACE SLIDES IN USE OF THE WEIBULL DISTRIBUTION FUNCTION

It was recognized above that the state of the occurrence of surface slides in a basin at an arbitrary state can be expressed by the area ratio which is the function of the precipitation. On the other hand, the Weibull Distribution Function which the author has employed has successfully presented the state of the yearly fluctuation of surface slides(3). Here, by combining both method, the hazard mapping of surface slides is presented.

Firstly, the foregoing results are summarized and then the method for mapping is presented. It is natural that the value of area ratio of a basin differs to each other according to the difference of the state and history of the occurrence of surface slides in a basin. The Weibull Distribution Function is one of the statistic density functions and originally adopted for the treatment of the experimental data and because of its easiness and conformity, it has come to be used frequently. The formula of this function is expressed below;

$$f(x)=m\alpha^{-m}(x-\gamma)^{m-1}\exp(-((x-\gamma)/\alpha)^{m}) \quad \text{--- (2)}$$

Three parameters included are the location parameter: γ, the scale parameter: α and the shape parameter:m respectively. Thus, the state of the distribution of surface slides of a basin at an arbitrary time can be expressed by these three parameters. The author has already recognized that when the number of surface slides increase yearly in a basin, α and m increase, but γ decreases, and confirmed that the values of three parameters fluctuate in accordance with the transition of the slide numbers.

Area ratio and Weibull parameters

Table 3 indicates the number of slides, the area ratio a/A and values of three parameters of five survey basins(Figure 6). These basisns have different situations concerning the occurrences of surface slides;for exemple:numerous slides have just occurred, the number of slides is increasing or decreasing and so on. Figure 7 shows the relation between Weibull parameters and area ratio . The scale parameter α and the shape parameter m increase with the increase of a/A, and location parameter γ decreases inversely. So, the conditions of the occurrences of surface slides could be presented by a set of Weibull parameter values at an arbitrary value of a/A and in that case, the scale parameter is the most effective one. Following formulas to calculate Weibull parameters using the value of the area ratio were derived using data in Table 3.

$$\alpha = 37.5091(a/A)-0.1272 \quad \text{---------(3)}$$
$$m = 18.2635(a/A)+0.4645 \quad \text{---------(4)}$$
$$\gamma = -10.5580(a/A)-0.0614 \quad \text{---------(5)}$$

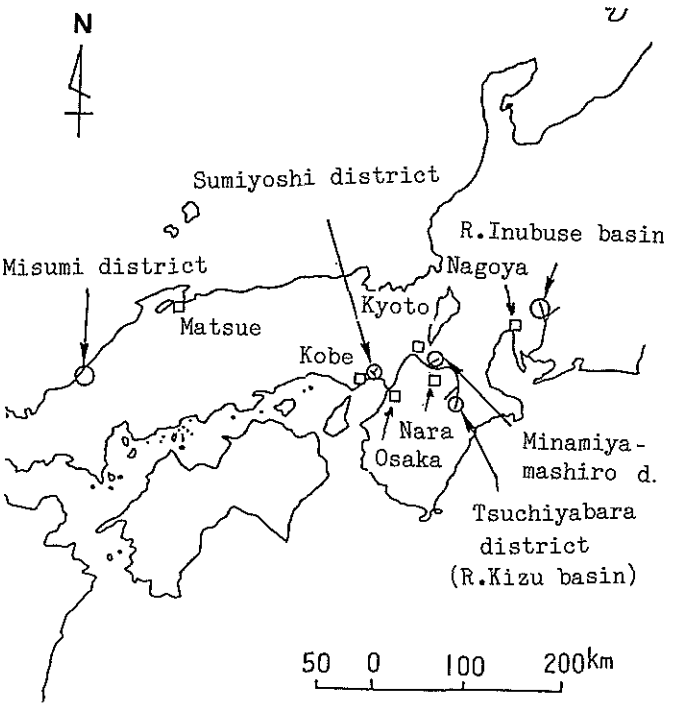

Figure 6--The location map of the survey areas

Table 3--Yearly fluctuation of Weibull parameters

(i)Tsuchiyabara district

Year	Total number of slides	Area ratio	Parameter α	m	γ
1966	1109	0.0282	1.011	0.994	-0.353
1971	1768	0.0450	1.573	1.155	-0.441
1976	1936	0.0492	1.802	1.240	-0.528

(ii)Minamiyamashiro district

Year	Total number of slides	Area ratio	Parameter α	m	γ
1954	1725	0.0254	1.030	1.059	-0.412
1963	2435	0.0359	1.346	1.162	-0.437
1971	1745	0.0257	0.983	1.039	-0.368
1983	614	0.0090	0.324	0.732	-0.182

(iii)Sumiyoshi district

Year	Total number of slides	Area ratio	Parameter α	m	γ
1966	937	0.0196	0.685	0.801	-0.316
1967	1296	0.0403	1.587	1.215	-0.544
1971	623	0.0130	0.448	0.771	-0.216

(iv)Misumi district

Year	Total number of slides	Area ratio	Parameter α	m	γ
1976	355	0.0007	--	--	--
1983	6396	0.0117	0.468	0.836	-0.239

(v)R.Inubuse basin

Year	Total number of slides	Area ratio	Parameter α	m	γ
1964	1321	0.0049	0.067	0.000	0.116
1972	4054	0.0151	0.626	0.934	-0.291

SIMULATION OF THE FUTURE SLIDE DISTRIBUTION AND MAPPING

Of five districts investigated hitherto, in the case of Tsuchiyabara district(R.Kizu basin), the number of surface slides continues to increase . So, the author tried to simulate the plane distribution of slides and to draw them on the map . The simulation was done according to the flow chart shown in Figure 8 and following procedures;

1) As a basis, the distribution map of surface slides existing in 1971 was used and the area ratio was a/A = 0.0450(Table 3). 2) Establish maximum precipitation of each year and calculate annual value of area ratio. 3) In five years from 1971 to 1976, the increment of surface slides is a/A = 0.0042. 4) Substituting a/A = 0.0450 into formulas;(3),(4) and (5), the values of parameters were calculated as follows: α = 1.718, m = 1.363 and γ = -0.581. 5) Calculate by the equation (2), the ratio of each mesh(75mx75m) containing zero to nine slides, and multiplying them by the total number of meshes of the basin(1678 for Tsuchiyabara district), the real number of each mesh is estimated. Table 4 indicates the values of real and estimated number of meshes. 5) Draw the distribution map indicating hazardous mesh suffering from the occurrence of surface slides by the number of slides in 1976.

Table 4--The estimated and real number of each mesh containing slides in 1976 (Tsuchiyabara district:R.Kizu basin)

Number of slides in each mesh	Real Number	Real Ratio	Estimated Number	Estimated Ratio
0	719	42.8	682	40.6
1	416	24.8	530	31.6
2	286	17.0	280	16.7
3	156	9.3	120	7.2
4	55	3.3	45	2.6
5	28	1.7	15	0.9
6	10	0.6	5	0.3
7	5	0.3	1	0.1
8	2	0.1	0	0.0
9	1	0.1	0	0.0
Total number of slides:	1936		1742	
Total number of meshe:	1678		1678	

Morphlogical analysis

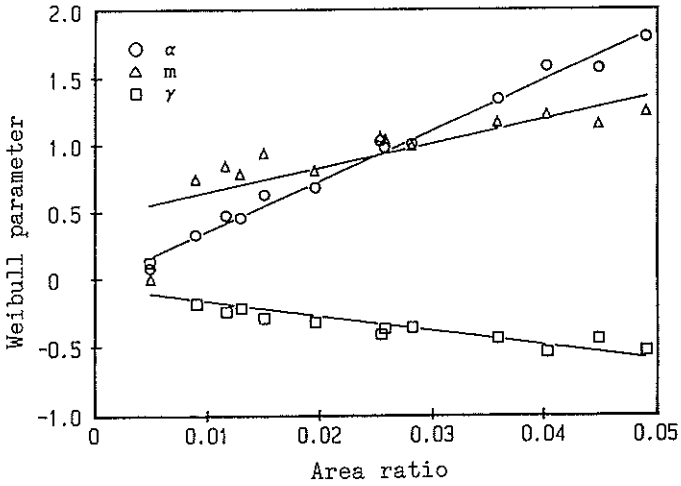

Figure 7--Relation between the Weibull parameter and the area ratio

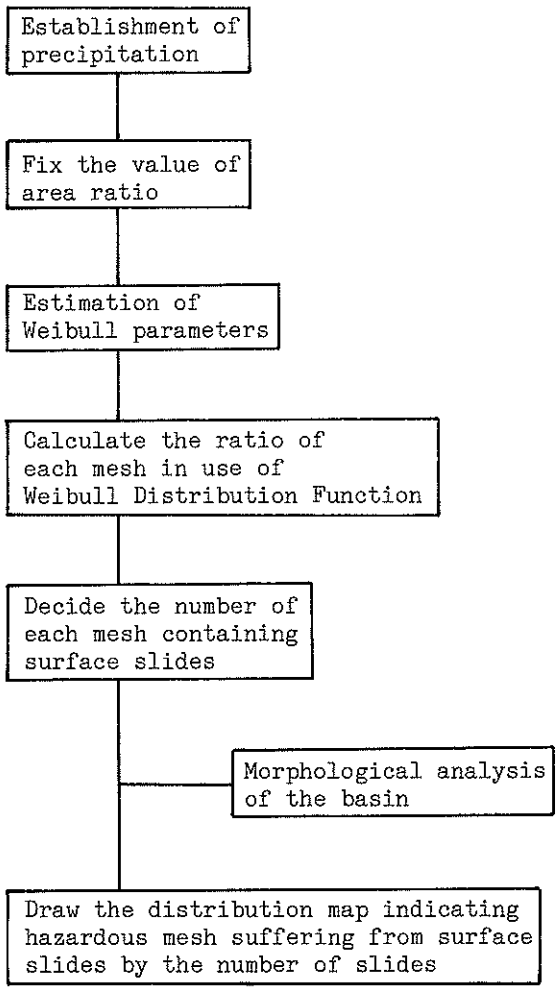

Figure 8--Flow chart to map the hazardous zone of surface slides

Before drawing the map, subsequent morphlogical analysis was done.

In general, a knick point in the longitudinal profile of a stream is recognized as the place

where mass movement occurs vividly and many slides also occur at this point. The knick point is located at the uppermost point of a river where a stream line disappear on the topographical map. A point of abrupt change of the inclination seen in the longitudinal profile of a slope can be the point of the occurrence of surface slides and this point can be distinguishes as where the relief of a mesh suddenly diminishes, in other words, the inclnation of the slope turns from steep to gentle when going upstream or going upwards on the slope on the relief map. In the first meaning, the stream line distribution map and in the second meaning, the relief map were used.

The mesh on which the knick point is found and the mesh whose relief indicates the steep inclination are not always the same. So, both when two conditions are overlapped and when either condition is satisfied, the increase of number of slides in the mesh is decided, the former preferentially. As the total number of the meshes is limited, the meshes which are to be increased were selected carefully considering the topographical conditions surrounding them.

Figure 9--Simulated distribution map of surface slides

Distribution map of the future slides

As for the total number of the surface slides, the real number exceeds the estimated value by 194 . This is due to the difference of the number of meshes containing more than three slides in them. The estimated number of meshes containing one slide in them is fairly large. The ratio of the estimated value to the real value is 1.3, so this value could be considered as the safty factor and to prepare for the dangerousness of the disaster using hazard map, this value never seem to indicate the excess value.

Figure 9 shows the numerical map of simulated plane distribution of slides. The circled numerals in Figure 9 are those who make good guesses. There are 600 meshes among 1687 meshes, of which the place of the occurrences of slides were guessed and the ratio of the guess is about 35.8pct. Of meshes containg zero slide, there are 350 meshes among 682 meshes could be guessed and in this case, the ratio is 51.3pct. Consequently, the simulation could be considered to be done successfully, considering the complexity of the process of the mass movement on the mountain slopes.

ACKNOWLEDGEMENTS

The author greatfully acknowledge the contribution given by M. Ken Ashida, Master of Agriculture of Kyoto Prefectural University, for his contribution to discussion and drawing figures.

REFERENCES

(1) UCHIOGI Tamao 1971. Landslide due to One Continual Rainfall. Journal of Japan Soc. of Erosion Control Eng.: No.79, 21-34
(2) YOSHIMATSU Hiroyuki 1977. The Estimation of Expression on Landslides. Journal of Japan Soc. of Erosion Control Eng.: No.102, 1-9
(3) HIURA Hiromasa 1988. Hazard Mapping in Use of Surface Slide Transition Model. 1988 International Symposion "INTERPRAEVENT 1988 - GRAZ"; 297-313

Experimental Study on Impact Load on a Dam Due to Debris Flow[1]

Iwao Miyoshi[2]

ABSTRACT

When a dam is struck by mud or debris flow, it is put under a great impact load and sometimes is destroyed. To prevent such destruction, it is important to perform basic research about the impact load on a dam due to debris flow.

Thus, we have made an experimental study and tried to establish a method to estimate such a impact load on the dam. The experiment was performed with glass beads of 5mm in diameter as bulk solid, in an open channel which is 7m in length, and 15cm in both width and depth. In these experiments, the load on the dam was measured by a dam-type load measuring device, and simultaneously the behavior of the debris flow was observed by a high speed video (200 frames per second). In the high velocity area, the load consisted of the dynamic pressure on the flow, and most agree at each point in time with the one assessed from the flow's momentum variation. However there is no method to estimate debris flow's momentum variation on an obstructed object. Consequently, a model is proposed to estimate quantitatively the deformation of the flow and the load on the dam. The results from the computer simulation of this model agree well with the experimental results.

INTRODUCTION

Debris flow is one of the most disastrous phenomena in mountain area. This is a flow of the mixture of soil, cobble, boulder, and water, that run down with great energy. The debris flow has given huge damage to our life. To prevent this kind of disaster, we have made great efforts, and have built a great number of dams, as one of these efforts. Dams have a certain effect on the control of sediment transportation, and usually the energy of the debris flow is attenuated or completely dissipated by the time it reaches a dam or by a dam itself. Recently in Japan, where steep mountains are close to cities, the debris flow is stopped by a dam directly. However, when such a flow strikes a dam, it generates a great impact load, sometimes destroying the dam. In such a case, the debris flow increases its energy by taking up the sediment and water on the dam and the situation becomes more dangerous. To prevent such accident, it is important to establish a method to estimate the impact load on a dam, when the debris flow strike it.

The impact load of debris flow can be roughly categorized in two groups by means of the generating mechanism (Mizuyama,1979). One is the load generated when boulders or floodwood in the flow hit the dams (solid impact load), and the other one is the load when the hydraulic bore of the debris as a fluid hits the dam (fluid impact load). The former tends to cause partial break of the concrete dam and the latter tends to cause large scale destruction of the dam. Therefore, from the stand point of disaster prevention, it is rather important to be able to estimate the fluid impact load.

In Japan, the dynamic fluid load of the debris flow that decides the design strength of the concrete dam is accounted for from the dynamic pressure of debris flow as the steady jet flow as seen in follow equation.

$$F = Dqv = DAv^2 \qquad (1)$$

where F is the load, D is the bulk densi-

1. Paper presented at the XIX World Congress of the International Union of Forestry Research Organizations, Montreal, Canada, August 5-11, 1990.
2. Department of Forestry, Kyoto University, Japan.

ty of the fluid, q is the discharge, v is the velocity, and A is the cross sectional area of the fluid. The dynamic pressure of the steady jet flow is the pressure on the wall during the steady jet flow changes its direction on the wall.

Several previous works on the impact load on fluid theory can be seen. But if the behavior of the debris flows different from that of regular jet flow, then reconsideration is required.

Hirao et al.(1970) made an experimental study on impulsive force on the bank due to hydraulic bore. In their experiment, the pressure on the wall, which was fixed in the channel in right angle, was measured, when it was hit by hydraulic bore of a few kind of fluid running down the channel. They reported that the measured load on the wall was 1.0-4.5 times lager than the load that calculated from the dynamic pressure of the flow as the steady jet flow. But the mechanism of load generation was not referred in this report. Miyamoto and Daido(1983) also studied on the impact load of mud-debris bore on the bank. In this work, the load was discussed theoretically and some experiments had be made. But some simplifications in their theory make it hard to apply to actual phenomena directly. Some more previous works on similar themes can be seen, but those are not enough to estimate the impact load of the debris flow yet.

In this paper, both the load and the behavior of the head part of debris flow is made clear on the basis of results of experiments and the load is discussed with the deformation of the flow head.

EXPERIMENT

A diagram of experimental apparatus is shown in Fig.1. The flow channel was made of steel and transparent acrylic board so that the side view of the flow can be observed. The size of the channel is 7m in length, 150mm in both width and depth. The channel bed was roughened by gluing glass beads (5mm in diameter) onto it. The channel's angle of inclination was 16 degree. Bulk solid were spherical glass beads with a diameter of 5mm and a specific gravity of 2.53. At the upper end of the channel, main and sub water supply device were attached, and at the bottom, dam-type load measuring instrument was set. The front face of the dam was at a right angle to the channel direction and the size of loading board is 120mm height and 150mm width. The load on the dam-type measuring instrument was measured by a dynamic strain meter and recorded by a oscillograph. As the same time, the side view of the flow on the dam was recorded by a high speed video recorder (200 frames per second).

The glass beads were put on the channel bed on the upper side of the dam making a movable bed 4m in length with 50mm depth. The glassbeads were saturated entirely by water from the sub water supply device, and then, the pre-determinded volume of water from the main water supply device was released all at once, and this forced the glassbeads from

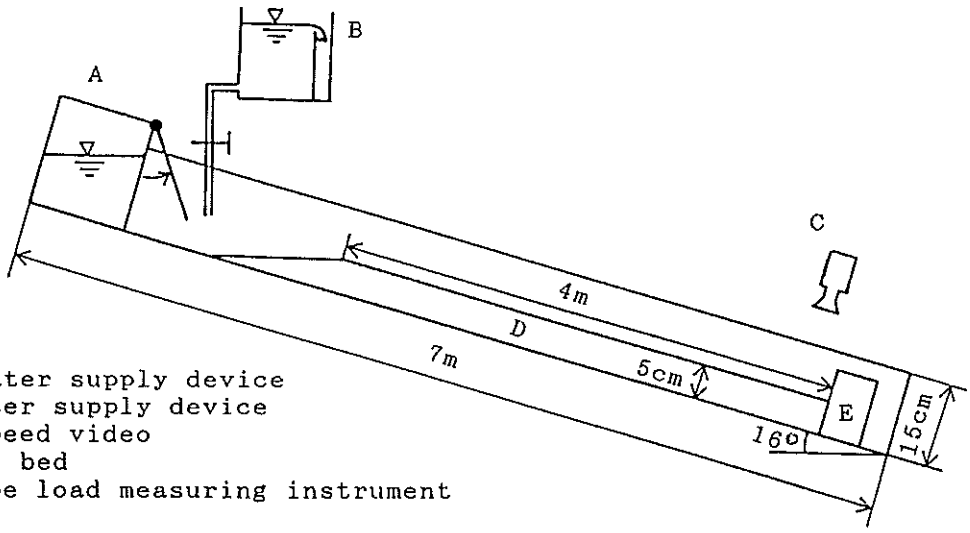

A : Main water supply device
B : Sub water supply device
C : High speed video
D : Movable bed
E : Dam type load measuring instrument

Fig.1 Diagram of experimental apparatus

the movable bed to move downstream as a debris flow. The velocity of the debris flow could be controlled by the volume of water in the main water supply device. The debris flow was checked by the dam at the bottom of the channel; the load on the dam was measured and the behavior of the flow was recorded from the channel side by the high speed video recorder. The record of both the load and the behavior of the flow were to be analyzed on the same axis of time. For this purpose, a pilotlamp was turn on in the site of the video recorder, and simultaneously in common circuit, a signal was sent to the oscilograph.

The flow's velocities were in the range of 0.4m/s to 2m/s. In all cases, distinct hydraulic bores could be observed and the flow could be considered as a steady flow at the dam point. The load on the dam measured in the experiment was recorded by the oscirograph. The measured loads can be classified in three types by the variation in time as shown in Fig.2. The load in type A has a clear peak in a very short time (from 0.01 to 0.07second) after impact; the load in type B also become maximum in very short time, but doesn't have a clear peak; the load in type C increases rather slowly. The relationship between the velocities and the measured maximum loads are shown in Fig.3. The measured maximum loads increased with the velocities and each type of the load has its velocity range. The morphology of the flow on the dam, when maximum load generated, varied with the velocity or/and type of the load. Fig.4 shows the side views of the each type's typical flow, when the maximum load was recorded. In the case of type C, when the maximum load generated, the dam was filled with debris. In this case, the load is relatively small and can be explained as the static load of debris. On the other hand, in the case of type A and B, in spite of rather larger maximum load, the static load is much smaller than that of type C. This means that, in the case of type A and B, the maximum load mainly consists of dynamic load. Consequently, it is important to estimate this dynamic load so as to estimate the impact load on the dam.

In general, the dynamic load of debris flow has been discussed in comparison with the dynamic load of the steady jet flow in the same profile. Fig.5 shows the relationships between the velocities and the maximum measured load per cross section of the bore. The broken line "P" in Fig.5 is the dynamic pressure of the steady jet flow, calcu-

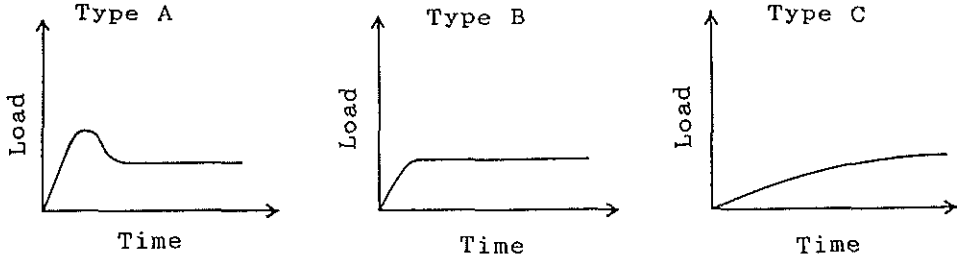

Fig.2 Type of load

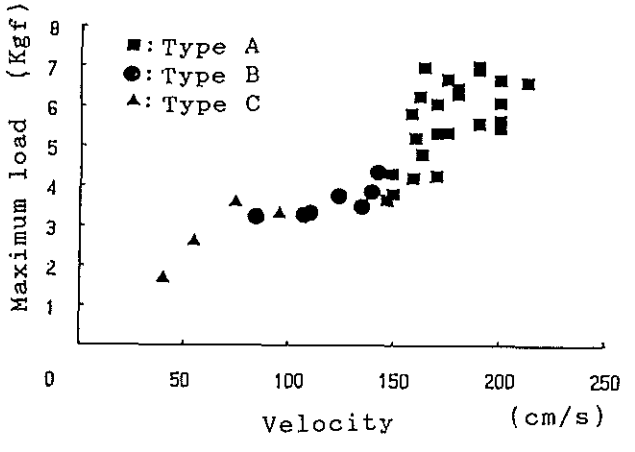

Fig.3 Relation between velocity and measured load

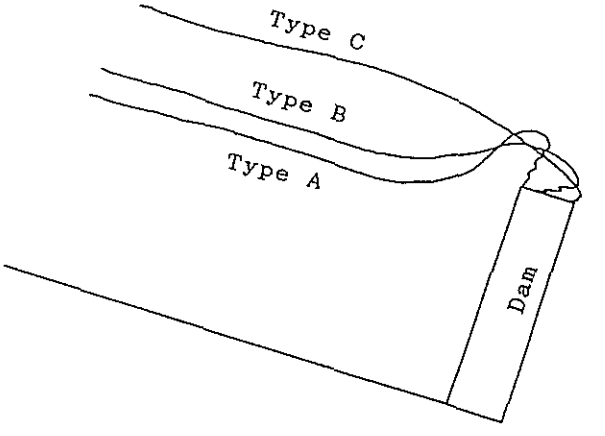

Fig.4 Flow morphology when maximum load generated

lated in the relationship of eq.(2).

$$P = Dv^2 \qquad (2)$$

The bulk density was determined to be $1.4gf/cm^3$ from results of preliminary experiments. This figure shows that the maximum load is larger than the one due to the dynamic pressure of steady jet flow at each velocity.

Fig.6 and Table 1 shows the variation of the form of flow's head part and the measured load. After impact, the debris flow change its direction along the dam-front surface just like the behavior of the jet flow. From 0.05 to 0.06 second after impact, the head part jumps up above the dam, and makes overflow. The maximum load measured at this point. Then the debris begins to stop and makes sedimentation from the corner between the channel bed and the dam face, and static part grows to the final sedimentation. The sedimentation makes the impact angle larger between the flow and the dam face and the load on the dam becomes smaller.

Fig.7 shows the relationship between the velocity and timelag (the difference of time between the moment at which flow's head touch the dam face and at which the load become maximum). The timelag seems to be in inverse proportion to the velocity. In other words, the length of the head part of the flow, that reach the dam until maximum load arises, is constant (about 10cm in this experiment), in spite of the difference in velocity. This means that the shape of the flow's head has an important role in the mechanism of load generation and that this part's properties should be adopted in estimating the impact load.

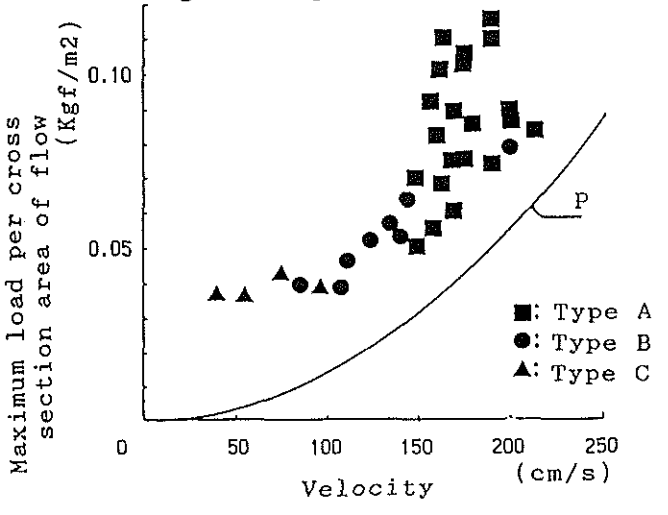

Fig.5 Relation between velocity and maximum load per cross secsion area of flow

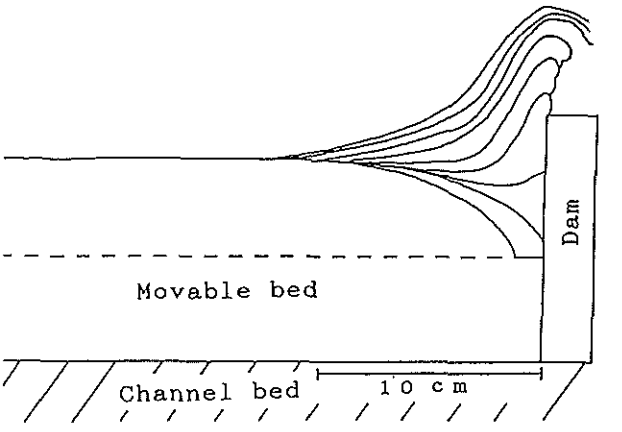

Fig.6 Morphological variation of debris flow's head at intervals of 0.01 second

Time (sec)	Load (Kgf)
0.01	1.66
0.02	4.04
0.03	4.26
0.04	4.78
0.05	5.21
0.06	5.46
0.07	5.15

Table 1 Variation of impact load with time

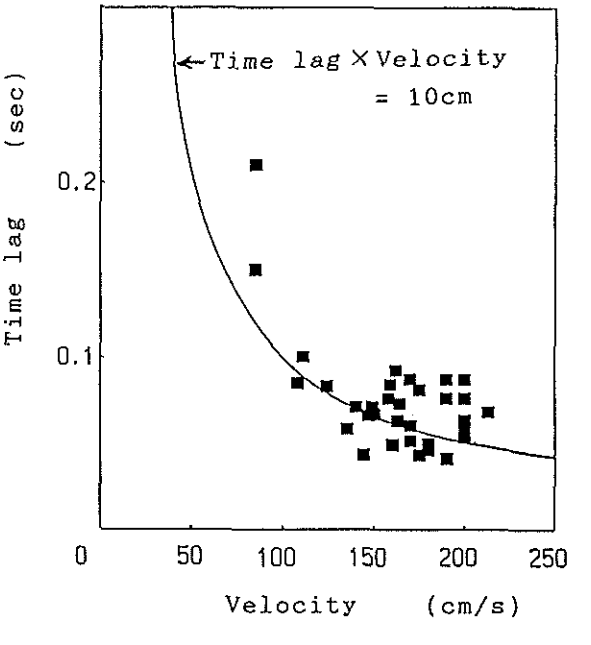

Fig.7 Relation between velocity and time lag

A DISCUSSION OF THE LOAD ON THE BASIS OF MOMENTUM VARIATION OF THE FLOW HEAD

In this chapter, the mechanism of load generation will be discussed in the relation with the variation of the load and the deforming process of the flow head.

If the flow is in a fully steady state before the impact point, the debris flow' head, that include enough part concerning the generation of the impact load, can be treated as a series of momentum points. On the assumption that the flow depth of this part is equal in each section, the discussion can be made in two dimension. Then, this part is expressed as a plane with some mass on X-Y two dimensional axis, as shown in Fig.8, and the surface line is described as a function h(x,t). At the time t, this fluid part exists in 0<x<xe, and the center of gravity on X axis xg is in the relation of

$$\int_0^{xg} h(x,t)(xg-x)dx = \int_{xg}^{xe} h(x,t)(x-xg)dx \qquad (3)$$

The center of gravity given by this equation varies with the deformation of the flow head, and is defined as a function of time xg(t). Then, the acceleration of the gravity center is also defined as a function of time ag(t) as

$$ag(t) = \frac{d^2xg(t)}{dt^2} \qquad (4)$$

It is the dam that gives the force which makes this acceleration, thus the load on the dam is described as follow.

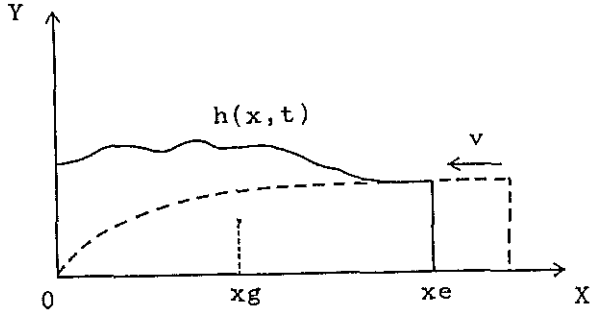

Fig.8 Model of flow head as a system of material points

$$F = DB \int_0^{xe} h(x,t)dt \cdot \frac{d^2xg(t)}{dt^2} \qquad (5)$$

where, B is the width of channel. As a consequence, the load on the dam is regulated by the function h(x,t) that express the surface line of the flow head.

These way of analysis was applied in results of the experiment. In this analysis, the head part of the flow, that include enough part concerning the generation of the impact load, is considered to be cut off and be independent from the following flow, as shown by the broken line in Fig.9(a). Fig.9(a) shows the morphology of the flow head at each 0.01 second interval after impact on the dam, that was observed in the experiment by the high speed video. The variation of the flow' gravity center is calculated from this morphological variation and the average loads that should be generated on the dam during each 0.01 second are

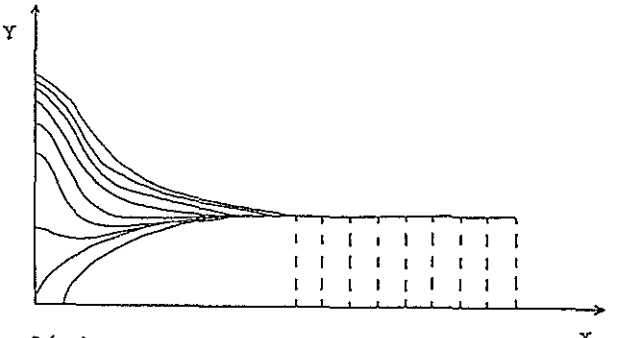

Fig.9(a) Behavior of the system of material points in flow's head at interval of 0.01 second

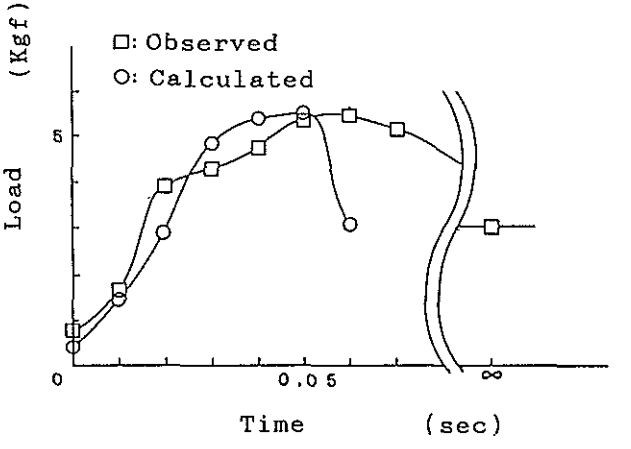

Fig.9(b) Relation between measured and calculated load

calculated from this and the bulk density. It is determined that the bulk density used in the calculation is to be $1.4 g/cm^3$. The comparison between the measured and the calculated load is shown in Fig.9(b). The two loads are in good agreement until the maximum point, and this means that the impact load of the debris flow is regulated by the deformation of the debris flow head. After the maximum point, the measured load becomes lager than the calculated one. This difference may be caused by the static load due to sediment of the debris.

FLOW MODELING AND COMPUTER SIMULATION

The impact load of the debris flow is regulated by the deformation of the debris flow head, as described in previous chapter. Therefore, the best method to roughly calculate the impact load is by estimating the deformation process of the flow head quantitatively using the initial conditions (flow velocity, flow depth, bulk density). Although h(x,t) may have complex form affected by many factors, here a simple model is proposed that is analogous to the behavior of a jet flow checked by a perpendicular wall.

In this model, some functions are prepared. The original flow depth is to be described as a function of the distance from the flow front H(x). The bulk density in each part of the flow is also to be described as a function of the distance from the flow front too, to take up the effect of the density distribution in x direction. As shown in Fig.10, the debris flow flows from x direction to y axis which represent the dam face with keeping initial velocity. The flow come to y axis and shift its position on the surface of original flow at each time in order from the front and, as a result of a series of this behavior, the fluid goes up to y direction along y axis. when the fluid shifts its position, each part of the flow changes its flow depth from H to Hd. Hd at each time is decided by R which is the ratio of Hd and H (R=Hd/H). R is also a function of the distance from the flow front. These functions of the distance from the flow front can be transformed to the functions of the time by means of velocity. Therefore the load on the dam and the morphology of the flow head at each time can be obtained by completing these functions of time as Ht(t), Dt(t), Rt(t). The load can be described as a function of time as

$$Ft(t)=Dt(t)Ht(t)Bv^2+\frac{Bv}{2}\cdot\frac{d}{dt}(Dt(t)Ht(t)^2Rt(t)) \quad (6)$$

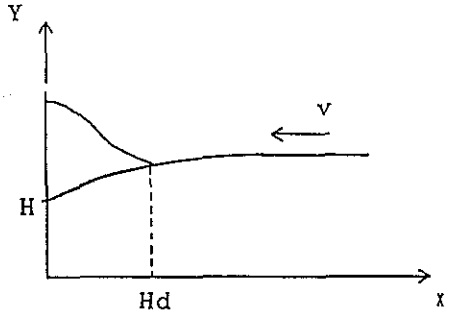

Fig.10 Flow deformation model

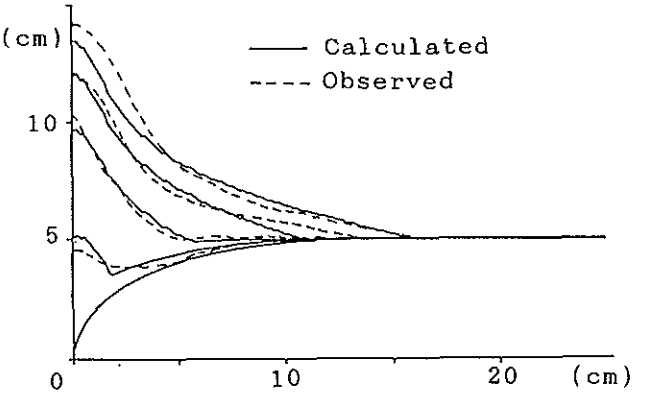

Fig.11(a) Comparison between observed and calculated morphology of debris flow head. (Each line indicates 0,0.1,0.3,0.5,0.7 second after impact)

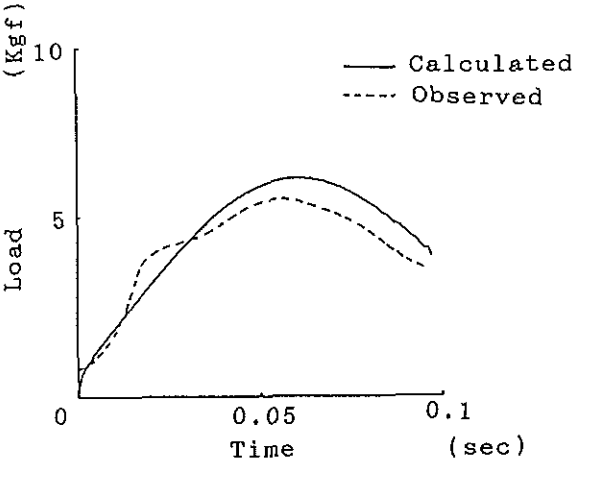

Fig.11(b) Simulated result of impact load on high velocity(1.70m/s).

After some transformations are made on this equation, the maximum load can be expressed by giving each value of composing functions Dt, Ht, Rt and their time differential functions (Dm, Hm, Rm, D'm, H'm and R'm respectively) at that time.

$$Fm = KDmHmBv^2 \qquad (7)$$

$$K = 1 + \frac{HmR'm}{2v} + \frac{RmH'm}{v} + \frac{D'm}{2Dmv} \qquad (8)$$

Where K is a coefficient that mean the ratio between the maximum load and the load by dynamic pressure of a steady jet flow in same profile.

Now this modeling is applied to the experiment. The composing functions are decided as follow.

H(x), the function that represents the flow depth, is to be described in a simple form that suits the morphology of the flow head in each experimental run, as follow

$$H(x) = \frac{H10+10a}{10^b} \cdot x^b - ax \qquad (9)$$

where, H10 is the flow depth at 10cm from the front; a and b are the parameters that are decided in each run for better suitabilities, which have the range of 0.5-0.7 and 0.6-0.7 respectably. This function is applied to about 20cm length in the flow front. D(x), the function that represents the bulk density in each part of the flow, is decided on the basis of the preliminary experiment, as a empirical equation.

$$D(x)=0.4+(0.15x)0.5-0.025x \qquad (10)$$

R(x) is the function that represents the deforming property of the flow, and also considered to express the ratio between the velocity components rise along the dam face and these which turn back to upstream after impact. This function is also decided so as to suit the experimental result.

Fig.11 is the comparison between the observed and the calculated morphology of the flow's head and the load on the dam. The velocity of this flow is 170cm/s a 1 the flow depth at 10cm from the front is 4.8cm and parameter a and b in equation (9) are 0.5 and 0.6 respectively. The function R(x) used in this calculation is

$$R(x)=1.7+0.07x-1.1\cos(0.2x) \qquad (11)$$

In this function, the x is given in cm unit. This function of the distance is

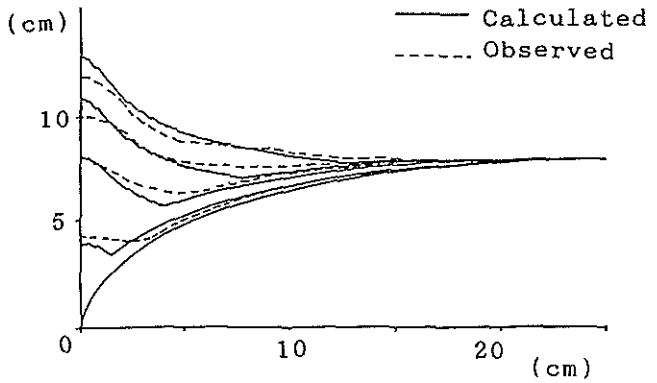

Fig.12(a) Comparison between observed and calculated morphology of debris flow head. (Each line indicates 0,0.1,0.3,0.5,0.7 second after impact.)

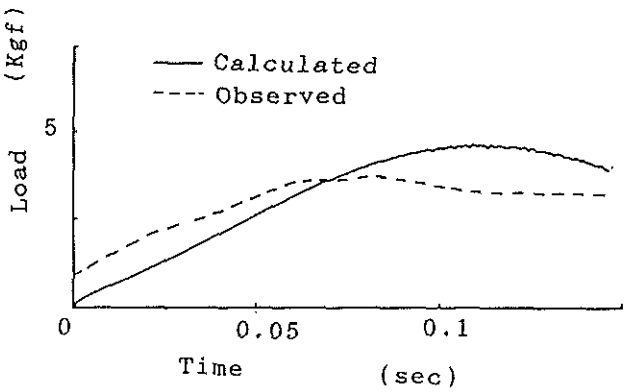

Fig.12(b) Simulated result of impact load on low velocity.

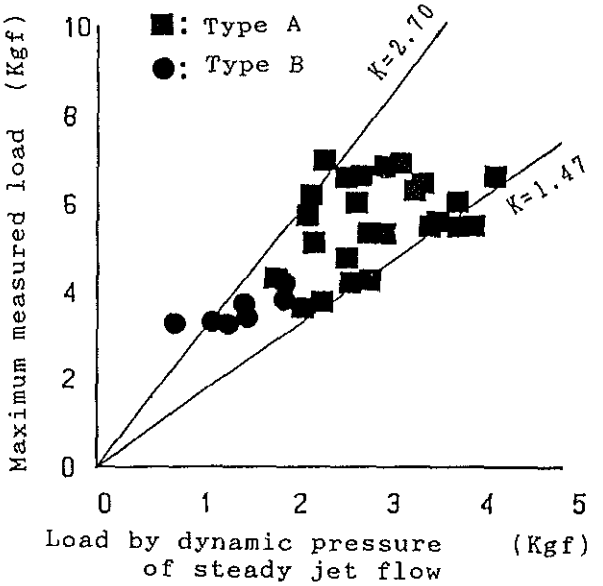

Fig.13 Relation between load by dynamic pressure of steady jet flow and measured load.

transformed to function of the time with the velocity (170cm/s) as

$$Rt(t)=1.7+11.9t-1.1\cdot\cos(34t) \quad (12)$$

Both the deforming process of the flow and the load on the dam are well simulated. Fig.12 is the simulated result of another experimental run, by same R(x). The velocity of this flow is 108cm/s, and the flow depth at 10cm from the front is 6.3cm, and the parameters of the flow depth function a, b are 0.7 and 0.7. The calculated results can be said to agree well with the observed one in spite that function R(x) is decided to suit for other experimental run. The difference of the load between the calculated and the observed after the maximum point is most likely caused by the effect of overflow above the dam, which is ignored in this model.

The estimation of the maximum load is one of the most important problem in the practical aspect. The maximum load can be estimated with the model and the functions above. With these functions and the condition that the maximum load arises when vt=10cm in this experiment (see Fig.7), eq.(9) is transformed to

$$K = 1.013+2.86a(b-1)+(0.135+0.286b)Hm \quad (13)$$

Since Hm is in the range of 4.1-6.3 and parameter a is 0.5-0.7, b is 0.6-0.7 as the results of the experiments, K should be in the range of 1.47-2.70. Fig.13 is the relationship between the load by the dynamic pressure of steady jet flow and the maximum measured load. The calculated value of K expresses the entire tendency of the experimental results.

CONCLUSION

The impact load on the dam when debris flow strikes it was measured and the behavior of the flow was observed in the experiment. In the low velocity area, the measured load could be explained as the static load by the sediment of debris. On the other hand, in the high velocity area, the measured load was rather great and corresponded to the momentum variation of the debris flow head. Then a model was proposed that estimate the characteristic momentum variation of the debris flow. Both the load on the dam and the deformation process of the flow could be well simulated by means of this model. The measured maximum load was 1.47-2.70 times larger than the load by the dynamic pressure of the steady jet flow in same profile of each debris flow.

In this way, the impact load on the dam due to debris flow has been made clear and, although more investigation will be required to apply this model to practical situations, the impact load can be estimated at least on an experimental level.

REFERENCES

Hirao,K. et al 1970. An Experimental Study on Impulsive Force due to Hydraulic Bore. Journal of Japan Society of Erosion Control Engineering No.76 : pp.11-16.

Miyamoto,K. and Daido,A. 1983. Study on the Impact load of Mud-Debris Bore on the Bank. Memoirs of the Research Institute of Science and Engineering, Ritumeikan Univ. No.42. : pp.61-79.

Miyoshi,I. and Suzuki,M. 1990. Experimental Study on Impact Load on a Dam Due to Debris Flow. Journal of the Japan Society of Erosion Control Engineering No.169. : pp.11-19.

Mizuyama,T. 1979. Estimation of impact force on dam due to debris flow and its problems. Journal of the Japan Society of Erosion Control Engineering No.112 : pp.40-43.

Sediment Dynamics of a High Gradient Stream in the Oi River Basin of Japan[1]

Hideji Maita[2]

Abstract: This paper discusses the effects of the valley width for discontinuities of sediment transport in natural stream channels.

The results may be summarized as follows: 1)In torrential rivers, deposition or erosion depend mostly on the sediment supply, not on the magnitude of the flow discharge. 2)Wide valley floors of streams are depositional spaces where the excess sediment from the upper stream area is temporarily deposited. In the erosional process that follows, the sediment runs off down stream in a way that can be explained by an exponential process.

Numerous researches in the area of sediment control work in mountainous areas have been carried out. However, our understanding of the effect of discontinuities in the history of sediment transport is still insufficient. In order to gain a fuller understanding, it is first necessary to examine the morphology of streams in their natural state without sediment control structures. With this in mind we selected the Higashigochi basin of a small tributary of the Oi river as our study area. During 1982 the basin was subjected to a period of intense rainfall of more than 900mm. This released abundant sediment, about 150,000m^3 in the observed reach. As a result the morphology of the stream changed. Taking this opportunity, we were able to study and come to a greater understanding of the dynamics of sediment transport. This paper analyzes a series of changes in the morphology of a high gradient gravel-bed stream that resulted from nine floods.

STUDY AREA

Topography and Geology

The Higashigochi river basin, with a drainage area of about 28 km^2, is a small tributary of the Oi river system emptying into the Pacific side of Honshu Island. A 2406 meter peak, located at the north corner of the basin is the highest point,

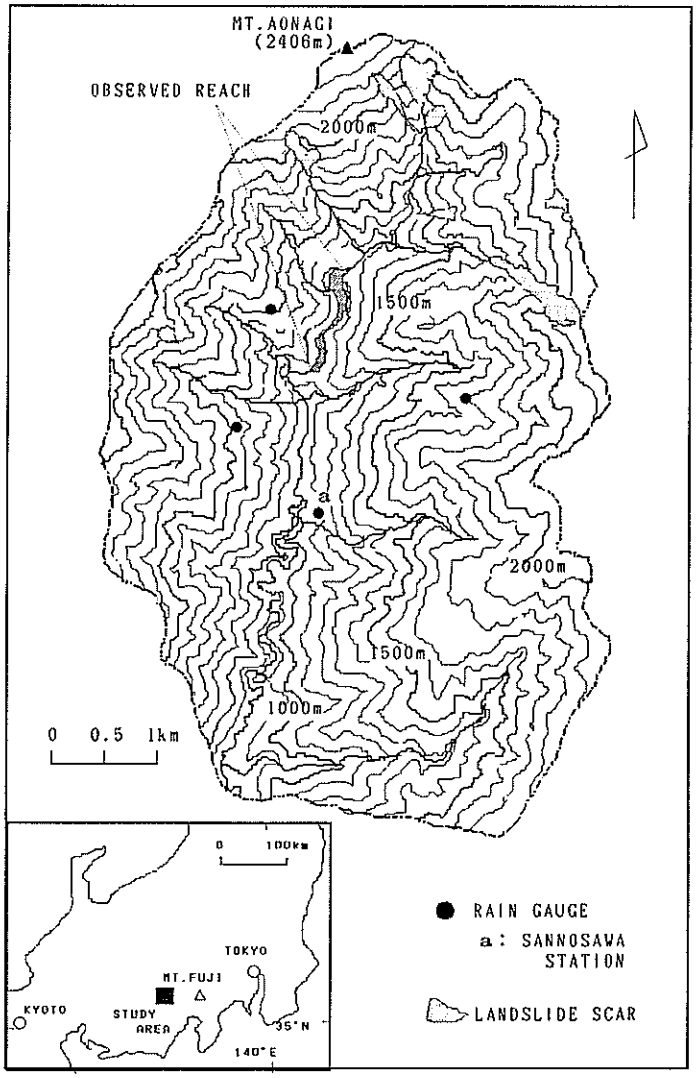

Figure 1--The study area.

[1]Presented at the Subject Group S1.04 Technical Session on Geomorphic Hazards in Managed Forests, XIX World Congress, International Union of Forestry Research Organizations, August 5-11,1990, Montreal, Canada.

[2]Assistant Professor of the Institute of Agricultural and Forest Engineering, University of Tsukuba, Ibaraki, Japan

while the elevation of the confluence with the main river, about 770 meters, is the lowest point in the study area. This gives a relief of about 1640 meters over a linear distance of 7.5 km. Reflecting this high relief, slopes are in general very steep with an average of about 38° (Fig. 1).

The bedrock is mainly composed of shale and sandstone from the Cretaceous period. The rock is generally fractured because the basin is situated in the high, uplifting zone of the Japanese Southern Alps.

As a result of these topographical and geological conditions, the ratio of landslide scars to the area of the basin is 2.9 percent and this figure reaches 7.6 percent in the upper basin.

Stream Channel Shape

The longitudinal profile of the Higashigochi river is shown in Figure 2. This figure shows that the stream is steep and the profile can be divided into three parts in terms of its gradient. The lower part, with a gradient of about 1/30, the middle part with a gradient of about 1/20 and the upper section the gradient of which is more than 1/10. The observed reach was located in the upper section. As to the planar shape of the stream, the meander and the variation of channel width is remarkable.

Climate

According to the climatic records at the Sannosawa station (Fig. 1), the average rainfall between the months of April and November from 1970 to 1981 was about 2,500 mm. Consequently, the mean annual precipitation may reach about 3,000 mm, but it is very variable.

The mean annual temperature is 9.8°C, with the highest temperature occurring in August and the lowest in January. Temperature records of daily maxima and minima suggest that freeze/thaw processes are normally active from the latter half of November to the first half of April (Fig. 3).

Vegetation

Vegetation is predominantly deciduous below the 1,500-1,800 meter zone and conifers dominate at higher elevations. Below the 1,500-1,800 meter zone, Japanese cedar (Chryptomeria japonica D. Don), Japanese cypress (Chamaecyparis obutusa S. et Z.) and Japanese larch (Larix leptolepis Gordon) have been planted.

Observed reach

The observed reach extended about 1 km, where the stream, coming through the V-shaped narrow valley first meets a wide floor of about 40 to 130 meters. Then the stream again enters a narrow valley section at the end of the observed reach (Fig. 4). The gradient of the stream bed in the observed reach ranges from 1/8 to 1/15.

Because no modification of the channel of the reach by sediment control structures had been undertaken, we were able to examine the morphology of the channel in its natural state.

METHOD

In this research we regarded the actual stream channel itself as the place for the field experiments. As a result, various measurements

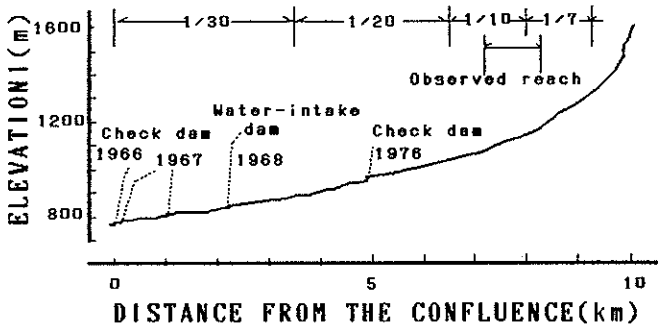

Figure 2--The longitudinal profile of the Higashigochi river.

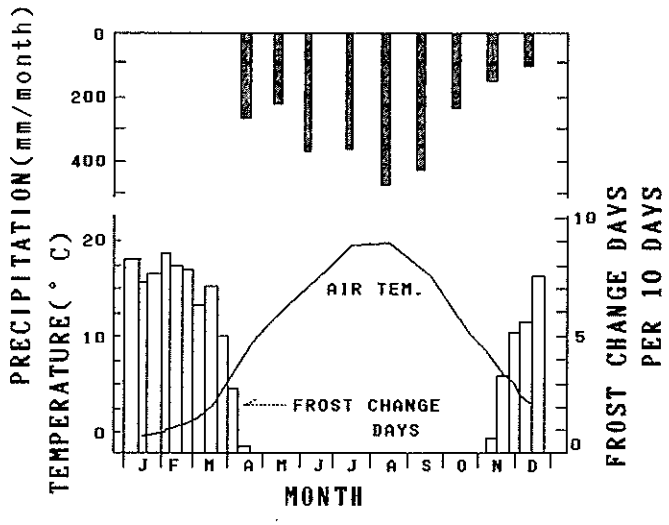

Figure 3--The climate of the study area.

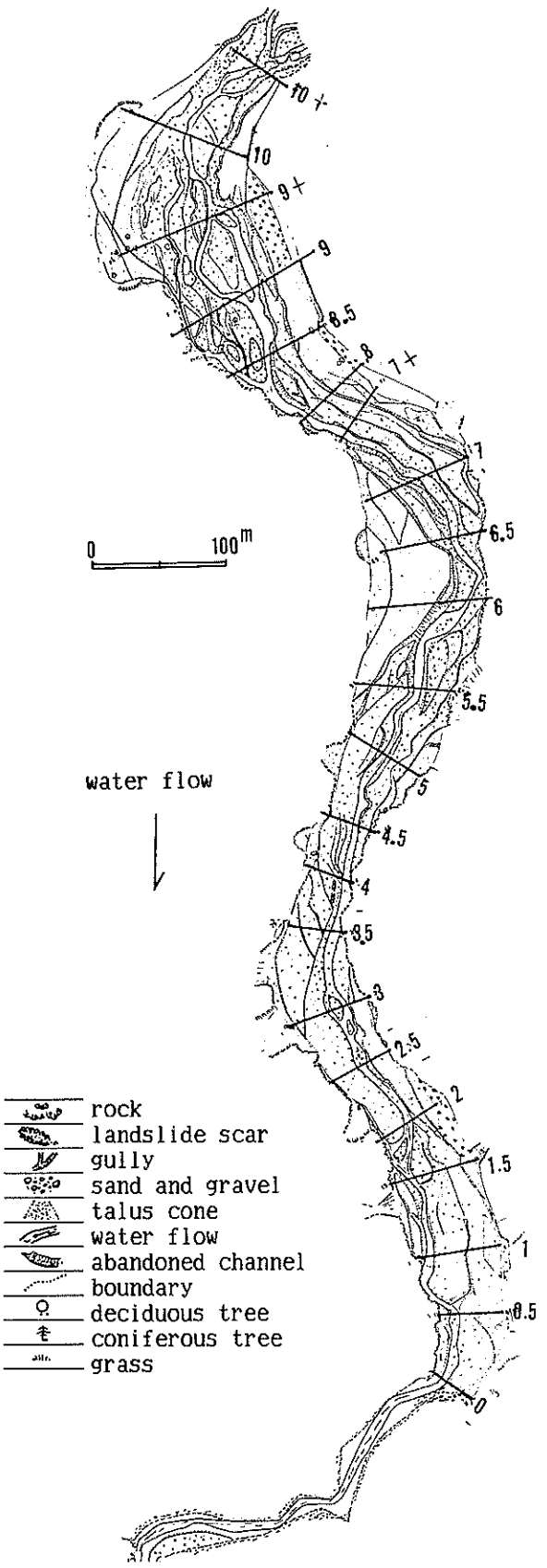

Figure 4--The observed reach after the 8209 flood and the location of the cross sections

were carried out in the study area. In order to record a sequence of changes in the channel morphology of the observed reach, whenever a river bed fluctuation occurred over the period 1979 to 1985, the leveling of 22 cross sections of the observed reach at intervals of about 50 meters was carried out(Fig. 4). Plane surveying was mostly carried out at the same time. The vertical and horizontal distribution of the grain size of the stream bed was investigated after the river bed fluctuations in September 1980 and September 1982. In order to measure the volume of the deposits on the bedrock of the observed reach, seismic prospecting was carried out after the river bed fluctuation in August 1981.

Rainfall was measured by several rain gauges placed around the basin (Fig. 1) and the flood discharge was calculated by a storage function run-off model below (Maita et al. 1984).

$$Sl=KQ^{P}, \quad P=0.6, \quad K=8.6A^{0.14}, \quad Tl=2.5A^{0.14}re^{-0.4}$$

Here, Sl is the hypothetical storage depth of rainwater over a basin considering the time lag Tl between rainfall excess re and flood discharge Q, and A is the area of a basin.

SHAPE CHANGES OF THE STREAM CHANNEL

Threshold Rainfall

Nine river bed fluctuations were confirmed in the observed reach from 1979 to 1985. Table 1 shows the largest values recorded for the continuous rainfall and hourly rainfall measured at several precipitation stations. It also shows the maximum calculated peak discharge at the end of the observed reach for each of the rainfall events and when a river bed fluctuation occurred.

Table 1--The magnitude of rainfall and discharge for each flood.

flood name	continuous rainfall (mm)	max. hourly rainfall (mm/h)	peak discharge (m^3/s)
7910	260.0	31.5	32.8
8009	229.5	37.0	14.8
8108	289.0	29.0	25.9
8208	933.0	69.5	96.9
8209	564.0	34.5	54.5
8305	296.0	29.0	26.4
8308	851.0	40.5	74.4
8309	330.0	33.0	34.7
8506	411.5	38.0	54.5

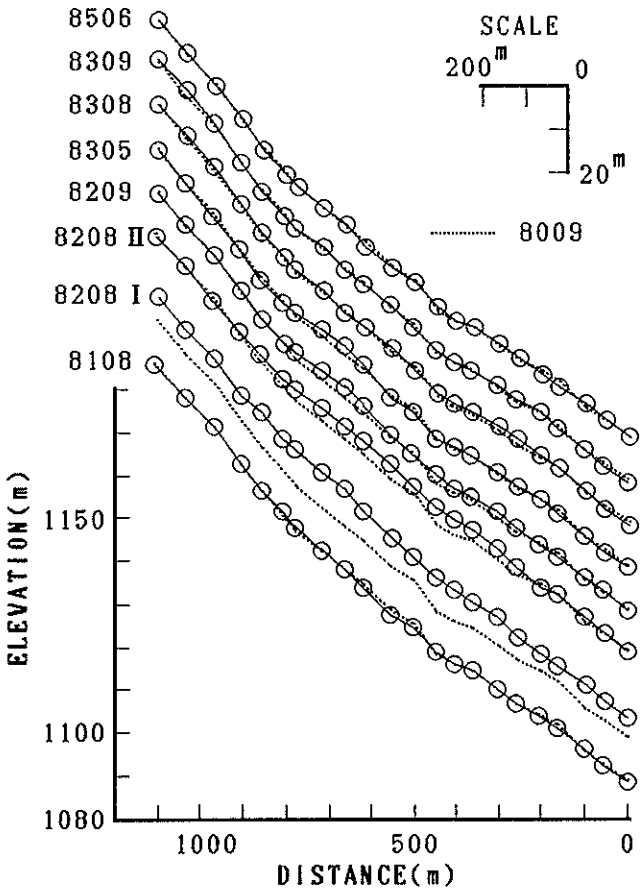

Figure 5--The changes in the lowest longitudinal stream bed profile in the observed reach.

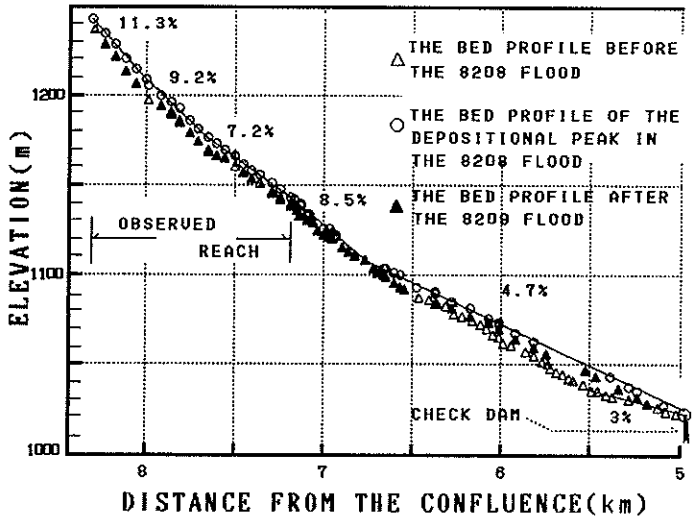

Figure 6--The changes in the longitudinal bed profile of the 3.3 km of stream between a check dam and the observed reach before and after the 8208 flood.

From the figures in Table 1, it seems that a continuous rainfall level of about 200 mm or a maximum hourly rainfall of about 30 mm is the threshold rainfall for a river bed fluctuation in the Higashigochi river basin. Such figures occurred about once every 1.3 to 1.5 years.

Changes of Channel Shape

Figure 5 shows the lowest longitudinal stream bed profile in the observed reach. The profile, formed by the 8208 flood (the flood in August 1982), is divided into two stages. One, shown as 8208I in Figure 5, is the bed profile of the depositional peak. The other, shown as 8208II, is the profile after the recession flow of the 8208 flood partially eroded the buried bed. Because of the clarity of the profile changes, each profile is compared to the profile after the 8009 flood (the flood in September 1980). Other floods were named in this manner.

Figure 6 shows the longitudinal stream bed profile of the approximately 3.3 km of stream between a check dam and the observed reach before and after the 8208 flood. As shown in Figure 4 and 5, the large deposition of the 8208 flood was caused by a continuous rainfall of 933 mm and an hourly rainfall of 69.5 mm (a recurrence interval of more than 30 years), which Typhoon no. 10 produced between August 1 and 3, 1982 (Fig. 7). This event raised the stream bed from 3 meters to 8 meters. Subsequently, rapid erosion ensured that the bed profile regained its former shape very rapidly. As shown in Figure 6, the check dam had no influence on the deposition in the observed reach caused by the 8208 flood. Besides it was noted that there was almost no drift wood debris in the observed reach in spite of such a large flood.

Figure 8 shows the changes in the cross sectional channel profiles in the observed reach. The black shaded parts of the diagram represent deposition. Erosion is shown by the unshaded area between the lines describing the cross section. The large deposition almost flattened the bed in the observed reach. After the flood, incision of the stream bed meant that these profiles nearly recovered their former shape. The recovery was more rapid in the narrow part of the valley than in the wide part.

Figure 9 shows the changes in the planar shape of the stream bed in the observed reach. The large deposition not only caused large changes in the planar shape but also the location of the thalwegs. The erosional process of the stream bed meant that the shape of the bed returned to its former shape and the thalwegs returned to their former positions.

Thus, large depositions have a marked effect on the stream bed but these changes are not permanent and the erosional process causes the channel shape to revert to its former one.

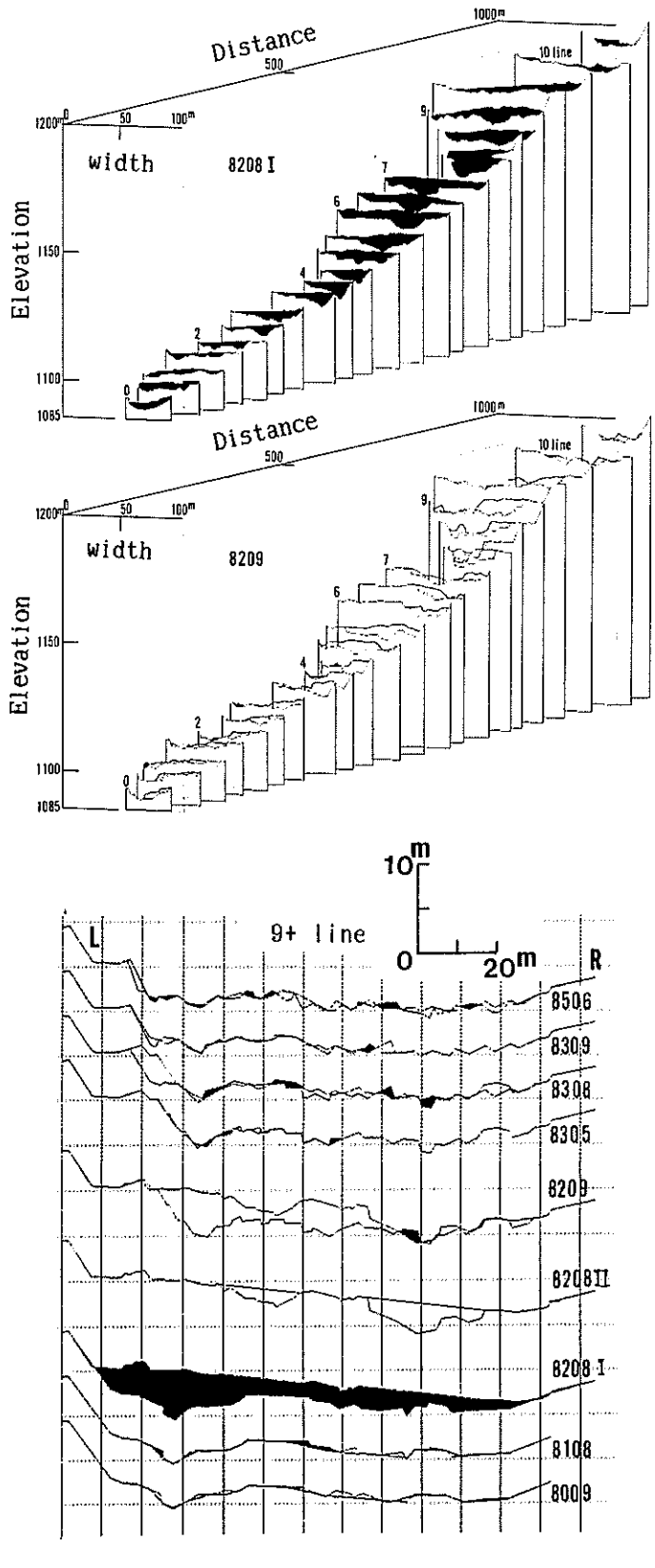

Figure 8--Some examples of the changes in the cross sectional profiles in the observed reach.

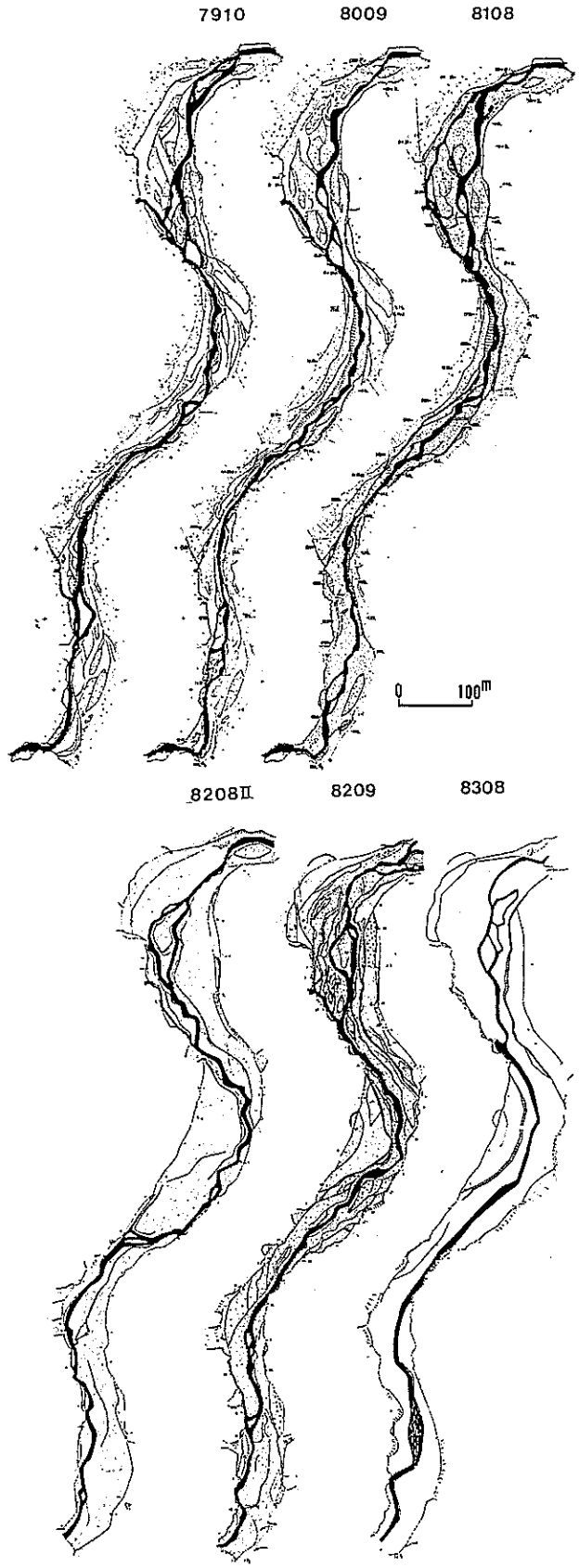

Figure 9--The changes in the planar shape of the stream bed in the observed reach. The black shaded parts of the diagrams represent the low water flows.

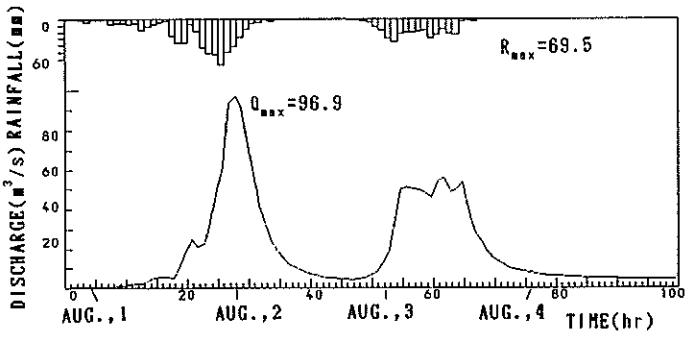

Figure 7--The observed hyetograph in the study area and the calculated hydrograph at the end of the observed reach in the 8208 flood.

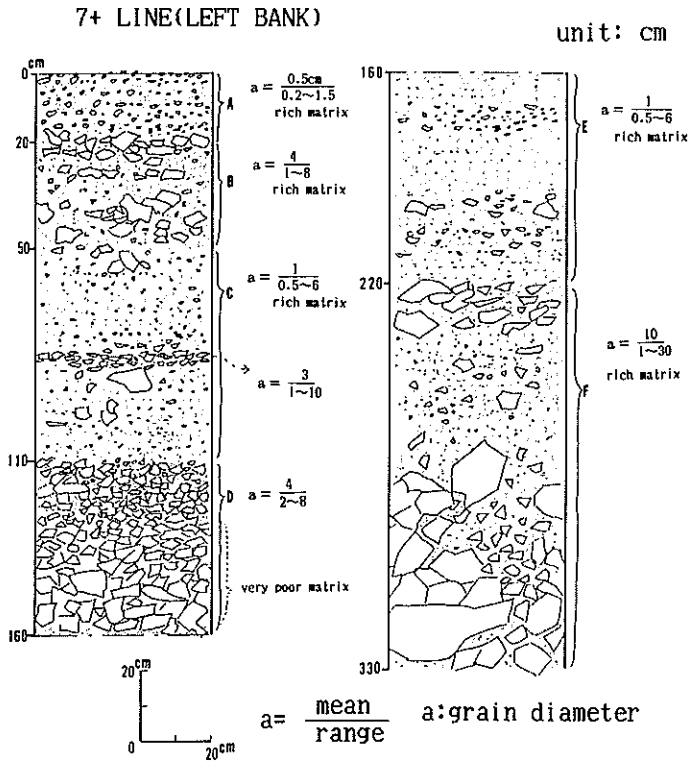

Figure 10--The structure of the deposit formed by the 8208 flood at 7+ line.

Structure of Deposits Formed by the 8208 Flood

Figure 10 shows the structure of the deposit formed by the 8208 flood at 7+ line shown in Figure 4. Although the deposition was formed by one flood there are several parts with laminar structures. As Iseya et al.(1990) described, it is thought that this structure was formed when a shallow and high velocity flow transported heterogeneous sediment, raising the bed at a high rate. Because of the large deposition, the grain size of the stream bed became smaller. On the other hand, erosion caused the grain size to become larger as the smaller sediment was removed from the stream bed.

QUANTITATIVE CHANGES OF RIVER BED FLUCTUATION

Changes of the Volume of Deposit

Figure 11 shows the changes of the volume of the deposits on the bedrock in the observed reach. This was found by using the volume of the river bed fluctuation and cross sectional bedrock profiles measured by seismic prospecting in October 1981. The volume of the river bed fluctuation can be obtained by the following steps. First, as shown in Figure 12, the volume of the river bed fluctuation of the segment is calculated by the equation below.

$$V=((E11+E12+...)+(D11+D12+...)+(E21+E22+...)+(D21+D22+...))L/2$$

Here, V is the volume of the river bed fluctuation of the segment, L is the distance between two adjacent cross sections, E11,E12,..etc, and D11,D12,..etc, are the areas surrounded by the two cross sectional profiles before and after a flood at the A1 cross section. E11,E12,..etc, represents the area eroded and is negative, D11,D12,..etc, represents the deposited area and is positive. E21,E22,..etc, and D21,D22,..etc, represent the same variables measured at the A2 cross section. The volume of the river bed fluctuation of the observed reach can be obtained by taking the sum of the volumes of each segment. Thus, the overall volume may be positive or negative in sign.

As can be seen from Figure 11, the volume of the deposits was decreased gradually to about 120,000 m^3 by the process of erosion between 1980 and 1981. But the 8208 flood in 1982 deposited sediment of more than 150,000 m^3 and the total volume of sediment on the bedrock increased to 270,000 m^3. After that, it decreased rapidly to about 130,000 m^3. As the changes between 1982 and 1985 show, the erosional process continued in the observed reach after the 8208 flood despite the fact that there were some large rainfalls in this period. This means that there was little sediment in the upper basin of the observed reach because unstable debris had been mostly swept from the stream beds and the slopes of the upper basin by the heavy rainfall associated with the 8208 flood.

ANALYSIS AND DISCUSSION

Figure 13 shows the relation between the absolute value of the river bed fluctuation in the observed reach and the peak flow discharge. This peak flow discharge was adopted as an index of the magnitude of discharge. As the graph shows, the volume of the river bed fluctuation is not always large in comparison with the increase of flow discharge and it seems probable that the ordering of the floods is an important factor. To attempt to unravel this complicated

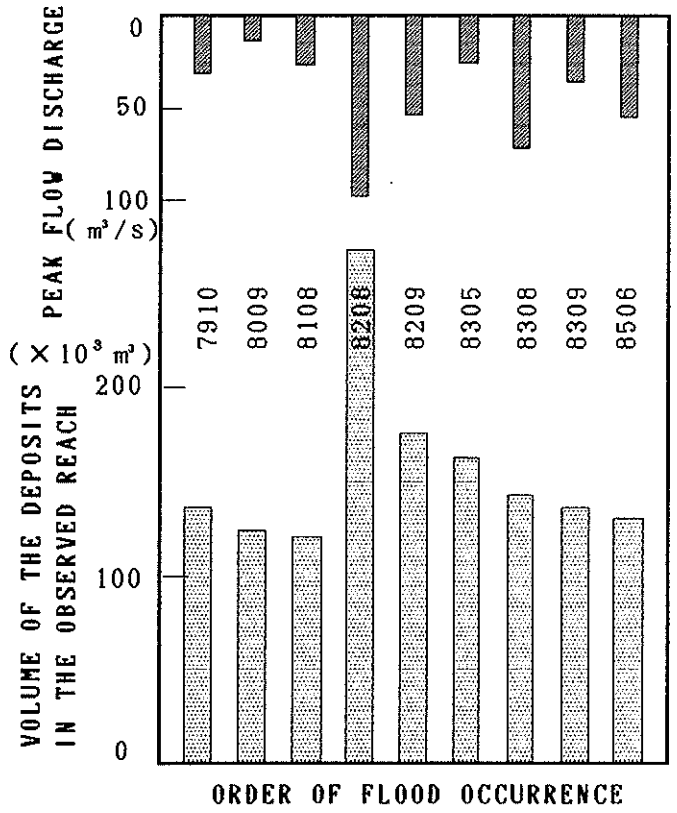

Figure 11--The changes of the volume of the deposits on the bedrock in the observed reach.

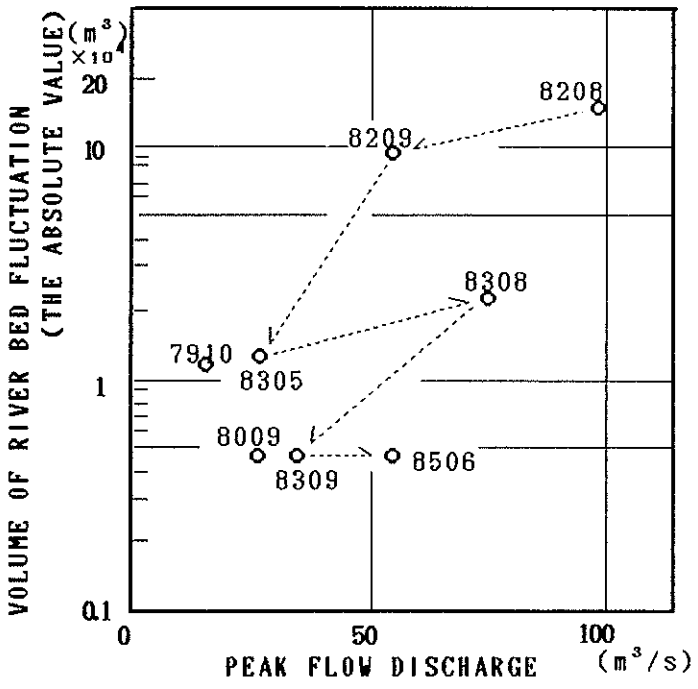

Figure 13--The relation between the absolute value of the river bed fluctuation in the observed reach and the peak flow discharge.

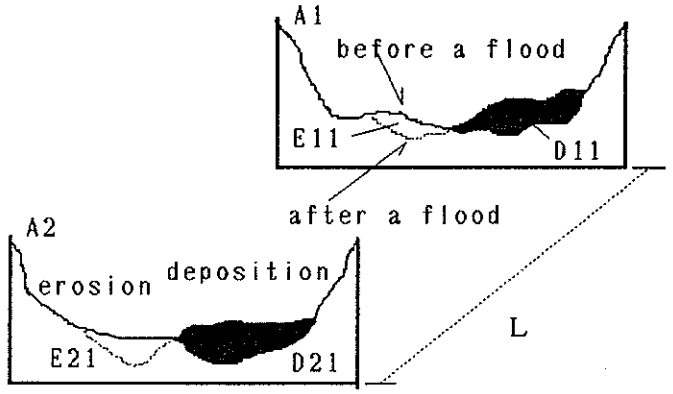

Figure 12--The schematic diagram to obtain the volume of the river bed fluctuation.

relationship, the idea of the specific volume of the river bed fluctuation was introduced. The specific volume was obtained by dividing the volume of the river bed fluctuation by the peak discharge adopted as an index of the flood discharge.

Figure 14 shows the specific volume of the river bed fluctuation in the observed reach arranged in the order in which the floods occurred. As this graph shows, a regularity is apparent. The specific volume decreases exponentially in the erosional process following the large deposition of the 8208 flood. As shown in Figure 15, this regularity of the erosional process in the observed reach can be expressed by the following exponential equation.

$$S(t) = -\alpha \exp(-\beta t) \qquad \alpha > 0,\ \beta > 0$$

Here S is the specific volume of the river bed fluctuation per unit distance, t is the occurrent order expressed as 1,2,.. etc, during the erosional process. In the case of the series of events in the observed reach α is 3.3 and β is 0.8.

Valley Floor Width and River Bed Fluctuation

Figure 16 shows the different ways in which the specific volume decreases during the erosional process, depending on the width of the valley . This difference can be expressed in terms of the parameters of the exponential equation above. In the wider parts of the valley in the observed reach (average width 72 meters), α is 3.3 and β is 0.8. In the narrower parts in the observed reach (average width 50 meters), α is 5.0 and β is 1.4. Thus, as the valley becomes wider β decreases. It is believed that β can be used as an index to shown how the valley floor width influences the volume of the river bed fluctuation.

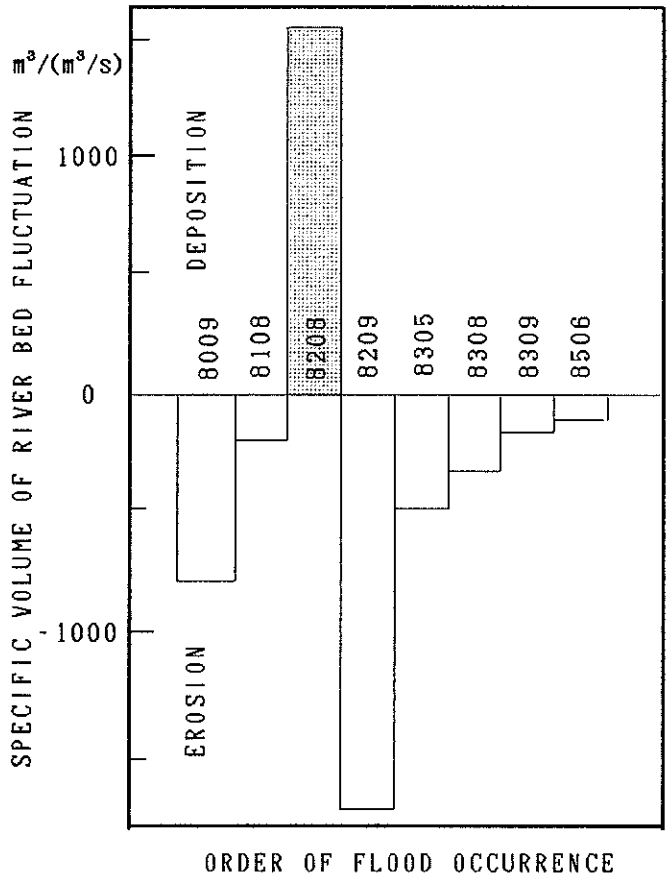

Figure 14--The specific volume of the river bed fluctuation in the observed reach arranged in the order in which the floods occurred.

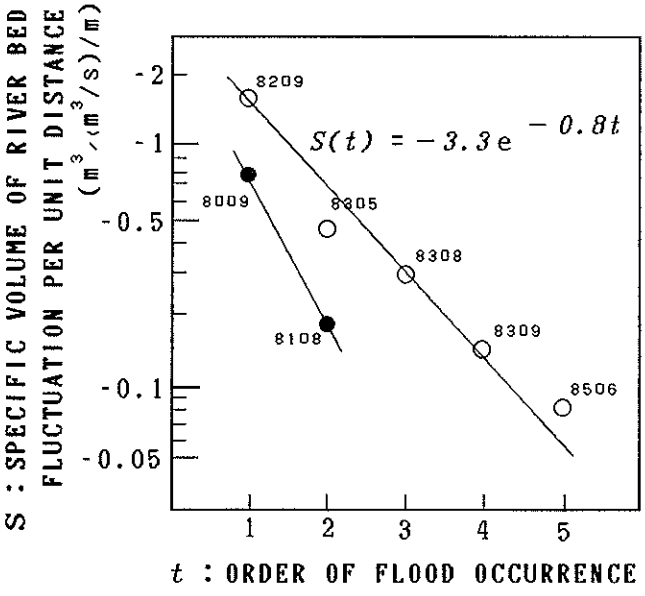

Figure 15--The exponential relation between the specific volume in the observed reach and the order of the flood occurrence during the erosional process.

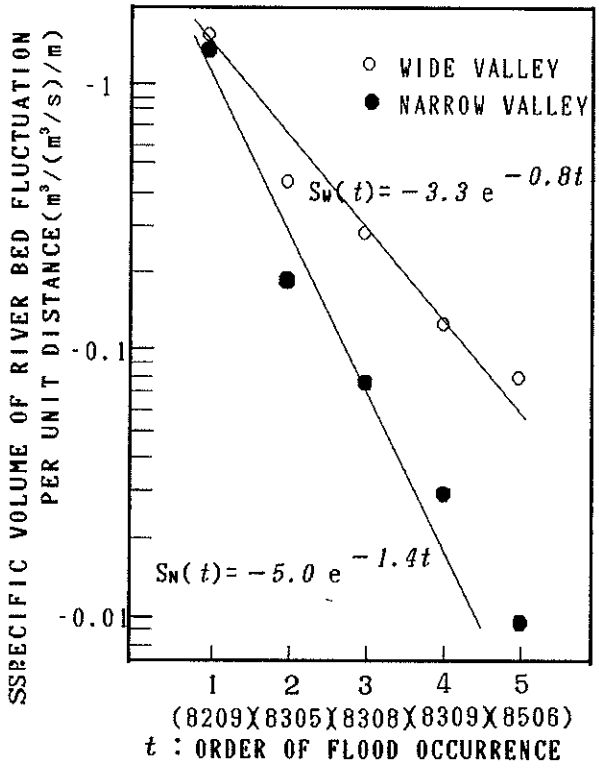

Figure 16--The different ways in which the specific volume decreases during the erosional process, depending on the width of the valley.

CONCLUSION

The magnitudes of the flow discharge and the river bed fluctuation did not exhibit a one to one correspondence. We were able to find a regularity in the quantitative changes by arranging the river bed fluctuations in the order of the occurrence of the floods. This implies that the history of sediment transport plays an important role. That is to say, when little unstable debris remains in the upper reaches and slopes of the basin, a trend towards the erosion of the river bed continues even if a larger flood occurs. Thus, in torrential streams in headwater regions, deposition or erosion depend mostly on the sediment supply, not on the magnitude of the flow discharge.

The valley floor width is closely related to the dynamics of sediment transport. In the erosional process, the specific volume of the river bed fluctuation decreases rapidly in narrow valley floors, but only decreases slowly in wide floors. On the other hand, in the depositional process, the wider the valley floors are, the more sediment from the upper reach they can retain. Therefore, the wide valley floors of a stream are depositional spaces where the excess sediment from the upper stream area is temporarily deposited. In the erosional process that follows, sediment runs off down stream in a

way that can be explained by an exponential process. In other words, wide valley floors represent spaces that retard sediment transport.

ACKNOWLEDGMENTS

I thank Michio Kaijo, Motoyuki Sunasaka, Teruo Otsubo, Toru Endo, Akira Takinami, Masanori Wade and Kunihiro Segawa, Agricultural and Forestry Research Center, University of Tsukuba, for their assistance to the field work.

REFERENCES

Iseya, Fujiko; Ikeda Hiroshi; Maita Hideji. 1990. Fluvial deposits in a torrential gravel-bed stream by extreme sediment supply: sediment structure and depositional mechanism. The 3rd International Workshop on Gravel-Bed Rivers, Florence,Italy, September 25-29,1990.

Maita, Hideji; Otsubo,Teruo; Kaijo, Michio. 1984. Hydraulic geometry in a natural torrent. Transactions, the 95th Meeting of the Japanese Forestry Society: 641-643 (in Japanese).

Snow-Cover Condition in Japan and Damage of the Sugi (*Cryptomeria Japonica* D. Don)[1]

Hideaki Taira[2]

Abstract: Japan is one of the most snowiest regions in the world. Particularly the mountainous area of Honshu (the main island), along the Japan Sea has heavy snow in winter. In some places, snow piles up more than four meters and the ground is coverd with snow about one hundred and forty days a year. The sugi tree is widely planted in snowy regions, and snow-pressure damages, such as basal bending, occure in juvenile stands, and after that crown snow-damage, such as stem breakage, happen in younger stands about 10~30 years-old. Basal bending is formed by the difference in recovery rate between the upper part and the lower part of the stem during growing season. Root damage occurs when the stem is prostrated, and the compression wood is formed in the process of the reelection of the fallen stem. Crown snow-damage happens during the condition of comparative warm air temparatures ranged from three degrees below zero to three degrees above zero. The strength of the stem against crown snow-damage depends on the diameter of the tree, tree taper,constunt μ for the root, and the modulus of elasticity. Pulling up the fallen stem, and controlling the tree density are important in preventing these snow damage.

Introduction: It is said that Japan is the snowiest region in the world. The Japan sea area of Honshu has a lot of snow every year. Though the snow protects plants from severe coldness in winter and is an important source of water, it also is the cause of damages such as basal bending and stem breakage. The sugi is an important spicese for reforestation in Japan and the total area of sugi reforestation exceeds 4.15 million ha., making it about 48 percent of the total artifical forest in Japan. The sugi is widely planted in snowy regions, but suffer many kinds of snow damages every year. Basal bending, stem breakage,stem bending and uprooting are recognized problems in the sugi reforestation, and these snow damages are classified in to two types; one is snow-pressure damage which occurs in younger aged trees untill they are about ten-years-old and the other is crown snow-damages which occur in trees over ten years old. But the types of snow damage depends on the snow-cover condition. The author will talk about the relationship between the snow-cover condition in Japan and the type of snow damage, the mechanism of main snow damage and its control.

THE SNOW COVER CONDITION IN JAPAN AND SNOW DAMAGE

The mean annual maximun snow depth of Japan is shown in Fig-1. A high percentage of snowy areas are distributed along the Japan Sea, and in some areas, snow depth exceedes four meters.In contrast there is only about 10~50 centimeters in the area along the Pacific Ocean, and the mountainous area of Shikoku and Kyushu island, and most areas of Shikoku, Kyushu and the southern part of the main island have less than 10 centimeters.

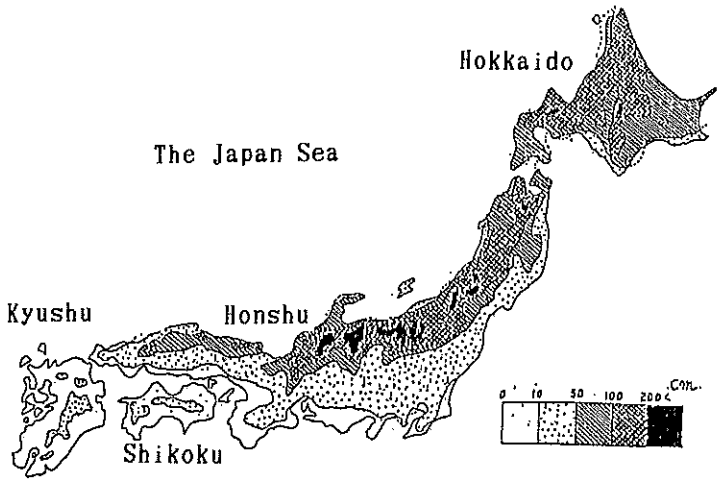

Fig.—1. Distribution map of annual maxmun snow depth

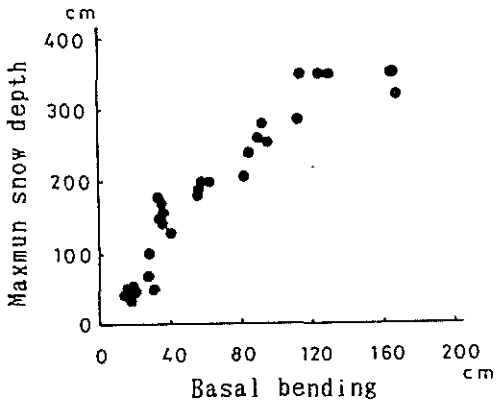

Fig.- 2. The relation between annual maxmun snow depth and basal bending

Quality of snow also varies. There is dry snow in Hokkaido, and the northern and mountainous areas of Honshu, but in the area along the Japan Sea there is wet snow which sticks easily on trees. Snow pails up on the tree crown, and causes stem breakage, which is called crown snow-damage. Also in the Pacific Ocean area of Honshu, crown snow-damage occurs when tropical low pressure passes by the Pacific Ocean and brings wet snow in early spring.

The relationship between basal bending and the mean annual snow depth are shown in Fig-2. Basal bending is about 20 centimeters in the areas where snow depth is below 1 meter. As the snow depth reaches 2 meters, basal bending increase over 60 centimeters, and at depths over 2.5 meters, basal bending increase to 178 centimeters. Basal bending increases as the snow depth increases.

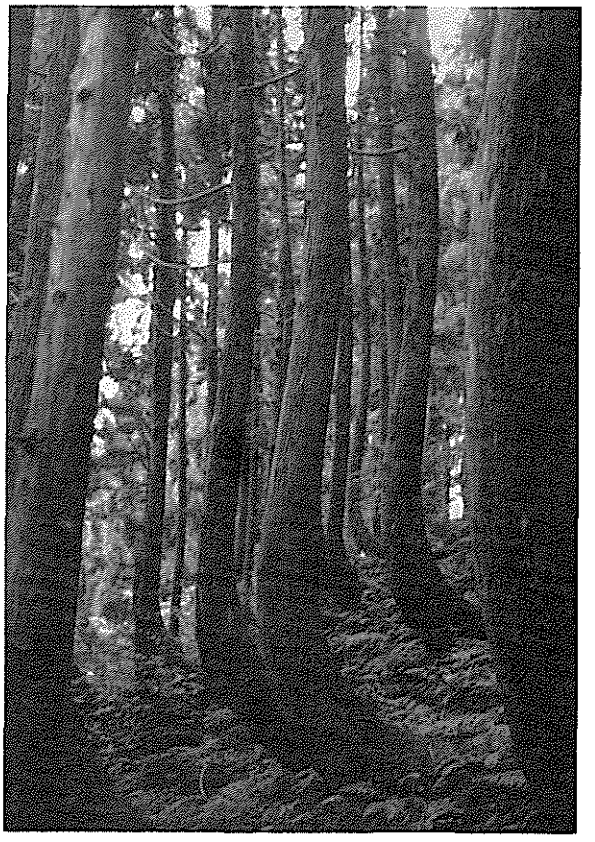

Fig.- 3 Basal bending of cryptomeria

Fig.- 4. Crown snow-damage of cryptomeria

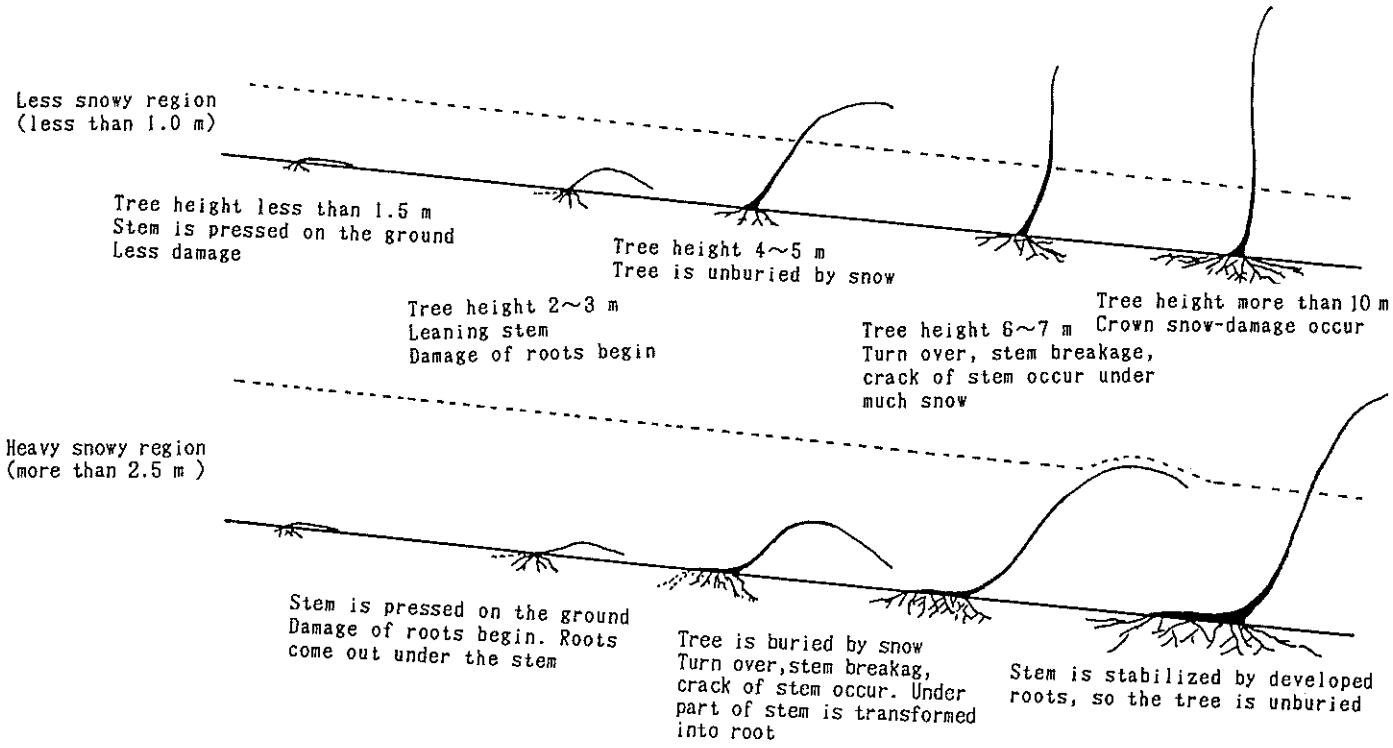

Fig.- 5. Variation of snow damage of cryptomeria by relation between snow depth and tree height

The extent of tree damage varies according to the snow depth and tree height(Fig-5). In areas with snow depths of less than 1.0 meters, only trees less than 2.0~2.5 meters in height are prostrated in winter. Root damage is not serious and stem breakage which becomes fatal seldom occurs. As the tree reaches more than 2.0~2.5 meters in height, the stem does not prostrate with average snow fall depth. However, in heavy snow the possibility of stem breakage and cracking at the bottom of the stem increases and many trees fall and pull out their roots. Snow damage on trees varies from the pulling out of roots to stem breakage (als ocalled crown snow-damage). Crown snow-damage occurs in trees more than 10 meters in height because the stem becomes stiff (and hence, resistant to bending) and the roots are large enough to resist stem prostration. In regions of heavy snow, the young stem repeatedly prostrates and the uprooting of the trees is common. The new roots develop under the part of stem still touching the ground, and the tree then develops resistance against futher prostration. The effects of snow damage during the growing stages rangs from the pulling out of roots to the cracking of the basal stem and stem brakage. In areas with depths of over 2.5 meters of snow, the ratio of dieing trees due to snow damage increases drastically, and it is difficult to forest the sugi in this area.

THE MECHANISUM OF MAIN SNOW DAMAGE

Snow Pressure Damage

The stem of the sugi leans with the initial snow fall and is buried by subsequent snow falls. The snow-covered stem is pressed down by the weight of the accumulated snow and subsequent sedimentation of snow, and is subjected to elastic strain, elastic after-strain and permanent deformation.

In younger trees (one to two years) where stems are soft and thin, the stress is mainly put on the stem and the stem does not lean from the base when the snow press it down on the ground. But,for trees more than three-years-old (height :

1.5~2.0 nmeters), the stem leans from the base because of the increase in its bending stiffness.

In early spring after the release of snow pressure,the stem begins its straightening process with rapid, simple elastic recovery, then elastic after-strain follows. The stem completes its recovery through elastic after-strain until the end of April or early May at which time the stem resumes its recovery with growth and the formation of compression wood. For one-and two-year old trees, stem straigthening is completed by the middle of June or early July; after that, some of the trees increase in weight with tree growth, and this also contributes to the basal bend formation (Fig-6).

Since straightening of the stem with growth is great in one-, two-and three-year-old trees, there is less basal bending on these trees. On the other hand, since straightening of the leaning stem decreases with age, there is greater basal bending in older trees.

The recovery rate observed at each stem positions varies in relationship to the stem's distance from the base. The nearer the stem is to the base, the slower the recovery rate. This difference in recovery rate at various stem positions causes basal bending (Fig-7).

The basal bending of the sugi increases every year. During the early stages of growth, snow depth has no effect on the basal bending of the sugi, but, when the tree attains a height of more than 1.5 meters, increase in snow depth greatly affects stem prostration resulting in greater basal bending. In addition to the two factors mentioned, the slope of the site also affects basal bending. If the snow depth and the height of tree are the same, the amount of stem prostration is affected by the degree of slope. As the slope steepens, the amount of stem prostration increases resulting in greater basal bending.

When the stem is prostrated by snow, the roots suffer damage at the upper part by stretch, at the lower part by pressure, and at the left and right sides by twist. The left and right twisting of the roots, however, does not badly injure them so that they can develop well on both side of the slope. Roots on the down slope side are only slightly damaged due to an increase on the compression force. But roots on the upper slope side are the ones that are severely damaged. They are pulled out,resulting in poor root development.

Therefore, mature bent trees have deformed roots and large side roots (Fig-8). In areas with snow depths of less than 1.0 meters, most of the trees more than 2.5 meters in height are not easily prostrated and the amount of stem prostration is small. Hcnce, the damage on roots is not so severe and the roots develop normally. In areas of heavy snow, beside root damage and deformation, the lower part of the stem is transformed into roots. When this stem touches the ground due to the weight of snow, roots start to develop from it and the part touching the ground is transformed into a main root.

Roots on both the side and the lower part of the slope are not easily damaged and hence, can develop well. The transformation of the lower part of the stem into a main root increases the resistance of tree against prostration by snow. Morever, the tree is not readily buried in the snow because the transformed main roots effectively prevent stem prostration.

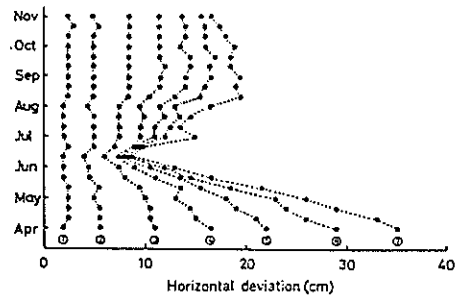

Fig.- 6. Process of straightening of the prostrated stem of a typical 2-year-old tree

① At 5cm above the ground
② 10 〃
③ 20 〃
④ 30 〃
⑤ 40 〃
⑥ 50 〃
⑦ Top

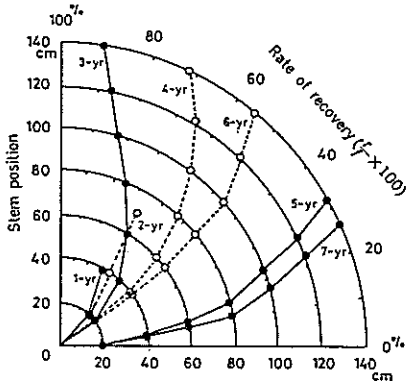

Fig.- 7. Relationship between the deviation from former position (f) and rates of straightening of prostrate stems ((r/f) x 100) at each position during a growing season

Fig.- 8 Deformation of roots

After basal bending is stabilized, surface roots on the down slope develop and the diameter of the lower stem increases towards the down slope. Therefore, the curve of the lower part of the stem is apparently corrected.

Crown Snow-Damage

Snow damage after basal bending has stabilized is called crown snow- damage. It is the phenomena in which the stems are broken by an accelerating snow load on the tree crown. This is roughly classfied into breakage of the stem, breakage of the tip of the stem, and uprooting. Uprooting is the predominant damage among trees less than twenty-years-old, and is sometimes difficult to distinguish from snow pressure damage. Breakage of stem is common in twenty-to thirty-years old stands, and this stand is most sensitive to snow crown damage. In stands More than thirty-years-old, the breakage of the tip of the stem is common, but it is not serious. Also trees with larger stems are more resistant to crown snow-damage than those with smaller stems. But it is difficult to evaluate tree strength against snow crown damage by the shape factor of stem. It is only a comparative standard and it dose not become an absolute one. As mentioned before, crown snow-damages is the phenomena in which the stem is broken by an unendurable snow load, so crown snow-damages can look as if the broken stem is a failure of the tapered column receiving an eccentric compressive load of snow, i.e. the buckeling load (P_{cr}) of stem can be estimated by the following equation.

$$P_{cr} = \sigma^2 \bullet \gamma_s^2 \bullet E \bullet I_o / L^2$$

γ_s^2 : satisties following the equation

$$\tan \gamma / \gamma = -1 / \beta / \alpha - \mu \bullet \gamma^2 \bullet L^2 \bullet I_o / L$$

δ : ratio of taper the stem

β : $1 - \delta$

E : Mudulus in elasticity

L : Height of gravity of a snow-laded crown

I_o : Second moment of cross cection base at the stem

It is understood from the equation that the strengthen against snow crown damage is determined by the diameter of the stem, the taper of the stem, the height of gravity of a snow-load, modulus in elasticity in bending, the μ-index whose value was obtained from the regression coefficient between the turning angle of the tree stem and the turning moment at the stem base. The estimated breaking load is 200~500 kilogram of trees about 20 centimeters at diameter breast height and is agreed with the experimental load which is gotten from broken trees receiving vertical loads as shown Fig-11.

CONTROL METHODS OF MAIN SNOW DAMAGE

Many methods of controlling snow damage have been adapted in the past.Of these control methods, the author will mentioned the most useful ones in this paper.

Snow Pressure Damage

As the cause of basal bending of young trees is stem prostration by snow, pulling up the fallen stem is the most effective method of

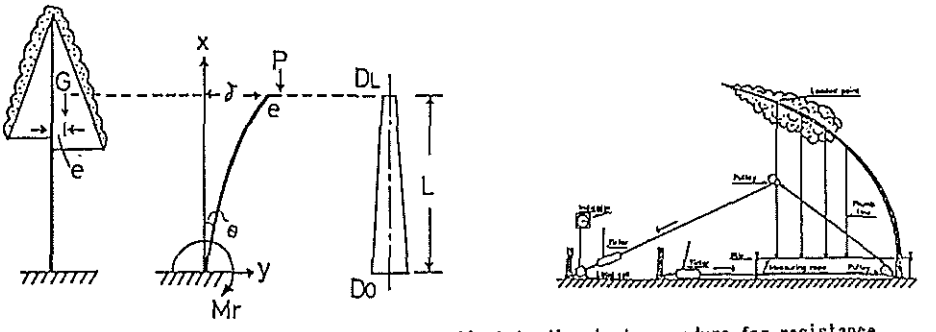

Fig. 11. Diagram of snow-loaded tree and vertical loading test procedure for resistance of tree stem (Nakatani and others, 1984).
Legend: G: the center of gravity of a snow-laden crown, e: horizontal displacement of the center of gravity of the snow-laden crown from the stem axis, P: snow load, θ: turning angle at the stem base, L: height of the center of gravity of the snow-laden crown from the ground, δ: deflection at the height L, D_B: diameter at the stem base, D_L: diameter at the height L.

control. In regions of heavy snow, slant planting which deforms the roots is adaptable because the deformed roots is unsusceptible to stem prostration. Fertizetion increases tree growth, but basal bending also increases at the same time. The degree of basal bending is different largely among the cultivares, so planting of small bend cullivares is an effective way to reduce basal bending. But, it is hard to lean with initial snow, so cultivares with a small degree of basal bending were less frequent in stems leaning under snow, but many stem breakage were observed in heavy snow regions (with snow depths over 1.5 meters).

Crown Snow-Damage

One of the most effective methods for controlling crown snow-damage is to decreas the height/diameter ratio by controlling stand density. The most desirable stand density is 800 ~1200/per hectare at planting, and repeated thinnings are requied when the competition occurs in the stand as the tree grow. Also, as modulus in elasticity in bending is different in the cultivarer, it is important to choose cultivar with large modulus in elasticity in bending for forest owners in the area of much crown snow-damage.

LITERATURE CITED

Fujimori, T.; Matsuda, and Kiyono, Y. 1987. Stand structure and snow damage in relation to stand age -Sugi plantations in Fukui prefecture in the 1981 heavy-snowfall-. Journal of Japan forest society 69(3): 94-104.

Kato, A.; Taira, H. and Nakatani, H. 1986. Differences of snow damage and resistive performance of tree stem in three Sugi cultivars. Bulletin of the Toyama prefectual forest experiment station 11: 7-17.

Kato, A.; Nakatani, H.; Taira, H. and Aiura, H. 1988. Estimation snow-load required to cause stem failure in Boka-sugi stand. Journal of the Toyama forestry and forest products research center 1: 1-6.

Katsuta, M. and Matsuda, K. 1984. Differences in the damage from snow crowning among Cryptomeria japonica cultivars (1). Rinboku no ikusyu (Forest tree breeding) 131: 12-17.

Kitamura, M. 1981. Uber die Schneeshaden des Sugi-Bestandes in Schneereichen Gebiet Japans. Beitrage zur Wildbacherosions Lawinenforschung (4). FBVA. Wine: 257-262.

Maeda, T.; Miyakawa, K. and Tanimoto, T. 1985. Vegitation and regeneration of beech forest in Gomisawa (Niigata Prefecture).- Performance of Sugi planted in beech forest zone and a proposal for natural regeneration in the zone -. Bulletin of the government forest experiment station 333: 123-171.

Nakatani, H.; Kato, A.; Taira, H.; Iijima, Y. and Sawada, M. 1984. Deflection and resistance performance of tree stems subjected to snowload in sugi stands, Journal of the Japan wood research society 30(11): 886-893.

Nitta, R. 1983. The variety of heavy-snowfall conditions causing disastrous forest damage during the winter of 1980/81, Trans. 94th meeting of Japan forest society: 727-728.

Shidei, T. 1954. Studies on the damages on forest tree by snow pressures. Bulletin of the government forest experiment stastion 73 : 1-89.

Taira, H. 1982. The influence of differences in the degree of initial snow throw effected by early winter snow on basal bending in young sugi(Cryptomeria japonica D. Don). J. Jap. For. soc. 64: 453-460.

———. 1984. The process of bend forming and

reerecting of the lower part in the stem due to the snow pressure and the tree weight increase in Tateyama sugi (Cryptomeria japonica D.Don). Beitrage zur Wildbacherosions -und Lawinen-forschung(5).FBVA. WIEN: 139-147.

———. 1985. Basal-bend formation in young sugi (Cryptomeria japonica D.Don). J. Jap. For. soc. 67:. 11-19.

———. 1986. Eeffects of inclined planting, fertilization and tying up the stem with rope on characters in young sugi (Cryptomeria japonica D,Don).J. Jpn. For. soc. 68:333-337.

———. 1987. The study of mechanism of Sugi basal bending and its control methods, Bulletin of the Toyama prefectual forest experiment station. 12: 80.

———. 1988. The role of snow in coniferous stem bend formation Beilrage zur Wildbacherosions -und Lawenenforschung(7). FBVA. WIEN. 275-283.

Takahashi, K. and Nitta. R. 1984. Wind' s role in snow damage distribution at two man-made forests, Trans. 95th meeting of Japan forestsciety: 309-310.

Tsukahara, H.; Ohtani, H. and Suto. S. 1975. The bending of root sides of the forest trees planted by Cryptomeria seedlings on the steep stands in the heavy snowry region. Jurnal of Yamagata agriculture and forestry sociaty. 32: 21-30.

Study on Shearing Force and Impact Force of a Volcanic Mud Flow on Mt. Sakurajima[1]

Yoshinobu Taniguchi[2]

Abstract: Two kinds of shearing stress meters (type A and type B) were set on the channel bottom in the Arimura River and the Mochiki River on Mt. Sakurajima. Volcanic mud flows take place there about 100 times a year. The results of the surveys demonstrated that the actual shearing force of a volcanic mud flow on Mt. Sakurajima was from 0.46 to 2.50 kgf/cm^2. The actual impact force caused by collisions of big stones, which were contained in a mud flow, with the channel bottom was calculated theoretically at about 15 times greater than the dead loads of the stones. The collision of stones in a mud flow caused great abrasion of concrete.

A great number of volcanic mud flows take place every year on Mt. Sakurajima in spite of little rainfall. They often damage both dams and channels, and also threaten the inhabitants of Sakurajima. In this study, the magnitude of the actual shearing force of a volcanic mud flow was researched in order to make clear the mechanism of the destruction and the abrasion of a dam or a concrete channel in torrents of Mt. Sakurajima. The data were analyzed by the theories of hydraulics and the collision of an elastic body. The cause of destruction and the abrasion of a dam or a concrete channel by mud flows could be clarified to some extent from the results of these surveys.

SEDIMENT YIELD ON MT. SAKURAJIMA

Mt. Sakurajima, which lies in the southern part of Japan (Fig. 1), is one of the most active volcanoes in Japan. It is

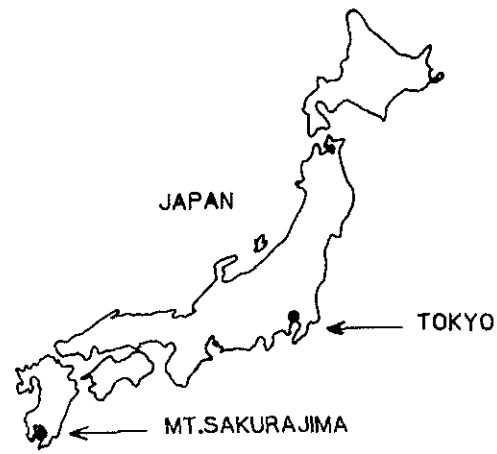

Fig. 1 Map of Japan

located in Kagoshima Bay and has an area of 80 km^2 and circumference of 52 kilometers. There are three craters on Mt. Sakurajima: Kitadake Crater (1117 meters above sea level), Nakahake Crater (1060 meters), and Minamidake Crater (1040 meters). Minamidake Crater is currently erupting vigorously. Table 1 shows the volcanic activities of Mt. Sakurajima for the past 20 years (Osumi Public Works Office, 1986).

Lately the baring of mountain slopes has been making conspicuous progress on Mt. Sakurajima in line with the vigorous volcanic activities. The baring of the slopes has been caused by both the effect of fall from the eruptions and the action of sulphur gas from smoke emissions of the Minamidake Crater. The receding of vegetation on the slopes in the upper reaches of each torrent has continued on Mt. Sakurajima, and the baring of the g downwards year by year. A number of gullies have formed on the slopes. These slopes have been suffering from rapid erosion, and they have been producing a great amount of sediment for the last 20 years. Fig. 2 shows a picture of the slopes around the Kitadake Crater. There is no vegetation in this area, and many rills and small gullies have already formed on the slope.

Some of the geomorphological factors in reference to mud flows were analyzed by

[1]Presented at the Subject Group S1.04 Technical Session on Geomorphic Hazards in Managed Forests, XIX World Forestry Congress, International Union of Forestry Research Organizations, August 5-11, 1990, Montreal, Canada.

[2]Yoshinobu Taniguchi: (1985) 58-2811. Professor of Agriculture and Forest Science. Faculty of Agriculture, Miyazaki University, Miyazaki 889-21, Japan

Table 1 Volcanic activities of Mt. Sakurajima

year	number of occurances eruptions	smoke emissions	earthquakes
1965	29	36	10312
1966	44	225	17117
1967	127	511	35174
1968	37	351	30383
1969	22	128	16801
1970	19	355	18264
1971	10	45	10974
1972	108	483	31949
1973	144	673	74883
1974	362	222	122795
1975	199	709	73297
1976	176	490	64055
1977	223	447	83491
1978	231	478	88334
1979	149	307	77261
1980	277	472	37338
1981	233	188	22182
1982	413	641	29402
1983	332	388	54032

using both a series of serial photographs from 1947 to 1984 and the report on the sediment yield on the slopes of Mt. Sakurajima (Osumi Public Works Office, 1988). These results are shown in Figs. 3-6.

Fig. 3 shows the expansion of the total area of these gullies in the 38 years from 1947 to 1984. The increase in their total area in the 26 years from 1947 to 1972 is less than that in the period since 1974. Volcanic activity became very vigorous after 1974. This fact shows that there should be a relationship between the number of mud flows and the volcanic activity since 1974. The same tendency also exists in the length of gullies (Fig. 4). This proves that the gullies have been considerably extended, and they have also expanded in width by the failure of

Fig. 2 Gullies on the slope of Mt. Sakurajima

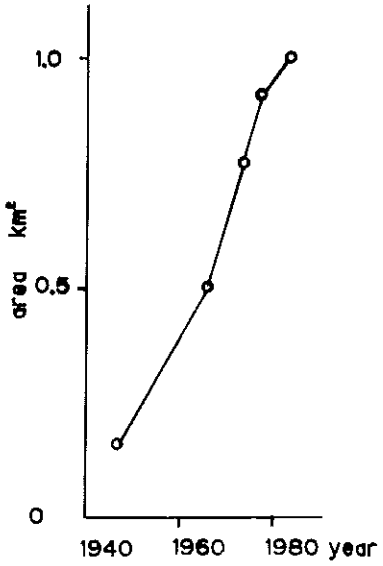

Fig. 3 Expansion of gullies

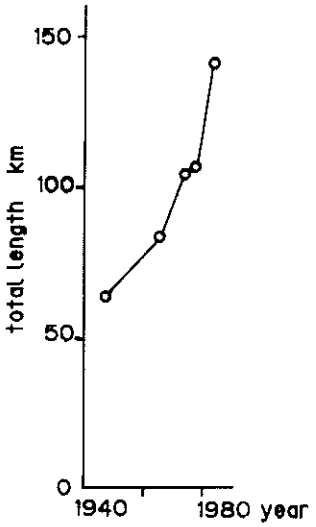

Fig. 4 Increase of total length of gullies

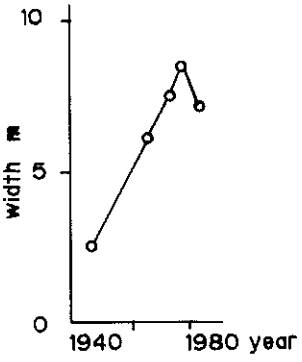

Fig. 5 Change of gully width

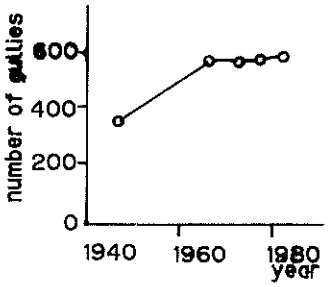

Fig. 6 Increase in number of gullies

sidewalls over the last 10 years (Fig. 5). An average rate of the expansion of the gullies in the 20 years from 1947 was only 0.13 m/yr. On the other hand, it increased to 0.76 m/yr in the 8 years from 1966. The latter is 5.9 times greater than the former. However, it has decreased since 1980, because fresh gullies began to form on the slopes. Fig. 4 shows the great extension of gullies. The number of gullies increased conspicuously in the 20 years from 1947 to 1966 (Fig. 6). This means that the formation of gullies had already ended during these years. Most of the sediment yield on Mt. Sakurajima is caused by the extension and the expansion of gullies. The volumetric rate of the sediment yield by the extension of gullies is 41 percent of the whole, and the expansion of them is 59 percent.

SURVEYING METHOD

A survey of the shearing force of a volcanic mud flow acting on a channel

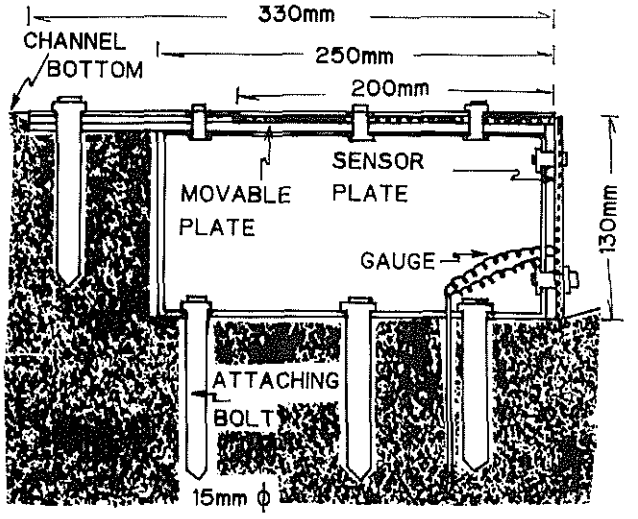

Fig. 7 Shearing stress meter (type A)

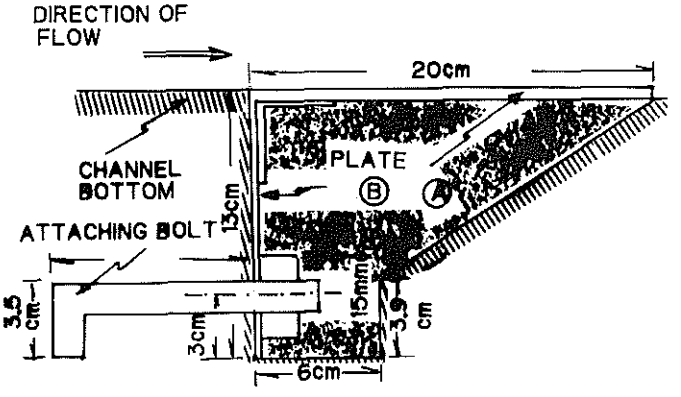

Fig. 8 Shearing stress meter (type B)

bottom has been going on in the Mochiki River since 1987 using the two kinds of shearing stress meters shown in Fig. 7 (type A) and Fig. 8 (type B). No data have been obtained from the type A survey up to the present, but some data have been gotten from the type B. In the type B, plate A is trailed downstream by the shearing force acting on its surface, and plate B is bent by the shearing force. As a result, a bending moment is generated in plate B. There should, however, be a balance between the shearing force and the bending moment. Accordingly, the shearing force acting on plate A (the channel bottom) can be easily measured by the magnitude of its deflection based on the theory of the deflection of a cantilever. The change in shearing force cannot be measured every time by this method, but the maximum shearing force can be easily measured using this meter.

When a dead load of 56.8 kilograms was applied to this shearing stress meter (type B) for the calibration of observed values, the average deflection of plate B was 8 millimeters. This meter is limited by the fact that plate B can not recover from its deflection, because a space caused by the bending moment forms between plate B and the wall of concrete to which plate B is attached (Fig. 8). This space is inevitably filled up by soil and sand which are contained in a mud flow whenever one runs down on plate A. On account of this, plate B of this meter cannot avoid increasing in deflection, whenever a bending moment acts on the plate. Of course, this happens on condition that the deflection is within the proportional limit of the strength of the material of which the plate is made.

SURVEYING RESULTS

Table 2 shows the volumetric concentration of the mud flow samples collected by the author in the Arimura River on July 18, 1987 in order to investigate the change of composition of a mud flow (Taniguchi and Takahashi, 1989).

The observed values of the shearing forces of several mud flows are shown in table 3. Some velocities of the mud flow, and the diameters of the stones in it are shown in table 4. They were measured on a video tape recorded by Osumi Public Works Office on September 24, 1988. One huge stone in the mud flow is shown in Fig. 9. These pictures were taken from that video. Fig. 10 is a picture of the measurement of the deflection of plate B in the Arimura River after the occurrence of the mud flow on October 6, 1988. No great number of huge stones gathered together at the front of that mud flow was observed.

Table 2 Grain size distribution and concentration of mud flow on July 18, 1987

	Collection Time		
	10 min.	15 min.	30 min.
grain diameter	distribution rate (pct)		
over 2000 $	1.0	1.0	2.9
840	3.5	3.1	7.7
500	5.8	6.9	12.9
250	22.2	22.4	32.5
105	58.9	52.2	37.0
74	6.2	4.1	5.1
37	2.2	4.	1.8
under 37	0.2	0.2	0.1
concentration (pct)	15.6	32.0	34.3
density (g/cm^3)	1.11	1.25	1.27

Table 3 Observed shearing forces of mud flows

date observed	shearing force kgf/cm^2	river
09/24/88	2.13	Arimura
10/06/88	0.462	Arimura
02/17/89	1.402	Arimura
02/17/89	2.502	Mochiki

Table 4 Stones' diameters in the mud flow on September 24, 1988 and their velocities.

stone	diameter (cm)	velocity m/sec
1	118	2.03
2	133	1.75
3	125	4.24
4	173	3.21
5	163	3.82
6	175	9.06
7	138	8.83
8	250	8.09
9	163	7.99
10	388	6.25

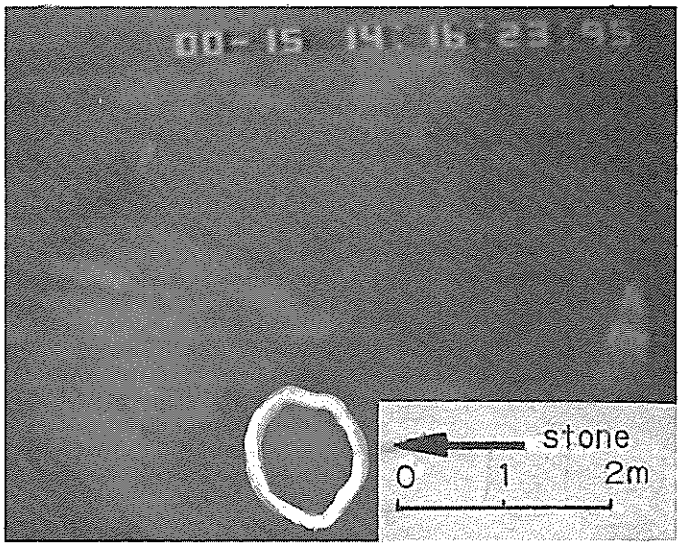

Fig. 9 Huge stone in the mud flow on September 24

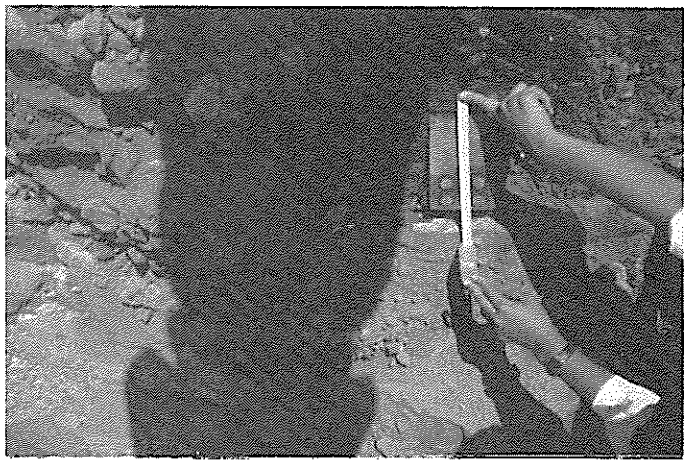

Fig. 10 Measurement of shearing force of a mud flow

DISCUSSION

The type B shearing stress meter is structurally a kind of cantilever. According to the theory of cantilever deflection, there should be a linearity between the shearing stress (τ) and the maximum deflection (δ) of the plate:

$$\delta \sim \tau \quad (1)$$

If it is supposed that the magnitude of the shearing stress (τ_0) already known acts on the shear plane (plate A), and that the deflection of plate B is δ_0, there should be the following relation between τ, τ_0 and δ, δ_0, using expression (1):

$$\tau / \tau_0 = \delta / \delta_0 \quad (2)$$

The shearing stress meter was tested by a dead load of 56.8 kilograms. As a result of that, the mean value of the deflections (δ_0) was 8 millimeters in the load test. When the above value of 8 millimeters is substituted into equation (2), the following is obtained:

$$\tau = 0.357\ \delta \quad (3)$$

Some data (δ= 6.0 centimeters, 1.3 centimeters and 4.0 centimeters in the Arimura River mud flow which took place on September 24, 1988, October 6, 1988, and February 17,1989, and 7.0 centimeters in the Mochiki River mud flow on February 17, 1989) were obtained. When these values were substituted into equation (3), the results of computations were shown in table 3 above.

It is, however, doubtful whether a linearity between these shearing forces and deflections of the plate might strictly exist in this case, because these observed deflections are conspicuously large.

However, seeing that these deflections began to occur in the test when the acting load had gone over 57 kilograms, it was evident that a shearing force at least greater than 0.29 kgf/cm^2 acted on the shear plane.

The shearing force of a mud flow acting on a channel bottom can be expressed as follows, taking the flow model of a mud flow shown in Fig. 11 into consideration:

$$\tau = \rho_D \, gH\sin\theta \qquad (4)$$

where ρ_D is the density of a mud flow; H is its water height; and θ is the angle of the channel slope. When the actually observed values of a density of 1.27 g/cm^3 and a water height of 1.0 meters in the mud flow of the Arimura River on July 18, 1987 are substituted into equation (4), the shearing

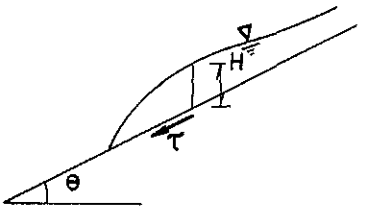

Fig.11 Flow model of a mud flow

stress (τ) becomes about 9 gf/cm^2. The computed value from equation (4) cannot prove that a large shearing stress as great as 0.5 ~ 2.5 kgf/cm^2 should occur even if there is a very large scale of a mud flow. Judging from that, it can be inferred that such a large shearing stress must be caused by the friction between stones and the channel bottom, because these stones are dragged along the channel bottom at a rather high speed.

Using the actual shearing force acting on the channel bottom, the size of a stone contained in the mud flow which took place in the Arimura River on September 24, 1988 could be estimated. When it was supposed that the density of a stone was 2.7 g/cm^3 and its frictional coefficient was 0.7, the size of a stone corresponding to the above shearing force of 2.13 kgf/cm^2 was calculated at about 60 centimeters in length for one side of a cube, or about 80 centimeters in the diameter of a sphere. Many stones corresponding to such sizes were observed on the video. Judging from that, it can be seen that the calculated value of the size of a stone is proper compared with the actual sizes. However, the maximum size of a stone in the Arimura River mud flow on September 24 was 3.8 meters. This proves that the concept of shearing force in the case in which a mud flow is regarded as only a fluid like water cannot be used for the solution of an actual problem like the abrasion of a concrete channel bottom.

When a mud flow accompanied by many stones flows on a channel bottom, its abrasion is very conspicuous, because the stones are dragged along the channel bottom. A great friction between the surface of the channel bottom and stones is generated.

The hydraulic drag force of a stone (a perfect cube or sphere) in fluid can be expressed as follows:

$$F = (1/2)\, C_D \rho_D \, V^2 A \qquad (5)$$

where F is the drag force; C_D is the coefficient of the drag force; V is the relative velocity between fluid and a stone; and A is the area of the application of the drag force. The value C_D became about 8 from the results of the computations on the mud flow which took place on July 18, 1987 in the Arimura River.

Supposing that C_D was 8, the density of a mud flow was 1.27 g/cm^3 (the value in table 2), the stone's diameter was 3.8 meters (the maximum diameter in the mud flow on September 24, 1988 in the Arimura River), and the relative velocity was 5.1 m/sec., the drag force of the mud flow could be estimated at 50 tons by equation (5). On the other hand, the frictional resistance of a stone on the channel bottom is estimated at 40 ~ 50 tons, using the value 0.76 as the coefficient of its friction. Judging from the above result, it can be seen that a mud flow with a water height of about 1 meter and a relative velocity of about 5 m/sec can easily carry a huge stone as large as 3 meters in diameter. The great friction is caused by many stones dragged along a channel bottom by a mud flow. There is another report that the temperature rose about 0.5 ~ 1.5°C in the Mochiki River when a mud flow ran down in the channel (Hirano, 1989). This shows that the frictional heat stated above might have a relation to the friction which was generated between the concrete channel bottom and the stones.

A mud flow also has the same characteristic as a debris flow. It greatly vibrates the earth around the stream when it flows at a high speed. The vibration is caused by the collision of stones with the concrete channel bottom or sidewalls of the stream. There are some reports that the vibrations caused by collisions between huge stones and the channel bottom have accelerated slope failures along torrents. This collision is also another important factor in the destructive damage of dams or concrete channels in torrents. The vibration caused

by the collision of a huge stone in a mud-debris flow was surveyed on the slopes of Mt. Yake in order to estimate the occurrence of a slope failure when the flow ran down in a torrent. An acceleration of 0.1 gal was observed at a point 15 meters from the centre of the torrent in cross section (Matsumoto Public Sabo Works Office, 1975). There might have been a great vibration near the centre. This problem should be taken into consideration to prevent dams or channels from being damaged in torrents.

The relationship between the strength of the concrete of a channel and the abrasion caused by the collision of stones contained in a mud flow is unclear even now. The impact force caused by the collision of an elastic body with concrete can be expressed as follows (Okubo, 1963):

$$(\sigma^2 / 2E)A\ell = W_0(S + \lambda) \quad (6)$$

where σ is the impact stress per unit area; E is the coefficient of the modulus of concrete; A is the area of the application of a force; ℓ is the length of a body; W_0 is a dead load S is the falling height of a body from a level; and λ is the compressed thickness of concrete. By solving equation (6), σ is obtained:

$$\sigma = \{2EW_0(S + \lambda)/A\ell\}^{1/2} \quad (7)$$

On the other hand, σ can also be expressed as follows:

$$\sigma = E(\lambda/\ell) \quad (8)$$

By substituting equation (8) into equation (6), σ can be solved:

$$\sigma = (W_0/A)(1 + \sqrt{1 + 2SEA/W_0\ell}) \quad (9)$$

When it is supposed that λ_0 is the thickness corresponding to a dead load (W_0), λ_0 can be expressed as follows:

$$\lambda_0 = W_0\ell/AE \quad (10)$$

When equation (10) is substituted into equation (9), σ can be solved:

$$\sigma = (W_0/A)(1 + \sqrt{1 + 2S/\lambda_0}) \quad (11)$$

The strain (λ) caused by the impact fo: of a stone which is contained in a mud can be solved, using equations (8) and (10):

$$\lambda = \lambda_0(1 + \sqrt{1 + 2S/\lambda_0}) \quad (12)$$

The dead load corresponding to the above strain can be estimated, using equations (8) and (12):

$$W/W_0 = 1 + \sqrt{1 + 2S/\lambda_0} \quad (13)$$

When it is supposed that D_0 is the actual stone's diameter, the converted diameter (D), defined here as the diameter of an imaginary stone which is assumed to be equal to the impact force caused by an actual stone with the diameter (D_0) stated above, can be calculated as follows, using equation (13) and both expressions of $W = \pi\rho_s D^3/6$, $W = \pi\rho_s D_0^3/6$:

$$D/D_0 = (1 + \sqrt{1 + 2S/\lambda_0})^{1/3} \quad (14)$$

where D is the converted diameter defined above; ρ_s is the density of a stone. When it is supposed that S is 10 centimeters, λ_0 is 1 millimeter, and stone's diameter is 3.8 meters (the maximum diameter in the Arimura River mud flow on September 24, 1988), the diameter (D) of an imaginary stone (the converted diameter corresponding to the impact force caused by an actual stone with a diameter of 3.8 meters is estimated to be about 9.4 meters. This means that the impact force has the same effect as a huge stone loaded on the channel bottom. It shows that channel works should be designed safely enough to prevent a concrete channel from destruction, because a channel may be attacked by a very high impact force.

If it is supposed that both areas of the application of forces, the dead load (W_0) and the impact load (W), are equal, W_0 and W can be expressed as follow:

$$W_0 = A\sigma_0 \quad (15)$$

$$W = A\sigma \quad (16)$$

When expressions (15) and (16) are substituted into equation (13), the following equation can be obtained:

$$\sigma/\sigma_0 = 1 + \sqrt{1 + 2S/\lambda_0} \quad (17)$$

σ_0 in equation (17) is the stress by the dead load derived from an actual impact stress (σ). The stress (σ) must be within the allowable strength of the concrete. It is generally said that the limit of the strength of concrete is about 250 kgf/cm^2. Accordingly, the maximum (σ) must be about 250 kgf/cm^2. If the same values as the above (λ_0 = 1 millimeter and S = 10 centimeters) are used here, σ_0 can be derived from equation (17):

$$250/\sigma_0 = 15$$

$$\therefore \sigma_0 = 16.\text{kgf/cm}^2$$

When the area of the application of a force is about 10 cm^2, the whole force becomes 167 kilograms, and a stone's diameter corresponding to this allowable force is calculated at 50 centimeters. However, the actual compressed thickness of the concrete of a channel must be less than the 1 millimeter assumed above. Then the value of σ_0 becomes smaller than 16.7 kgf/cm^2. Accordingly, the allowable diameter of a stone in a mud flow to prevent the destruction of a concrete channel must be less than 50 centimeters.

The above is a discussion from the point of view of the compressive strength of concrete. Shearing force is also a very important factor in the destruction of a concrete channel. It is generally said that the shearing strength of concrete is 1/4 ~ 1/7 of its compressive strength (Okada and Muguruma, 1989). Accordingly, the allowable size of a stone should be even smaller than 50 centimeters in diameter. It can be foreseen that the destructive action against a concrete channel will increase even more by dint of the shearing force caused by the friction of stones with a channel bottom, in addition to the compressive force by the impact. The Osumi Public Works Office began to carry out a survey of the abrasion of the channel concrete in the Mochiki River in 1988. That concrete channel was constructed to the strength of 160 kgf/cm^2. The mixing proportion of that concrete is shown in the following.

slump	water	aggregate fine	aggregate coarse A	aggregate coarse B	additive	cement
(cm)			(kg)			
8	158	700	600	600	2.5	252

A mud flow took place on October 6, 1988, a week after the channel works had been completed, and it abraded the concrete in the survey section. That mud flow could not be recorded on video tape, because it took place at night. The abrasion of the concrete was 2.5 centimeters in depth. The result of the strength test of the concrete reported that the strength on the 7th day after the mixing of that concrete was 110 kgf/cm^2.

Taking into consideration the fact that the shearing strength of concrete is about 1/7 of the compressive, the allowable compressive strength of 110/ kgf/cm^2 corresponds to an allowable shearing strength of 15.7 kgf/cm^2. The shearing force of the mud flow which took place on the Mochiki River on February 17, 1989, was 2.5 kgf/cm^2. As the mud flow on October 6, 1988, could not be recorded on video tape, its scale was unknown, but the marks of the water height in the channel after this flow nearly equal to the marks of the mud flow on February 17, 1989, in the same river. As both scales were almost equal, the value of 2.5 kgf/cm^2 was substituted for its shearing force. It resulted in the calculated value (the allowable shearing strength of the material, 15.7 kgf/cm^2) being larger than the observed ones. However, in the case in which such shearing force acts actually on a channel bottom as a repeated force, the shearing force of 2.5 kgf/cm^2 is not small as compared with the allowable shearing strength of the concrete (15.7 kgf/cm^2) stated above.

CONCLUSION

The results of surveys in the Arimura River and the Mochiki River showed that the actual shearing force of a mud flow on the surface of a channel bottom was about 0.5 ~ 2.5 kgf/cm^2. According to the theoretical calculations, the frictional force which should be caused by a stone of about 80 centimeters in diameter corresponded to the force of 2.13 kgf/cm^2 in the Arimura River mud flow on September 24, 1988. Such sizes of stones could be observed on the video. The impact force caused by huge stones in a mud flow was derived from the theory of the collision of an elastic body, and it proved that the impact force of a stone was several times greater than the dead load caused by that stone. When a shearing stress of about 2.5 kgf/cm^2 acted on a concrete channel with a compressive strength of 110 kgf/cm^2, the abrasion of that concrete was 2.5 centimeters in depth.

REFERENCES

Hirano, M. 1989. Report of research project, Grant in Aid for Scientific Research; 25 p. (in Japanese).

Matsumoto Sabo Public Works Office. 1975. Publication of surveys of Mt. Yake 7. Ministry of Construction: 37 p. (in Japanese).

Okada, K., and H. Muguruma. 1989. Engineering handbook of concrete. Tokyo: Heibon-sha Co., 404 p. (in Japanese).

Okubo, H. 1963. Strength of material. Tokyo: Shokoku-sha Co.; 40-41 (in Japanese).

Osumi Public Works Office. 1982. Report of the research work on sediment yield from the Kurokami River. Ministry of Construction; 13 p. (in Japanese).

Osumi Public Works Office. 1986. Sabo in volcano Sakurajima. Ministry of Construction; 8 p. (in Japanese).

Osumi Public Works Office. 1988. Sabo in volcano Sakurajima. Ministry of Construction; 5 p. (in Japanese).

Taniguchi, Y., and M. Takahashi. 1985. Experimental study on sediment yield and fluidization of soil mass in an area of active volcano. Proceeding of International symposium on Erosion, Debris Flow and Disaster Prevention-Tsukuba 1985: 133-138.

Taniguchi, Y., and M. Takahashi. 1989. Prediction for the escape from the strike of a volcanic mud flow in a torrent and the characteristic of its movement. Journal of the Japan Society of Erosion Control 44(4):26 p. (in Japanese).

Research of Wind Erosion Intensity in the Region of Subotica-Horgos Sands[1]

Velizar Velasevic and Ljubomir Letic[2]

Abstract: Wind is an important erosional process in the areas of steppe-savanna climate in Europe as typified by the Vojvodina plain in Yugoslavia. Cultivated and forested plots on the Subotica-Horgos Sands were used to study aeolian erosion processes. Wind erosion on the cultivated plot was 3-29 times greater than that occurring on a plot planted to forest trees. That erosion results in important losses of humus and nutrients. A practical equation estimating wind erosion from wind parameters is presented.[3]

Deflation processes in the zone of steppe-savanna climate in Europe are represented in the large plain of Vojvodina, which is a cornfield and a region of particular importance to Yugoslavia. The use of contemporary agricultural engineering, the inappropriate organization of the territory, destruction of protective green cover, and other unfavorable effects lead to the initiation and development of deflation processes of different intensities. This aspect of soil destruction affects, first of all, agriculture, water resources management, traffic, infrastructure, environment, etc. The region of Vojvodina is characterized by heterogeneous soil types, ranging from sands, black soil, chernozem, and smonitza to gleyed soil which, in given climate conditions, are differently threatened by the process of wind erosion. In this paper we shall point out the research on wind erosion (started in 1980) on the soils of light mechanical composition (potentially the most threatened soils), on the Subotica-Horgos Sands.

The Subotica-Horgos Sands are situated in the North-Northwest part of Vojvodina plain between the Danube and Tisa rivers. The average length of the Sands is 48 km and the average diameter is 5-11 km. The Sands cover an area about of 240 km^2. The Vojvodina plain is a well-known orchard-grape vine country, with more than 33 percent under vineyards and orchards, about 20 percent forests and woodlands, and over 34 percent under grassland. It is characterized by mildly undulating dune relief of northwest-southeast direction, as well as by a high level of underground waters, 2 - 8 m. As these Sands are in the zone of arid climate, at the boundary of steppe-savanna and slight woodland character, under the influence of pedogenetic factors, there can be distinguished different types of sand: grey-yellow, brown, black, black loamy, and saline sands with different production capacities.

METHOD OF RESEARCH

A comparative method of stationary observation by wind-gage stations has been applied on specially selected erosion plots, of which one, used for agricultural production, has not been protected ("U"), while the other ("P") has been protected with forest plantings, figure 1.

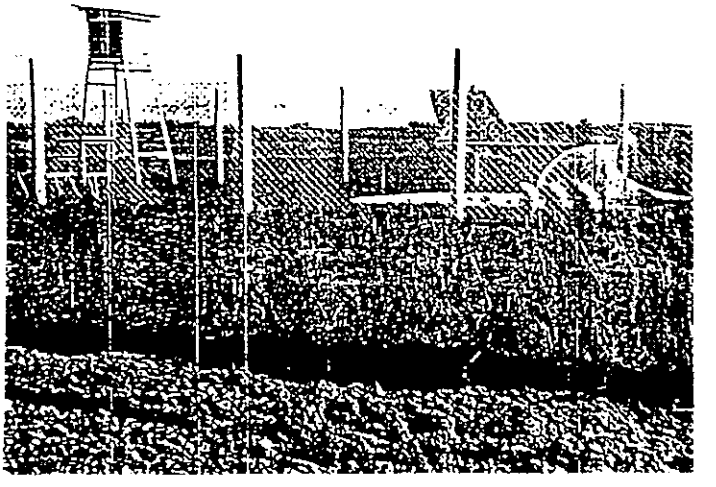

Figure 1--Experimental wind-gage station records deflation processes.

[1]Presented at the Subject Group S1.04 Technical Session on Geomorphic Hazards in Managed Forests, XIX World Forestry Congress, International Union of Forestry Research Organizations, August 5-11, 1990, Montreal, Canada.

[2]Faculty of Forestry, University of Beograd, Beograd, Yugoslavia.

[3]Abstract supplied by Session Chairman.

Table 1. Average monthly and annual deposition quantities (E_n kg m^{-1}) Loc. "U" and loc. "P"

E_n	Months												
	Jan	Feb	Mar	Apr	May	June	July	Aug	Sep	Oct	Nov	Dec	E_n
Loc."U" (kg m^{-1})	0.272	0.765	0.504	0.693	0.306	0.350	0.507	0.106	0.136	0.116	0.040	0.062	3.857
Loc."P" (kg m^{-1})	0.017	0.026	0.028	0.047	0.053	0.038	0.040	0.039	0.025	0.019	0.014	0.010	0.356
Relation U/P	16	29	18	15	6	9	13	3	5	6	3	6	11

Table 2. Average monthly velocities (m s^{-1}) at 0.05 m above ground frequencies (pct) and storm winds (12.3 m s^{-1}) NW and N directions.

Parameters	Months												
	Jan	Feb	Mar	Apr	May	June	July	Aug	Sep	Oct	Nov	Dec	Average
Velocity (m s^{-1})	8.10	8.49	8.13	6.24	7.89	9.36	7.11	8.61	6.97	9.59	7.45	7.05	7.92
	4.32	-	9.01	4.90	7.13	5.53	5.89	9.67	-	7.73	8.12	4.38	6.67
Frequency (pct)	23.42	11.88	7.21	6.23	5.76	9.32	17.25	2.25	4.04	1.96	1.84	8.84	8.33
	4.65	-	16.85	32.51	0.77	11.40	6.24	1.20	-	5.77	10.44	10.17	10.00
Force (K)	3.08	2.48	3.00	2.82	3.51	4.16	2.75	4.26	3.50	4.75	3.71	2.83	3.33
	8.47	3.13	3.04	3.38	5.44	3.59	4.15	5.23	1.00	4.25	3.81	2.92	3.85

Experimental stations record: quantity of aeolian deposition, wind frequency and velocity, air and soil temperatures, air and soil humidity, etc. Field data are analyzed in order to qualify and quantify the deflation process, as well as to define the conditions of climate and residual soil in which they occur.

RESULTS OF RESEARCH

The analysis of the data obtained at experimental stations "U" and "P" has proved significant differences in the distribution and intensity of deflatory processes, as well as in the parameters of climate and residual soil which affect them.

The data on the annual intensity of wind erosion, with 2.127-5.490 t km^{-1} per year, emphasize that unprotected areas (loc. "U") of the researched region are threatened by erosion, whereas the protected areas (loc."P") are subjected to deflation processes of about 11 times lower intensity, ranging from 0.247 to 0.444 t km^{-1} per year, average 0.356 t km^{-1} per year (table 1). According to the data in table 1, maximum values of wind erosion intensity occur in the first half of the year between January and July, amounting to about 80 percent total annual quantity of aeolian deposition, whereas the remaining 12 percent are deposited between August and December.

Therefore in the unprotected areas of the Subotica-Horgos Sands, deflation processes oscillate within categories II and III, starting from medium intensity erosion (2.0 - 5.0 t km^{-1} per year) to intensive erosion (5.0 - 7.0 t km^{-1} per year). In the protected areas of the Sands, deflation processes are reduced to the level of normal erosion (category I of erosion processes) with the intensity lower than 0.5 t km^{-1} per year.

The degree of hazard (comparison of protected and unprotected areas of the Sands) is included in the expression $B = I_{ee}^{p}/I_{ee}^{s}$, and ranges between 11 for annual and 171 for diurnal intensities of wind erosion. This points out the significant differences in the degree of hazard of the compared lands, which is conditioned by the buffering effect of protective plantings on the deflatory processes in the protected erosion plots.

The establishment of "erosion active" winds has been performed by the criterion of critical (initial) velocities ($V_s \geq V_{kr}$). Accordingly, the initial velocity necessary to move the mixture of D. Tavankut sands D_s = 0.18 mm, is about 3.0 m s^{-1}at the height of 0.05 m above ground. This denotes stormy winds (>12.3 m s^{-1}) as erosion active winds.

In the researched region of the Pannonian Plain, by the "Modified Method of Instrumental Analysis", the following dominant winds have been distinguished: NW (14) and N (16) with the degree of dominance ranging up to 10 times. Average monthly velocities (at 0.05 m) and wind frequencies are presented in Table 2.

Stormy winds in the Subotica-Horgos Sands occur 48.96 percent in the period

Table 3. Average monthly air temperatures (ºC), precipitation (mm), relative air humidity (pct), and total soil moisture, loc. "U" and "P"

Climatic Factors	Loc.	Months Jan	Feb	Mar	Apr	May	June	July	Aug	Sep	Oct	Nov	Dec	Annual	VP*	NVP**
Air Temp. °C	"U"	-0.87	-0.54	6.07	10.01	15.58	17.63	20.16	19.81	16.64	10.88	3.91	0.41	9.98	16.64	3.25
	"P"	-1.52	-0.49	5.86	10.70	15.00	18.04	19.53	18.91	16.02	10.58	3.07	-0.04	9.64	16.64	2.91
Precip. (mm)	"U"	28.78	21.48	35.42	32.16	54.92	90.30	35.22	30.74	43.18	39.84	40.20	47.36	499.60	286.52	213.08
	"P"	31.36	22.88	37.48	34.38	57.44	88.76	39.66	25.70	46.24	44.26	41.62	49.26	519.04	292.18	226.86
Relative Humidity of Air (pct)	"U"	81.45	78.24	68.92	64.19	65.40	66.77	67.49	67.89	71.88	72.76	77.59	83.01	72.13	67.27	77.00
	"P"	88.66	81.06	72.57	68.31	67.32	70.44	69.34	72.27	75.70	77.73	82.96	86.54	75.91	70.56	81.25
Total Soil Moisture (pct)	"U"	3.82	6.52	2.68	3.36	3.32	2.30	2.42	2.56	2.68	3.96	4.96	7.04	3.80	2.80	4.80
	"P"	15.78	21.02	12.60	9.56	6.70	6.42	5.70	4.96	7.56	10.88	11.42	17.80	10.87	6.80	14.90

* VP denotes Vegetational Period
** NVP denotes Non-Vegetational Period

between 10 a.m. and 3 p.m. As per their duration, category II winds (60 - 360 min.) occur most frequently in March and October. In addition, it has been observed that erosionally active air currents of NW direction (14) are more favorable (warmer and drier air) to the development of deflation, than the winds of N (16) direction.

The degree of nonuniformness of air currents expressed through the factors of force (K) and frequency (percent) ranges between 1.0 and 9.6. These values for NW (14) and N (16) winds oscillate much less, averaging 3.33 and 3.86 (table 2) which is very significant for the evaluation of the aggressiveness of air currents.

The analysis of data (table 3) of the hydrometric regime of the researched erosion plots points to the significantly more humid regime on the protected erosion plot, which decreases the development of deflatory processes.

The analysis of aeolian deposit (E_n) and residual soil (O_z) resulted in several indicators of conditions in which deflation processes occur. The following are the most important ones:

Particle-size composition of the researched sands indicates a very "erodible soil". The content of erodible particles smaller than 1 mm (to the depth of 0.05 m) amounts to more than 99 percent, and the condition of erodibility is 40 percent of these particles.

Sand moisture (rough dispersion) is a very significant factor in the group of soil physical properties which condition the "pseudo cohesion" reducing the development of the deflation process. The content of total sand moisture (to the depth of 0.05 m) on the unprotected area ranges between 2.3 percent and 7.0 percent, and on the protected area it is 4.9 percent to 21 percent (table 3). The relation of moisture (W_z) and apparent cohesion (c) is defined by the function:

$$c = -0.23 + 0.16 \times W_z + 0.07 \times W_z^2 - 4.74 \times 10^{-3} \times W_z^3 + 8.58 \times 10^{-5} \times W_z^4,$$

and it has been established for W_z = 1 - 21 percent, with the corresponding values of cohesion of up to c = 6.79 kN x m^{-2}. On this occasion it has been observed that deflation processes occur at the soil moisture below 7 percent, which corresponds to cohesion below c = 3.0 kN x m^{-2}.

The analysis of the relation of chemical characteristics of the aeolian deposition (E_n) and the residual soil (O_z) points to the very significant indication of soil fertilization loss affected by deflation processes. It is denoted by the "deflation coefficient" presented in table 4.

Table 4. The degree of the damaging effect of deflation process expressed as deflation coefficient $mu = E_n \times O_z^{-1}$

Number	Nutrients	$mu = E_n \times O_z^{-1}$
1	Humus	5.7 - 16.2
2	$CaCO_3$	1.1 - 1.3
3	Total Nitrogen	3.2 - 14.0
4	Readily Available P	15.5 - 20.3
5	Readily Available K	6.4 - 14.3

By the research of correlation between aggressive factors of climate, resistances of soil particles, and the quantity of aeolian deposition in the conditions of the Pannonian Plain, the basic equation of wind erosion has been developed:

$$E_n = A \times e^{(B \times Qv)} \times T \qquad (kg\ m^{-1})$$

where:

- E_n - Quantity of aeolian deposition in kg m^{-1};
- A and B - coefficients of regression;
- e - base of natural logarithms;
- Qv - air flow in seconds through the observed cross section in $m^3 s^{-1}$;
- T - duration of each aggressive wind in s.

The formula is practical, as it is incomparably easier (with the aid of analytical evaluations and graphs of input parameters) to evaluate the erosion process, which otherwise calls for a rather complicated procedure of measurements.

CONCLUSIONS

By the analysis of data presented in the paper, it can be concluded as follows:

- In steppe-savanna conditions of the Pannonian Plain deflation processes represent a significant factor of soil destruction. They are factors which have adverse effects on the quality of the environment and, in general, on human activities in the region.

- Light soils (sands) of the Subotica-Horgos Sands are very erodible (containing more than 90 percent particles smaller than 1 mm) and they can be classified as category III wind erosion hazard (Chepil and Woodruff 1954) - soils not resistant to wind erosion, or as (III), category of intensive erosion (Letic, Lj. 1989) with 5.0 - 7.0 t km^{-1} per year of deflation.

- Deflation processes occur in the periods winter - spring (Jan - Apr) and summer (June - July) and they are caused by aggressive winds NW (14) and N (16), velocity above 3.0 m s^{-1} (at 0.05 m above ground).

- The researched soils are subject to the accelerated nutrient loss resulting in fertility loss.

- These researches have a practical value, as they widen and supplement the knowledge of the measures of struggle against the phenomena of deflation, i.e. the establishment of shelterbelt plantings (and other measures) in this part of the Pannonian Plain.

REFERENCES

Chepil, W.S. and N.P. Woodruff. 1954. Estimations of wind erodibility of field surfaces. Journal of Soil and Water Conservation 9:257-265, 285.

Letic, Lj. 1989. Istrazivanje intenziteta eoloske erozije na Suboticko-horgoskoj pescari, Disertacija, Beograd.

Svehlik, R. 1975. Vetrna eroze pudy na jinovychodni Morave, Sv. 20, C.S.R. ve ZH. Praha.

Velasevic, V. 1978. Zastita i unapredjenje suma Suboticko-horgoske pescare, Studija, Subotica.

The Forest Service, U.S. Department of Agriculture, is responsible for Federal leadership in forestry. It carries out this role through four main activities:

- Protection and management of resources on 191 million acres of National Forest System lands
- Cooperation with State and local governments, forest industries, and private landowners to help protect and manage non-Federal forest and associated range and watershed lands
- Participation with other agencies in human resource and community assistance programs to improve living conditions in rural areas
- Research on all aspects of forestry, rangeland management, and forest resources utilization.

The Pacific Southwest Research Station

- Represents the research branch of the Forest Service in California, Hawaii, American Samoa and the western Pacific.

Persons of any race, color, national origin, sex, age, religion, or with any handicapping conditions are welcome to use and enjoy all facilities, programs, and services of the U.S. Department of Agriculture. Discrimination in any form is strictly against agency policy, and should be reported to the Secretary of Agriculture, Washington, DC 20250.

GTR
PSW
130

Proceedings of the IUFRO Technical Session on Geomorphic Hazards in Managed Forests

August 5-11, 1990, Montreal, Canada

Printed on recycled paper